CRANFIELD UNIVERSITY

Jen-Rong Huang

OPTOELECTRONIC SPECKLE SHEARING INTERFEROMETRY

Centre for Photonics and Optical Engineering

School of Mechanical Engineering

PhD Thesis

CRANFIELD UNIVERSITY

Centre for Photonics and Optical Engineering

School of Mechanical Engineering

PhD Thesis

Academic Year 1995-6

Jen-Rong Huang

OPTOELECTRONIC SPECKLE SHEARING INTERFEROMETRY

Supervisor: R. P. Tatam

April, 1996

This thesis is submitted in partial fulfilment of the requirement for the Degree of Doctor of Philosophy

ABSTRACT

This thesis describes the implementation of enhanced signal processing techniques in electronic speckle shearing interferometry, including two-wavelength slope measurement, phase stepping, and heterodyning and stroboscopic illumination in vibration analysis. All the techniques were achieved using laser diode emission wavelength modulation.

Slope measurement using two-wavelength illumination can generate slope fringes in a mechanically passive manner and the fringe visibility is better compared to other illumination-shifting and object-tilting methods. Three simple geometric objects were measured using an x shear of 4 mm and $\Delta\lambda \sim 0.45$ nm. The results are in agreement with a theoretical analysis. The measurement accuracy can be further improved by calculating the simple equations of parameters in the fringe function.

A novel phase stepping technique has been demonstrated using laser diode injection current modulation. An unbalanced Michelson-interferometer arrangement, with a perspex block of 25 mm thickness inserted into the longer interferometer arm to maintain equal image magnification for the two images, was used to obtain a 2π phase shift for an optical frequency change of 7.25 GHz. The technique provides an additional phase stepping method in shearography with the advantages of removing an active phase-shifting component from the interferometer and a greater linearity in the phase shifts through the diode wavelength modulation.

In vibration measurement, heterodyning and stroboscopic illumination have also been successfully achieved in a mechanical passive manner. For shearing systems using a Michelson interferometer, heterodyning was originally difficult to perform. With the unbalanced optical configuration as used in the phase stepping work, heterodyning has been demonstrated to measure vibration motion ~5.5 kHz and the diode optical frequency modulation ~15 GHz. By pulsing the laser diode with an 11% duty cycle, stroboscopic illumination was performed to obtain cosine fringes along with greatly improved visibility. Phase stepping methods were then incorporated to automate the fringe analysis.

ACKNOWLEDGEMENTS

At first, I have to thank my supervisor Dr. Ralph P. Tatam for accepting me, a dumb guy without any optics background, as his student and continuously supervising me up to the final stage. I also need to thank Dr. Helen D. Ford for her assistance in experimental work and many discussions. Thanks also to all the other members in the optical sensors group especially Steve Staines, Dr. Hashim Atcha, Abdel Ezbiri and Alan Wilson.

Special thanks have to go to Dr. P. J. Bryanston-Cross at Warwick University for providing us the fringe analysis program and to his student Dr. P. H. Chan for helping me to make it work and also many discussions in image processing.

The four-year sponsorship from the Industrial Technology Research Institute (ITRI) and the Mechanical Industry Research Laboratories (MIRL) in Taiwan R.O.C. is deeply appreciated.

Finally, my sincere thanks to my parents, parents-in-law and all the family for their support, to my lovely wife Chun-Ping for her patience of accompanying a bad-tempered husband and being always there for me, and to my baby girl Tsu-Ying for behaving well when I was writing my thesis.

CONTENTS

FIGURES

TABLES

NOTATION & ABBREVIATIONS

Notation

A	aperture of the viewing lens
$A(r_o, t)$	motion of a sinusoidally vibrating object
$a_o(\underline{r}_o)$	amplitude of vibration motion
a_r	amplitude of reference beam modulation
C_x, C_y, C_z	coefficients in two wavelength slope measurement
c	free space velocity of light
D	diameter of the illuminated area
d_{obj}	average size of the objective speckle
d_{sub}	average size of the subjective speckle
E_1, E_2	electric fields of the image-sheared wavefronts
$E_o(\underline{r}_o)$	electric field of the object beam
$E_{o1,2}$	electric field of the object beam under the illumination of λ_1 and λ_2
E_r	electric field of the reference beam
$E_{r1,2}$	electric field of the reference beam under the illumination of λ_1 and λ_2
E_{tot}	interfere wavefront
e_1, e_2	amplitudes of the image-sheared wavefronts
e_o	amplitude of the object beam
e_r	amplitude of the reference beam
F	lens aperture ratio (f/number)
f_{max}	speckle cut-off frequency (maximum spatial frequency)
g_{min}	minimum speckle size
h	Planck's constant, or height variation of the object surface
I	intensity
$\langle I \rangle$	average intensity over many speckles
$I(\underline{r}_d)$	intensity at the camera (in the image plane)

I_1, I_2	$I_1=e_1^2$ and $I_2=e_2^2$, intensities of two image-sheared wavefronts,
I_{aft}	intensity in the image plane after object deformation
$I_{aft,\ k+1}$	phase stepped images after object deformation, k = 0, 1, 2
I_{bef}	intensity in the image plane before object deformation
$I_{bef,\ k+1}$	phase stepped images before object deformation, k = 0, 1, 2
$I_{E1} \sim I_{E4}$	phase stepped images before object deformation
$I_{E1}' \sim I_{E4}'$	phase stepped images after object deformation
I_o	e_o^2, intensity of the object beam
$\langle I_o \rangle$	mean value of I_o
I_r	e_r^2, intensity of the reference beam
$\langle I_r \rangle$	mean value of I_r
I_{sub}	intensity subtraction of two image frames
J_0	zero-order Bessel function of the first kind
J_1	first-order Bessel function of the first kind
L	laser cavity length
L_S	distance from the scattering surface to the observation screen
l_o	the object beam path length
l_r	the reference beam path length
M	image magnification
m	integer
n, n_b	refractive index
$\underline{n}_o$	unit vector of the viewing direction
$\underline{n}_s$	unit vector of the illumination direction
P(I)	probability density function of the intensity of a fully developed speckle
R	thermal resistance
$R_I(r)$	auto-correlation function for the image-plane speckle intensity
R_o	viewing distance
R_s	illumination distance
r	$[\ (\Delta x)^2 + (\Delta y)^2\ ]^{1/2}$, Δx and Δy are the distance between two adjacent speckles in x and y directions
$\underline{r}_d$	conjugate position vector of $\underline{r}_o$ in the image plane

$\mathbf{r}_o$	position vector of a point on the object
T	exposure period of image frame
T_m	temperature
t	time
U	distance between the object and the lens
u	x component of in-plane displacement
V	distance between the lens and the image plane
V_{aft}	camera voltage signal proportional to the intensity of speckle image after object deformation
V_{bef}	camera voltage signal proportional to the intensity of speckle image before object deformation
V_{sub}	$V_{aft} - V_{bef}$
v	y component of in-plane displacement
w	out-of-plane displacement
x, y, z	coordinate on the object surface, z is defined as the viewing (out-of-plane) direction, and x, y as the in-plane direction
(x_o, y_o)	conjugate point in the image plane corresponding to a point (x, y) on the object surface
α, β	proportionality constants
β_1	light propagation coefficient in an optical fibre
ΔI	subtraction of two images
Δi	injection current change
ΔL	path length difference in the unbalanced Michelson interferometer
ΔL_f	length change of the fibre wrapped around PZT
Δl	optical path length difference
ΔT_m	temperature change
$\Delta\phi$	phase change
$\Delta\phi_x$	phase change in a shearography system with x image shear
$\Delta\phi_{x1}, \Delta\phi_{x2}$	phase changes in the fringe patterns associated with the illuminating angles θ_1 and θ_2 respectively.
$\Delta\phi_y$	phase change in a shearography system with y image shear

$\Delta\lambda$	wavelength change
$\Delta\nu$	optical frequency change
$\delta\ell$,δl	optical path length difference between object and reference beams
δx	magnitudes of x shear
δy	magnitudes of y shear
δz	height variation
δu	x component of relative deformation between two image-sheared points
δv	y component of relative deformation between two image-sheared points
δw	z component of relative deformation between two image-sheared points
ϕ	phase difference between the object and reference beams
ϕ_1, ϕ_2	The phases of the image-sheared wavefronts
$\phi_o(\underline{r}_o)$	object beam phase
ϕ_r	reference beam phase
ϕ_s, ϕ_{s1}, ϕ_{s2}	speckle phases
γ_{max}	maximum tilt angle
γ_x	$\partial w/\partial y$
γ_y	$\partial w/\partial x$
λ	wavelength of light
λ_1 , λ_2	two wavelengths of light
$\lambda_{1,2}$	λ_1 and λ_2 occur in the same image frame
λ_{eff}	$\lambda_1\lambda_2/(\lambda_1 - \lambda_2)$, effective wavelength
$\partial z/\partial x$	surface gradient in x direction
$\partial z/\partial y$	surface gradient in y direction
ω	angular frequency of vibration
σ_o^2	variance of I_o
σ_r^2	variance of I_r
τ	period of vibration
θ	inclined angle of the collimated beams with respect to the object surface
θ_1, θ_2	two different illuminating angles lying on the yz plane
$\varphi_o(\underline{r}_o)$	phase of the vibration motion

φ_r	reference beam modulation phase
φ_v	phase of diode modulation
Ψ_i	angle of phase step
*	Hermitian conjugate
<>	time average

Abbreviations

A/D	analog to digital
ALU	arithmetic logic unit
CCD	charge-coupled device
CCIR	Comite Consultatif International Radio, an international standard
CNC	computer numerical control
CPU	central processing unit
CW	continuous wave
D/A	digital to analog
DiPSSI	digital phase stepping speckle interferometry
DSPI	digital speckle pattern interferometry
EOH	electro-optic holography
ESPI	electronic speckle pattern interferometry
FEM	finite element
FTM	Fourier transform
Hi-Bi	highly birefringent
LED	light emitting diode
LUT	look-up table
MOS	metal-oxide semiconductor
NDT	nondestructive testing
PZT	piezoelectric transducer
SOP	state of polarisation
TPSSC	temporal phase stepping correlation

1. INTRODUCTION

Electronic speckle shearing interferometry, also called electronic shearography, is an interferometric speckle technique for the direct measurement of gradients of surface deformation, gradients of vibration, and slopes (surface gradients) of test objects over an extended area. Essentially, the technique is performed by collecting image-sheared speckle patterns of a test object in its initial and deformed state. These two images, commonly recorded by a CCD camera, are stored electronically and correlation fringes generated, usually by subtracting the two images, represent the derivatives of surface deformations, as shown in Fig. 1.1.

The capability of shearography to directly measure deformation derivatives is advantageous compared to conventional out-of-plane sensitive interferometers in the calculation of bending moments and flexural strains of plate structures [1.1-1.4]. In shearography, differentiation of the deformation is performed optically such that only one single differentiation of the unwrapped phase map is necessary to obtain curvatures and hence bending moments, thus reducing errors from numerical differentiation.

Compared to interferometric methods with separated reference and object beams, e.g. out-of-plane sensitive electronic speckle pattern interferometry (ESPI) as shown in Fig. 1.2(b), shearography is more robust against environmental perturbations due to its common path optical configuration, Fig. 1.2(a). In shearography, the acquired images that depict gradients of object deformation are also more interpretable than those measured by ESPI systems in the qualitative evaluation of stress/strain concentration on the object surface [1.5,1.6]. An example is shown in Fig. 1.3. The above mentioned two characteristics of shearography are important considerations for in-situ industrial applications and non-destructive testing. During the past few years, research effort in shearography techniques has increased dramatically because of its potential application in industrial fields [1.7-1.12].

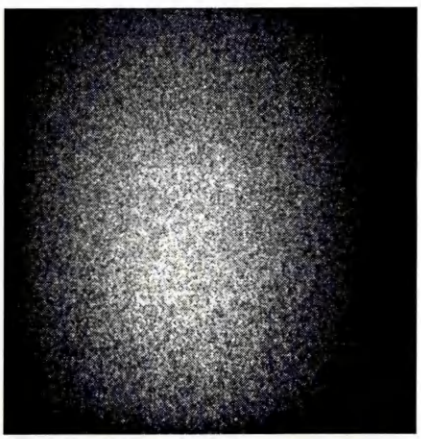

(a) Speckle image before object deformation

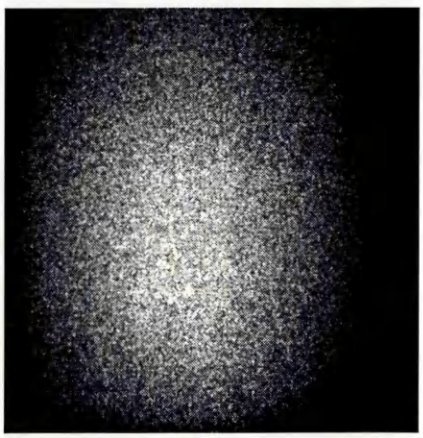

(b) Speckle image after object deformation

(c) Correlation fringes generated by the subtraction of speckle images before and after object deformation

Fig. 1.1 The generating process for correlation fringes in electronic shearography (the test object is a flat aluminium plate, 150 mm x 100 mm, mechanically loaded at the centre of the back surface and clamped around the edges)

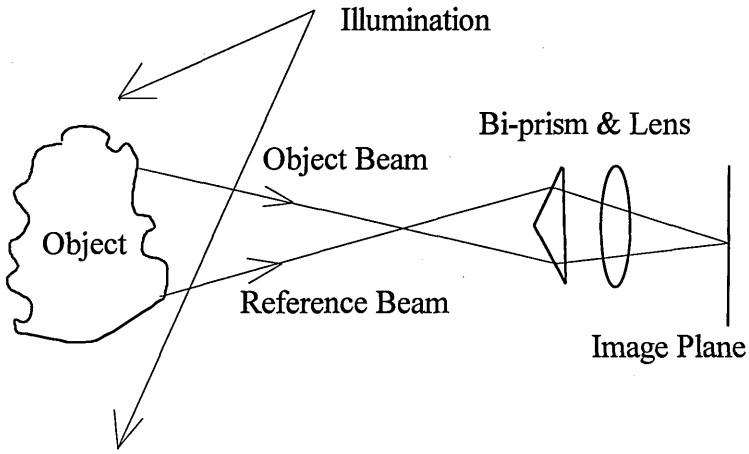

(a) Shearography with a common path optical configuration

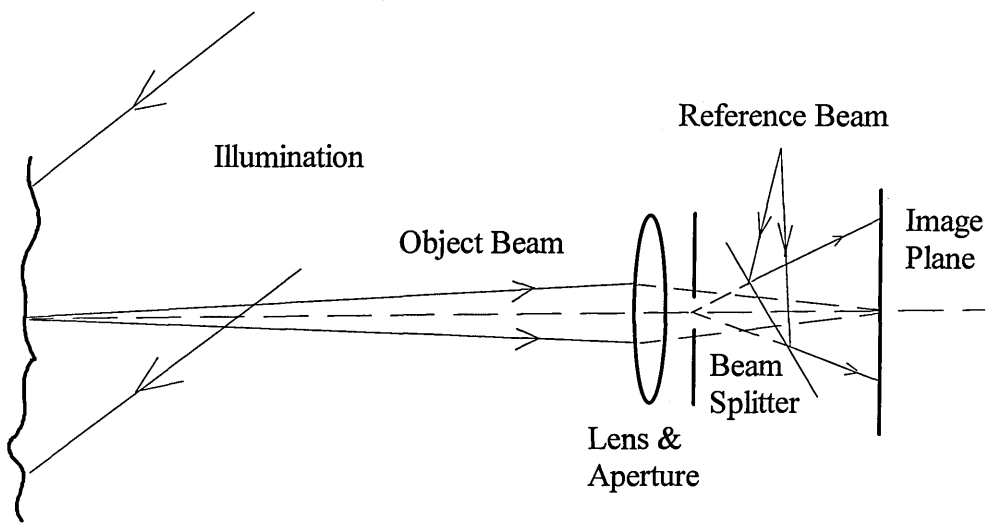

(b) Out-of-plane ESPI with separated reference and object beams

Fig. 1.2 Comparison of optical configurations between shearography and out-of-plane ESPI systems

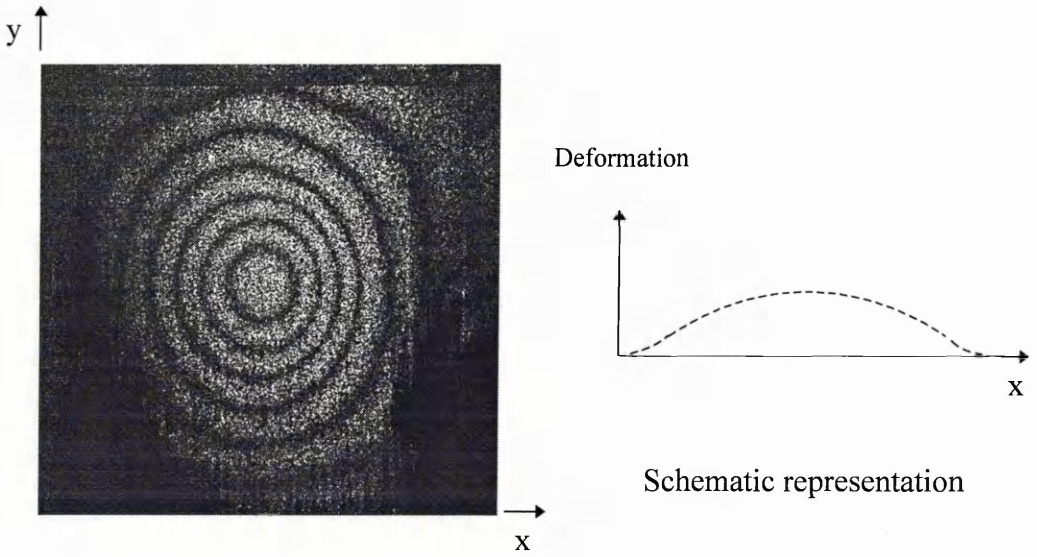

(a) Deformation fringes measured by out-of plane ESPI

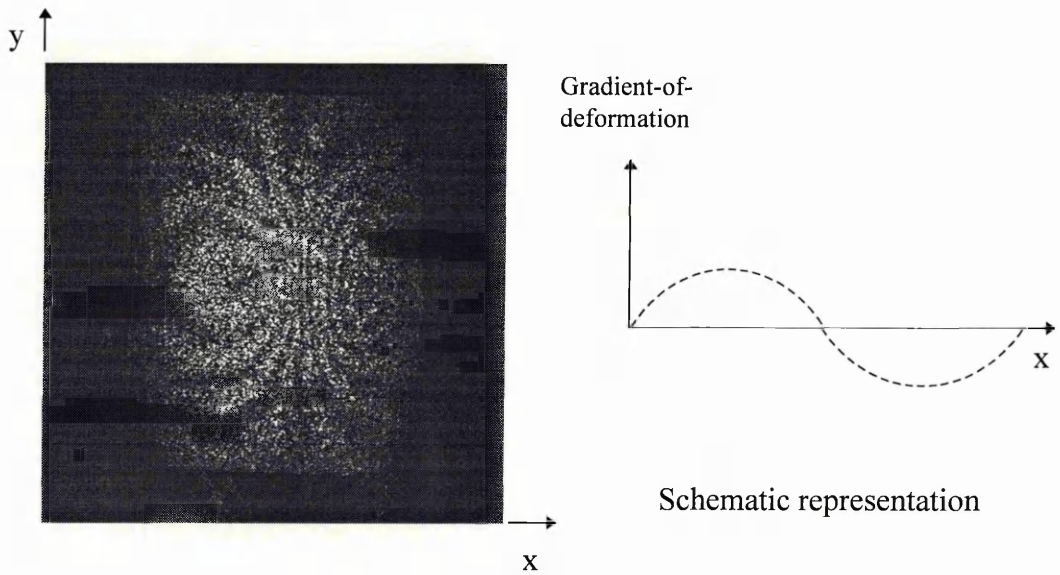

(b) Gradient-of-deformation fringes measured by shearography

Fig. 1.3 Comparison of fringes measured by shearography and ESPI in nondestructive testing (the test object is a composite carbon fibre coupon mechanically loaded at the centre of the back surface and clamped around the edges)

This thesis describes the implementation of enhanced signal processing techniques in electronic speckle shearing interferometry using laser diode wavelength modulation, including two-wavelength slope measurement, phase stepping in deformation measurement, and heterodyning and stroboscopic illumination in vibration analysis. The theory that verify these techniques is derived and experimental results are presented and discussed. Since electronic shearography is considered as part of electronic speckle pattern interferometry (ESPI) and its operation is similar to ESPI, comparisons of theory and experimental results of shearography and out-of-plane sensitive ESPI systems using similar techniques are also presented.

In chapter 2, the basic principles of ESPI and shearography are introduced, including the characteristics of laser speckle, various optical configurations for measurement of different sensitivity directions (e.g., out-of-plane, in-plane, speckle shearing), and electronic signal processing techniques that generate correlation fringes. Phase measurement techniques commonly used in the analysis of speckle fringes, e.g. temporal phase stepping techniques are also discussed.

The principles and operations of components and devices used in ESPI and electronic shearography systems, e.g. laser diodes, optical fibres, CCD cameras, and frame grabbers, are presented in chapter 3. The experimental set-ups for electronic shearography and existing ESPI systems utilised in this work are described.

At the end of chapter 3, we describe the program that has been written for this work, which integrates the electronic shearography and ESPI systems in a PC. The program, which has facilitated most of the functions needed, e.g. real time image subtraction, phase stepping and dithering, laser diode modulation and image input/output etc., has been a useful tool and is specific to the frame grabber that we used.

In chapter 4, slope measurement using an electronic shearography system is presented. It contains a review of full field optical methods in shape and slope measurements and discusses the characteristics of each technique. Two-wavelength contouring is a well

established technique in holographic and speckle interferometry, but the similar technique has not been reported for slope measurement in a shearography system before. The theory of this technique is described and measurements of conical, cylindrical, and spherical test objects are presented. Comparisons of experimental results with theoretical data are demonstrated to be in good agreement. This technique offers the advantage of being completely mechanically passive, non-contact and real-time compared to other slope measurement techniques in shearography.

In chapter 5, a novel phase stepping technique in shearography using laser diode injection current modulation is presented. To implement phase stepping using laser diode wavelength modulation, a path length imbalance in the interferometer is necessary for generating the phase difference between the two image-sheared wavefronts. This causes problems of different magnification and focal distances of the two images. These problems have been overcome by inserting a glass block into one arm of the interferometer, which also helps to increase the path length imbalance and is beneficial to this technique.

Heterodyning and stroboscopic illumination methods for vibration measurements, in electronic shearography, using laser diode wavelength modulation are presented in chapter 6. Techniques in vibration measurements using ESPI are reviewed in the beginning of this chapter. As in ESPI, the heterodyning technique is utilised to obtain phases and gradients of vibration amplitude from the fringe patterns generated in shearography. To implement this technique using laser diode wavelength modulation, the same optical configuration as in the phase stepping experiment was used and proved to work successfully. Heterodyning has been achieved in a mechanical passive manner in contrast to modulating the mirror mounted on a piezoelectric transducer. To improve fringe visibility and implement quantitative analysis of vibration fringes, stroboscopic illumination is performed by pulsing the laser diode to illuminate the vibrating object and synchronise with the peak of the vibration motion. The experimental results are presented and discussed.

In chapter 7, the work and contributions of this thesis are summarised. Future work such as the measurement of in-plane strain using shearography, simultaneously three-dimensional strain measurement using multi-wavelength shearography, and the separation of two sinusoidal vibration modes using stroboscopic illumination etc., is also discussed.

References

1.1 Leendertz, J. A. & Butters, J. N., An image-shearing speckle pattern interferometer for measuring bending moments. *J. Phys. E: Sci. Instrum.*, **6** (1973) 1107-10.

1.2 Takezaki, J. and Hung, Y. Y., Direct measurement of flexural strains in plates by shearography. *J. appl. Mechanics*, **53** (1986) 125-129.

1.3 Templeton, D. W. and Hung, Y. Y., Shearographic fringe carrier method for data reduction computerisation. *Opt. Eng.*, **28** (1989) 30-34.

1.4 Toyooka, S., Nishida, H. and Takezaki, J., Automatic analysis of holographic and shearographic fringes to measure flexural strains in plates. *Opt. Eng.*, **28** (1989) 55-60.

1.5 Hung, Y. Y., Shearography: New optical method for strain measurement and nondestructive testing. *Opt. Eng.*, **21** (1982) 391-395.

1.6 Hung, Y. Y., Shearography versus holography in nondestructive evaluation. *Proc. Soc. Photo-Opt. Instrum. Eng.*, **604** (1986) 18-29.

1.7 Ettemeyer, A., New techniques for nondestructive testing of piping systems in nuclear power plants. *Nuclear Eng. and design* **139** (1993) 183-185.

1.8 Maji, A. K., Satapthi, D. and Zawaydeh, S., Electronic shearography for inspecting steel bridges: a feasibility study. *SPIE*, Vol. 2004 (1993) 224-233.

1.9 Hung, Y. Y. and Long, K. W., Evaluation of residual stresses in concrete structures by digital shearography. *SPIE*, Vol. 2004 (1993) 27-33.

1.10 Shearographic inspection of a Boeing 737. *US Dept. of Transportation report no.* DOT/FAA/ CT-TN92/19 (1992).

1.11 Inspection of fabricated fuselage panels using electronic shearography. *US Dept. of Transportation report no.* DOT/FAA/ CT-TN92/26 (1992).

1.12 Hansche, B. D., Emerging nondestructive inspection for ageing aircraft. *US Dept. of Transportation report no.* DOT/FAA/ CT-TN94/11 (1994) chap. 6.

2. ELECTRONIC SPECKLE PATTERN INTERFEROMETRY

2.1 Introduction

The existence of speckle noise in holographic interferometry was originally considered as an annoyance which reduces the fringe quality. However, it was soon realised that speckle patterns are information carriers on an object surface. Measurement techniques in experimental mechanics based on speckle characteristics were then developed, which include speckle photography [2.1], speckle interferometry [2.2], and speckle correlation [2.3]. Speckle interferometry is one of these techniques which was developed from the basic principle of holographic interferometry. It can be used for the full-field measurement of static and dynamic surface displacement [2.2,2.4] without the need to record high resolution holograms. The replacement of photographic films for image recording by TV cameras in speckle interferometry facilitated the development of electronic speckle pattern interferometry (ESPI) [2.5-2.7]. The advantages of non-film processing, real time image display and nowadays directly digital image analysis capability initialised a specific research area which has been explored during the past two decades.

ESPI technique was first developed almost at the same time by three different groups [2.5-2.7]. Butters and Leendertz [2.5] at Loughborough University considered it as an extension of speckle interferometry, while Macovski et al [2.6] at Stanford University and Schwomma [2.7] at an Austrian company developed their systems from the holographic interferometry point of view. For more than two decade's development, there has been a considerable amount of research and publications in this field, and several commercial systems are now available [2.8-2.12]. In the past ten years, the rapid progress of new technology implemented in ESPI systems, e.g. semiconductor lasers, fibre optics and phase measurement techniques, as well as the price reduction of

components, such as PC-based frame grabbers, CCD cameras and personal computers, have increased the potential of using ESPI systems in more engineering applications. Three years after the publication of speckle interferometry, another interferometric speckle technique for the direct measurement of the derivatives of surface displacements was developed independently by Leendertz and Butters at Loughborough University [2.13] and Hung and Taylor [2.14]. The principle of this technique is similar to that of speckle interferometry, except that the two interfering wavefronts are reflected from the same object and laterally sheared with respect to each other. The technique was commonly called speckle shearing interferometry, or shearography. The recording of shearographic fringes using TV cameras instead of using photographic films was reported a few years afterwards [2.15].

The following sections of this chapter describe the basic principles of ESPI and shearography. At first, the characteristics of laser speckle are introduced. In ESPI, components of surface displacement can be measured independently by various optical configurations, which are discussed. Different electronic signal processing techniques that generate correlation fringes are then introduced. Speckle shearing interferometry is described in a separate section. Finally, phase measurement techniques commonly used in the analysis of speckle fringes are discussed. A detailed description of the statistical properties of laser speckle [2.16], ESPI [2.17-2.19], shearography [2.20,2.21], fringe analysis [2.22] and speckle techniques [2.23] can be found in the literature.

2.2 Laser speckle

Laser speckle is the grainy appearance observed when coherent laser light is reflected from an optically rough surface or transmits through a medium with random refractive index variations. Here, a surface is defined as optically rough when its surface roughness is in the order of, or greater than, the wavelength of light.

When laser light is reflected from such a surface, any distant point in front of the surface consists of many coherent wavefronts, each arising from a different microscopic element of the surface. The distances travelled by these wavefronts may differ from zero to many wavelengths depending on surface roughness and the geometry of the surface. Interference of the dephased but coherent wavefronts results in the granular pattern of intensity which is called "laser speckle".

Ennos described speckle patterns in two forms, objective speckle and subjective speckle [2.24,2.25], which are explained as follows.

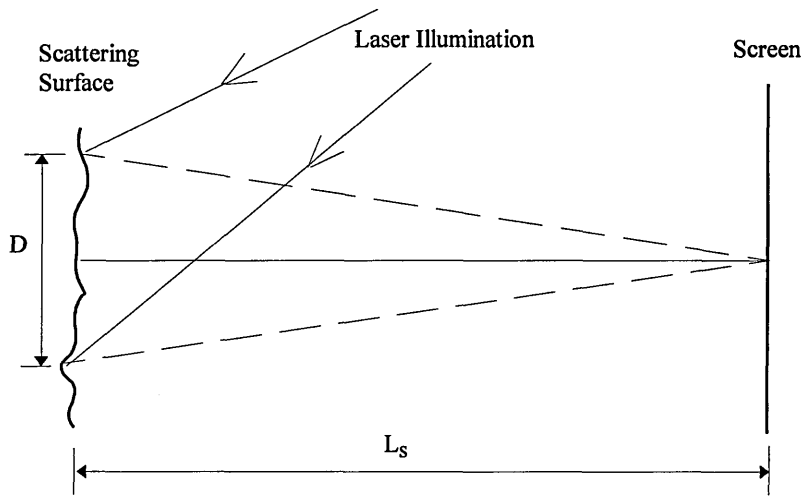

Fig. 2.1 Objective speckle observed on a flat screen

2.2.1 Objective speckle

Objective speckle is formed in front of an optically rough surface when it is illuminated by coherent light. A flat screen held at a distance from the scattering surface will have a speckle pattern projected on it, Fig. 2.1. The intensity structure of the speckle pattern depends on whether the speckles are fully developed or not. A fully developed speckle

is obtained when all the waves contributing to this speckle are coherent, which implies that the surface does not depolarise these waves. The probability density function of the intensity of a fully developed speckle is governed by a negative exponential relationship and expressed as [2.25]

$$P(I) = \frac{1}{\langle I \rangle} \exp\left(-\frac{I}{\langle I \rangle}\right) \tag{2.1}$$

where <I> is the average intensity of the speckle pattern. The most probable intensity of a fully developed speckle is zero, i.e. there are more completely dark speckles than those of any other intensity.

The size of the speckle is defined as the statistical average of the distance between adjacent regions of maximum and minimum brightness [2.24]. As shown in Fig 2.1, when the illuminated area of the object has a diameter D, the distance from the scattering surface to the observation screen is L_S, and the wavelength of light is λ, the average diameter (d_{obj}) of the speckle is given by the radius of the Airy disc and can be expressed as

$$d_{obj} \approx 1.22 \frac{\lambda L_S}{D} \tag{2.2}$$

From the above equation, as the illuminated area on the object gets smaller and the distance to the viewing plane increases, the observed speckles become larger. A similar expression to equation (2.2) was also derived by Goodman from the auto-correlation function of the intensity of the speckle field [2.16].

2.2.2 Subjective speckle

When an optically rough surface is illuminated by coherent light and imaged through a lens onto an image plane, as shown in Fig. 2.2, the speckle pattern on the image plane is termed *subjective* since the speckle pattern has been modified by the viewing system.

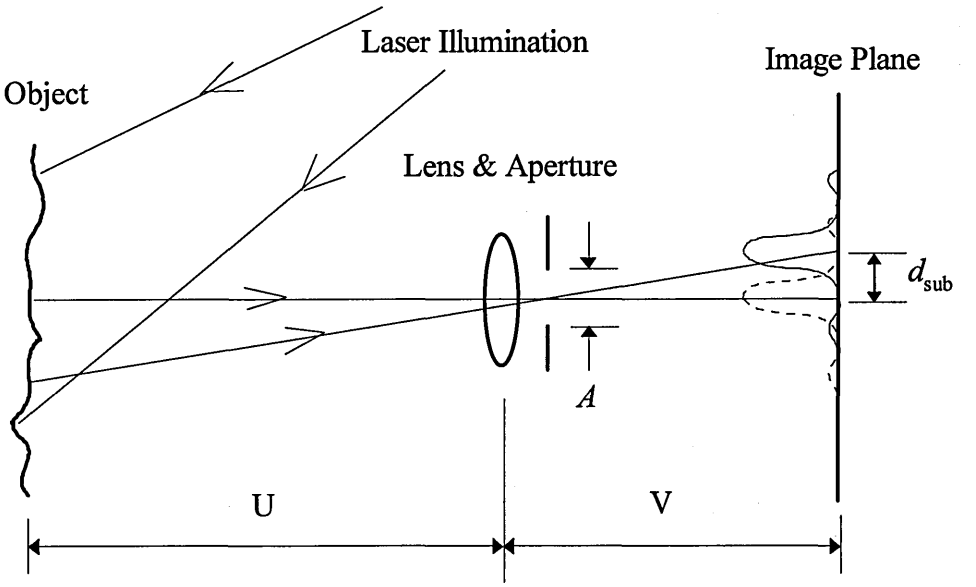

Fig 2.2 Subjective speckle observed on a image plane

The spatial distribution of subjective speckle is determined by the diffraction limit of the imaging system. The auto-correlation function for the image plane speckle intensity is expressed as [2.16]

$$R_I(r) = \langle I \rangle^2 \left[1 + \left| 2 \frac{J_1\left(\frac{\pi A r}{\lambda V}\right)}{\frac{\pi A r}{\lambda V}} \right|^2 \right] \tag{2.3}$$

where <I> is the average intensity over many speckles, A is the diameter of the viewing lens aperture, V is the distance of the lens to the image plane, r = [$(\Delta x)^2$ +

$(\Delta y)^2\ ]^{1/2}$ where Δx and Δy are defined as the distance between two adjacent speckles in x and y directions, and J_1 is the first-order Bessel function.

The speckle size d_{sub} is defined as the separation between the first two minima of the Bessel function and is given by [2.17,2.25]

$$d_{sub} = \frac{2.44\lambda V}{A} \propto (1+M)\lambda F \tag{2.4}$$

where, M is the magnification of the image and F is the lens aperture ratio (f/number). It can be seen from equation (2.4) that the size of the image speckle is dependent on the aperture of the viewing lens. The smaller the aperture being used, the bigger will be the size of the speckle observed in the image plane.

2.2.3 Speckle pattern correlation Interferometer

Speckle pattern correlation interferometry was first introduced by Leendertz in 1970 [2.2]. He showed that the intensity at a point in the speckle pattern varied cyclically for a specific movement of the object surface if the speckle field interfered with a reference beam of a certain geometry. That is, the speckles are interferometrically encoded by the addition of a reference beam. The intensity varied sinusoidally in a similar manner to a two beam interferometer. Correlation fringes were obtained by the superposition of a speckle image recorded in a negative film when the object was at rest with a speckle image recorded in a positive film when the object was displaced. The fringes obtained then represent the phase change induced by the surface displacement. This technique has been used to observe components of surface displacement coaxial to the viewing direction (out-of-plane displacement) and also perpendicular to the viewing direction (in-plane displacement) independently depending on the optical configuration used [2.2].

In ESPI, correlation fringes can be generated by subtracting or high-pass-filtering speckle images recorded by a CCD camera that resolves all or part of the speckles. The system resolution depends on the spatial resolution of the cameras and also on the speckle cut-off frequency (or the maximum spatial frequency, f_{max}) set by the aperture [2.17]

$$\frac{1}{f_{\max}} = g_{\min} \propto \frac{\lambda V}{A} \tag{2.5}$$

where g_{min} is the minimum speckle size. For a CCD camera with a pixel size of 11×11 μm^2, the minimum speckle size (g_{min}) resolvable by this camera is then 11 μm, i.e. the maximum spatial frequency $f_{max} = 9 \times 10^4\ m^{-1}$.

2.3 Optical configurations

As mentioned in the previous section, correlation of the interferometrically encoded speckle patterns before and after object deformation reveals the phase change on the object surface. However, the relationship between the optical phase change and the object deformation depends on the optical arrangement used. For speckle interferometry, in-plane and out-of-plane displacements can be detected independently, which is different from holographic interferometry and shearography. Optical configurations for the out-of-plane and in-plane measurements are described below.

2.3.1 Out-of-plane sensitive ESPI

An optical configuration for the measurement of out-of-plane displacement is a modified Michelson interferometer [2.2], of which one or both mirrors have been replaced by optical rough surfaces, as shown in Fig. 2.3. When the test object is displaced, the phase change $\Delta\phi$ is given by

$$\Delta\phi = \frac{4\pi}{\lambda} w \tag{2.6}$$

where w is the out-of-plane displacement.

An alternative arrangement for out-of-plane sensitive speckle interferometry is shown in Fig. 2.4. The surface is illuminated by a beam of laser light, the object beam, and the back scattered light is imaged by a lens onto the image plane. A reference beam from the same laser is directed to generate a pseudo on-axis mixing with the object beam. The phase change $\Delta\phi$ due to the out-of-plane displacement w is given by [2.17]

$$\Delta\phi = \frac{2\pi}{\lambda}(\underline{n}_o - \underline{n}_s)w \tag{2.7}$$

where $\underline{n}_o$ and $\underline{n}_s$ are unit vectors define the viewing and illumination directions respectively. When the viewing and illumination directions are collinear, equation (2.7) is simplified to become equation (2.6).

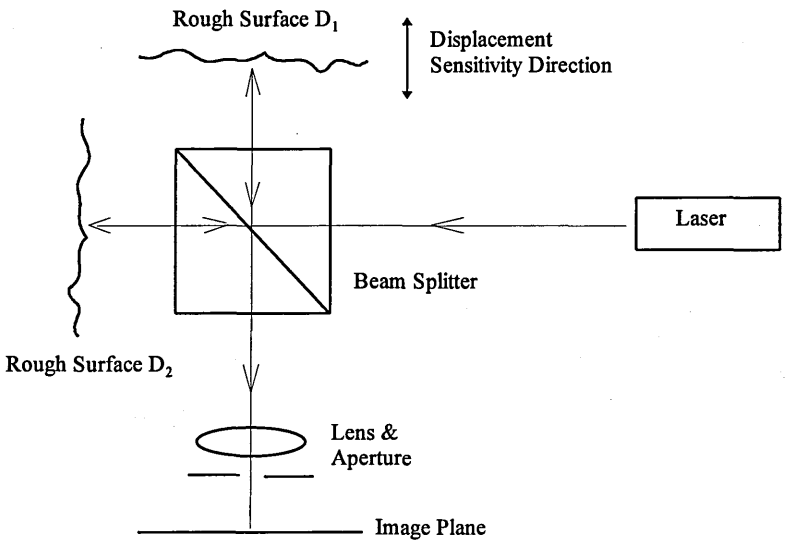

Fig. 2.3 A modified Michelson interferometer for out-of-plane speckle interferometry

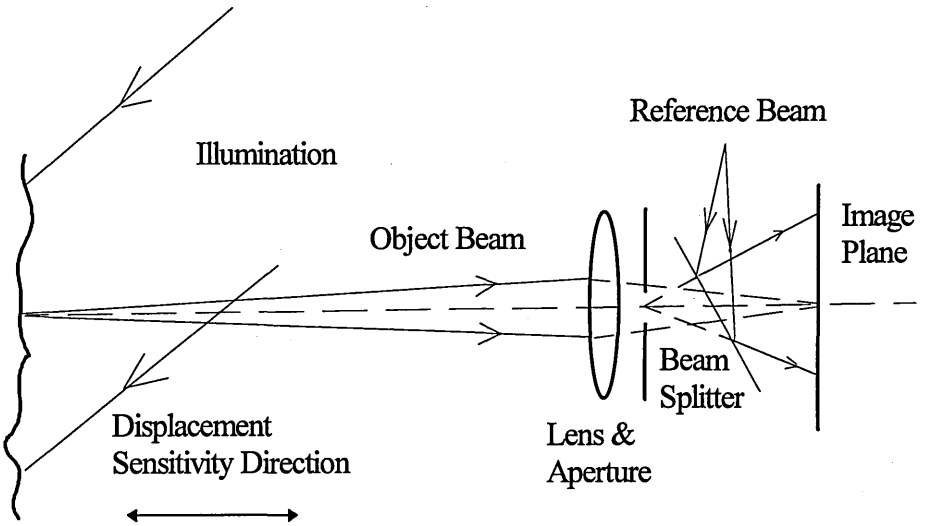

Fig. 2.4 A speckle interferometer with a smooth, in-line reference beam

2.3.2 In-plane sensitive ESPI

The optical configuration for the measurement of in-plane displacement is shown in Fig 2.5. The surface lying in the xy plane is illuminated by two collimated beams inclined at equal but opposite angles, θ, with respect to the x axis. The phase change $\Delta\phi$ due to the in-plane displacement d is given by [2.26]

$$\Delta\phi = \frac{4\pi}{\lambda} u \cos\theta \tag{2.8}$$

where u is the x component of surface displacement. If the two collimated beams have been rotated 90° with respect to the z axis (the viewing direction), the y component of surface displacement can also be detected. The measured in-plane surface displacements can be differentiated to calculate the in-plane strain on the object surface [2.27].

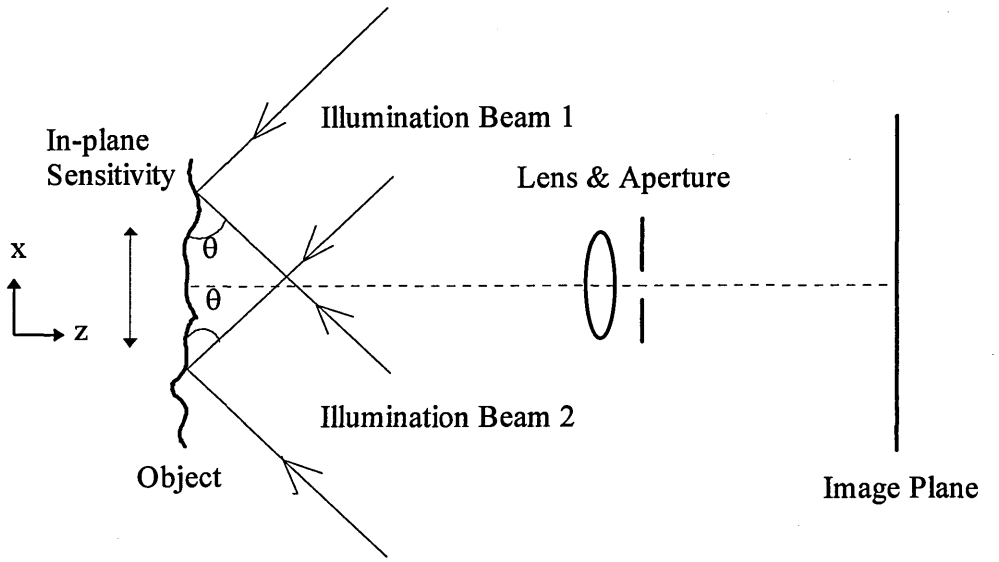

Fig. 2.5 In-plane sensitive speckle interferometry

2.4 Electronic signal processing

There are various signal processing methods for generating correlation fringes in ESPI and electronic shearography, e.g. static subtraction [2.17,2.47], high-pass filtering [2.17,2.48] and real-time image addition [2.17,2.30-2.33], sequential subtraction [2.28,2.41,2.49] and parallel processing of phase stepped images [2.35,2.36]. To explain how they work, we will use an out-of-plane ESPI system as an example. *For simplicity, the object and the reference beams are assumed to be of the same polarisation state and perfectly coherent through this thesis unless other conditions are specified.*

2.4.1 Static subtraction

Static subtraction is commonly used in the measurements of static deformation, slowly varying deformation, and contouring [2.17]. In this processing mode, one speckle image before object deformation is selected as a reference frame, and the incoming

image frames after object deformation are continuously subtracted from the reference frame.

For an out-of-plane ESPI system with a smooth reference beam, the complex amplitudes of the reference wavefronts E_r and the speckle wavefronts E_o scattered from the object surface before object deformation can be expressed as

$$E_o(\underline{r}_o) = e_o \exp i\left[\phi_o(\underline{r}_o) + \phi_s\right] \tag{2.9}$$

$$E_r = e_r \exp i\phi_r \tag{2.10}$$

where, e_r and e_o are the amplitudes of the reference and object beams, $\underline{r}_o$ is the position vector of any point on the object and ϕ_r is the phase of the reference beam. The object phase information expressed as $\phi_o(\underline{r}_o)$ is superimposed on a randomly varying speckle phase, ϕ_s , which remains constant during the small movement of the object surface. The intensity at the camera is defined by

$$I(\underline{r}_d) = \left\langle (E_o + E_r)(E_o + E_r)^* \right\rangle \tag{2.11}$$

where $\underline{r}_d$ represents a conjugate position vector of $\underline{r}_o$ in the image plane, * implies a Hermitian conjugate and < > denotes a time average. The intensity in the image plane before object deformation, I_{bef}, then becomes

$$I_{bef}(\underline{r}_d) = I_r + I_o + 2\sqrt{I_r I_o}\cos(\phi + \phi_s) \tag{2.12}$$

where, $I_r = e_r^2$ and $I_o = e_o^2$ are the intensities of the reference and object beams respectively, and $\phi = \phi_o(\underline{r}_o) - \phi_r$ is the phase difference between the object and the reference beams.

When the object is deformed, an optical phase change, $\Delta\phi$, occurs due to the surface displacement on the object. The intensity detected in the image plane, I_{aft}, becomes

$$I_{aft}(\underline{r}_d) = I_r + I_o + 2\sqrt{I_r I_o}\cos(\phi + \phi_s + \Delta\phi) \tag{2.13}$$

When the output camera signals (voltages) are proportional to the input intensities, the signals of the incoming image frames after object deformation (V_{aft}) subtracted with the signals of reference frame before object deformation (V_{bef}) are expressed as

$$V_{sub} = V_{aft} - V_{bef} \propto I_{sub} = -4\sqrt{I_r I_o}\sin(\phi + \phi_s + \Delta\phi/2)\sin(\Delta\phi/2) \tag{2.14}$$

where I_{sub} is the intensity subtraction of the two image frames. It can be seen from equation (2.14) that the subtracted signals have positive and negative values. To avoid the loss of negative signals (they are treated as zero intensity on a monitor), the subtracted signals are rectified and displayed on a TV or computer monitor. The first sinusoidal function in the equation has the speckle phase term ϕ_s in it which prevents it from producing cyclic fringes. Rectification of equation (2.14) therefore produces speckle correlation fringes modulated by the deformation phase change $\Delta\phi$. Despite the intensity variation in each pixel due to the randomly-varying speckle phase term, the bright fringes appear where $\Delta\phi = (2m+1)\pi$, and dark fringes appear where $\Delta\phi = 2m\pi$.

Although static subtraction is commonly used to measure static deformation, vibration fringes also can be generated by this processing method [2.15,2.28]. This is performed by selecting a reference frame when the object is stationary, and recording the incoming frames when the object vibrates. By this processing, the stationary areas appear to be dark fringes. To reverse these areas to become bright fringes, a π phase shift is introduced in the interferometer before recording the incoming frames [2.28].

2.4.2 High-pass filtering and real-time image addition

High-pass filtering is the earliest method to extract correlation fringes in the measurement of vibration motion [2.17,2.48]. In this method, a single image frame of time-averaged speckle pattern is first recorded. When an object is vibrating sinusoidally, the time-averaged speckle pattern is given by

$$I(\underline{r}_d) = I_r + I_o + 2\sqrt{I_r I_o}\cos(\phi + \phi_s) J_0\left[\frac{4\pi}{\lambda} a_o(\underline{r}_o)\right] \tag{2.15}$$

where $\underline{r}_o$ is the position vectors of a point on the object, $a_o(\underline{r}_o)$ is the amplitude of vibration motion, $\underline{r}_d$ represents a conjugate position vector of $\underline{r}_o$ in the image plane, and J_0 is the zero-order Bessel function of the first kind.

The image signals are high-pass filtered to remove the non-interference dc intensity and then rectified to display on a TV monitor. The resulting intensity on the monitor, I , is given by [2.17,2.29]

$$I \propto \sigma_r^2 + \sigma_o^2 + 2\langle I_r\rangle\langle I_o\rangle J_0^2\left(\frac{4\pi}{\lambda} a_o\right) \tag{2.16}$$

where σ_r^2 and σ_o^2 are the variances of I_r and I_o, $<I_r>$ and $<I_o>$ are the mean value of I_r and I_o. The first two terms in equation (2.16) are background noise and the last term, $J_0^2(4\pi a_o/\lambda)$, represents the fringes of vibration motion across the object surface.

A similar technique which combines real time image addition and high-pass filtering is also commonly used in a pulse laser ESPI system for deformation and vibration measurements [2.17,2.30-2.33]. For a two-pulse laser, the pulse timing and separation are variable. The addition of images illuminated by the two pulses enables the measurement under very unstable environments, even for the in-plane strain

measurement of high speed rotating objects [2.34]. These work is normally not applicable by using a CW (continuous wave) based ESPI system.

2.4.3 Sequential subtraction

Sequential subtraction was originally developed for the observation of vibration fringes [2.28,2.41,2.49], however it also can be used in two-wavelength contour/slope measurements.

In the method, any acquired image frame i (i =1, ...N) is stored as a reference frame and subtracted with the next incoming frame i+1. The subtracted signals are rectified and displayed. Frame i+1 then becomes the reference frame and subtracts with frame i+2, and then frame i+2 becomes the reference frame and subtracts with frame i+3 and so on.

To generate high visibility fringes in this processing mode, one arm of the interferometer needs to be modulated by a π phase shift between image frames, otherwise the subtraction of two identical speckle patterns will produce a total dark image and no fringes will be observed. For vibration measurement, the time-averaged speckle pattern is expressed as in equation (2.15). When a π phase shift is introduced between image frames, the subtracted signals are

$$I_{sub} = 4\sqrt{I_r I_o}\cos(\phi + \phi_s) J_0\left[\frac{4\pi}{\lambda} a_o(\underline{r}_o)\right] \tag{2.17}$$

By taking the absolute value of the subtracted signals (rectification), Bessel fringes with negligible dc noise are obtained. The whole process, as shown in Fig. 2.6, can be automatically processed and controlled by a PC with a frame grabber and a D/A board housed in it.

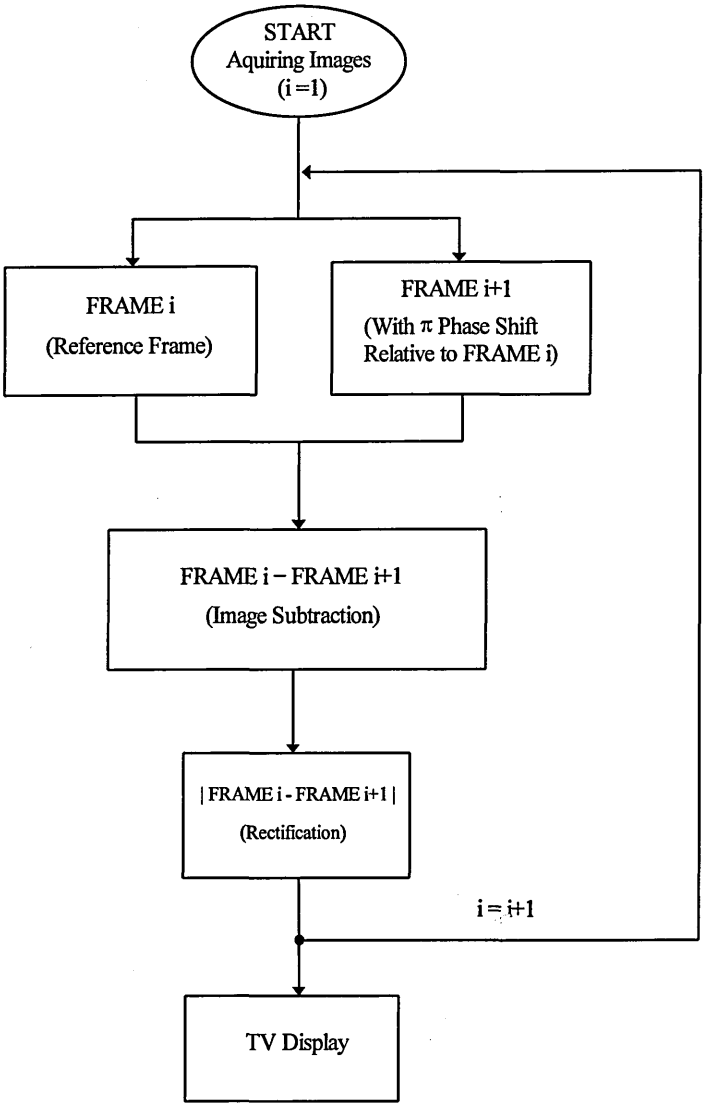

Fig. 2.6 The process of sequential subtraction

2.4.4 Parallel processing of phase stepped images

One method that uses pipeline parallel processors to process phase-stepped speckle images and generate correlation fringes in real time was reported by Stetson et al [2.35,2.36] and called " electro-optic holography (EOH) ". In this method, the phase of the reference beam is advanced by 90° between frames, and the fringe pattern is

generated from each set of four sequential TV frames by subtracting alternate frames, squaring and adding the two results.

For vibration measurement, each detected speckle pattern can be expressed as in equation (2.15). The four TV frames with 0°, 90°, 180° and 270° phase shifts then become

$$I_{E1} = I_r + I_o + 2\sqrt{I_r I_o}\cos(\phi + \phi_s) J_0\left(\frac{4\pi}{\lambda} a_o\right) \tag{2.18}$$

$$I_{E2} = I_r + I_o + 2\sqrt{I_r I_o}\sin(\phi + \phi_s) J_0\left(\frac{4\pi}{\lambda} a_o\right) \tag{2.19}$$

$$I_{E3} = I_r + I_o - 2\sqrt{I_r I_o}\cos(\phi + \phi_s) J_0\left(\frac{4\pi}{\lambda} a_o\right) \tag{2.20}$$

$$I_{E4} = I_r + I_o - 2\sqrt{I_r I_o}\sin(\phi + \phi_s) J_0\left(\frac{4\pi}{\lambda} a_o\right) \tag{2.21}$$

The following arithmetic processing is then performed:

$$(I_{E1} - I_{E3})^2 + (I_{E2} - I_{E4})^2 = 16 I_r I_o J_0\left(\frac{4\pi}{\lambda} a_o\right) \tag{2.22}$$

This produces a fringe pattern that is proportional to the reference beam intensity (essentially constant) , the image of the object, and the Bessel function of the vibration amplitude [2.36].

In static deformation measurement, four initial frames (I_{E1}, I_{E2}, I_{E3} and I_{E4} advanced by 90° phase steps) are stored before object deformation, and four corresponding frames (I_{E1}', I_{E2}', I_{E3}' and I_{E4}') are recorded after object deformation. The following arithmetic processing is then performed to generate deformation fringes [2.35]:

$$\left(I_{E1} - I_{E3} + I'_{E1} - I'_{E3}\right)^2 + \left(I_{E2} - I_{E4} + I'_{E2} - I'_{E4}\right)^2 = 32 I_r I_o \left(1 + \cos\Delta\phi\right) \quad (2.23)$$

As compared to equation (2.14) and (2.17), there is no $\cos(\phi+\phi_s)$ term in equation (2.22) and (2.23). This is the main difference between fringes generated by image subtraction and by EOH. The cosine term is actually a factor that makes pixels black when it equals zero, therefore fringe patterns with less black pixels (i.e. better fringe visibility) are obtained in this processing method [2.36].

2.4.5 Summary

Four typical electronic signal processing in ESPI have been introduced. Although each method has its own suitable application fields, some comparisons of their characteristics are listed as follows.

Image subtraction methods, either static subtraction or sequential subtraction, produce less noisy fringes than high pass filtering. There is almost no dc intensity left after image subtraction, but a certain dc intensity is residual after high pass filtering as seen in equation (2.16).

High pass filtering needs specific hardware to do the analogue processing. Normally, it is not available in commercial image grabbers.

Sequential subtraction can reduce the effect of slowly varying environmental perturbation, since the reference frame is updated in the image frame rate (25 Hz). This is especially beneficial to measurements using a fibre based ESPI system because the thermal drift effect is reduced. However, this method is not suitable for static deformation.

The method of EOH needs a parallel processor to real-time process the phase-stepped images and more digital storage boards are required to store those images and the intermediate results. The method can generates better fringes with less black pixels since the $\cos(\phi+\phi_s)$ term has been removed. However, this method is not suitable to a double pulsed ESPI system, because the current design obtains data from sequential TV frames with phase steps introduced between them. The two pulses are generally separated by a short time interval and occur within the same TV frame. The optics need to be redesigned to generate all the phase steps at once [2.35].

In this thesis, only two processing modes, static subtraction and sequential subtraction, are used for the correlation of speckle images. Practically, these two modes are enough for almost all the applications.

As described in this section, fringes in ESPI are generated by the correlation of speckle images. The intensity variation of pixels in these images is always very low because half of the dynamic range of the CCD camera is occupied by the non-interference terms (I_r and I_o), as expressed in equation (2.12). The image speckles also have a larger distribution in the lower intensity [2.25]. Normally, these image are linearly or nonlinearly enhanced, either by digital processing in the frame grabber or by analogue adjustments in a TV monitor, and then displayed.

Another concern of speckle correlation fringes is the speckle noise present in the image which reduces the quality of fringes. The smoothing of speckle fringes using different filters [2.37,2.38] and speckle averaging techniques [2.39-2.41] have been used to reduce speckle noise.

2.5 Shearography

In speckle shearing interferometry, wavefronts reflected from an object are first separated by a shearing device to become two images, one image is spatially translated with respect to the other, and the two images are then combined to interfere. The interference of the two waves gives information about the optical phase difference between two neighbouring points on the object. Correlation of the speckle pattern before object deformation with that after object deformation thus reveals gradient of surface deformation.

Various optical configurations has been reported to produce the image shear [2.13,2.15,2.20,2.42-2.47]. One of these is a Michelson interferometer arrangement [2.13] where the image shear is generated by tilting one of the mirrors as shown in Fig. 2.7. Another popular arrangement is the use of a glass wedge that covers half of a image lens [2.20], or a bi-prism in front of the whole lens [2.15] as shown in Fig. 2.8, to produces the shear. A Wollaston prism also can be used to generate the shear of two orthogonally polarised wavefronts [2.43,2.44]. Image shear generated by a Michelson arrangement placed after the image lens was recently reported [2.45]

Both the glass wedge (including bi-prism) and Michelson-interferometer arrangements are commonly used in shearography. However, the Michelson device has better sensitivity adjustment and flexibility than the other, e.g. the amount and direction of shear can be adjusted by only tilting the mirror, and phase stepping can be easily implemented by translating one of the mirrors.

In shearography, the magnitude of linear shear is normally measured by putting a reference ruler on the object. For an automatic and more precise measurement, techniques based on a reference pattern [2.50], moire effect [2.51] and digital correlation [2.52] also have been reported. The principles of shearography and comparisons of shearography with ESPI are described as follows.

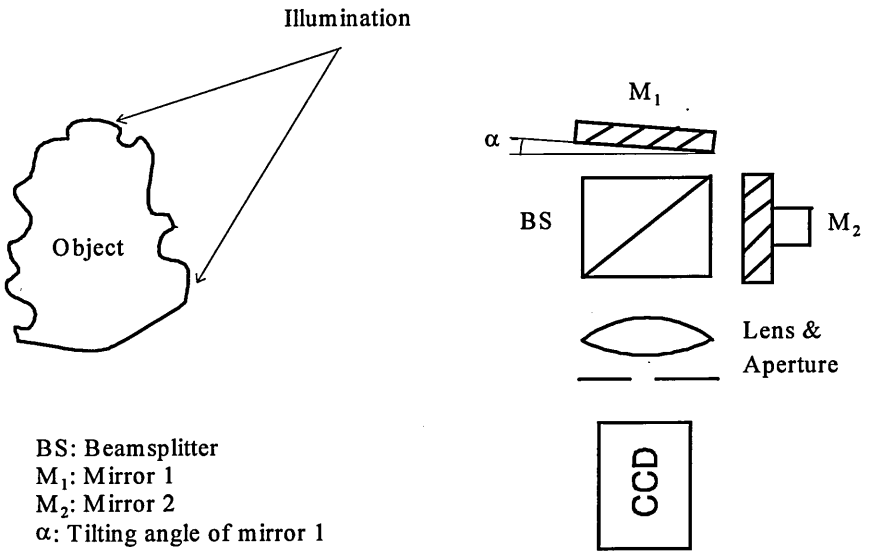

Fig. 2.7 Image shear generated by a Michelson interferometer arrangement

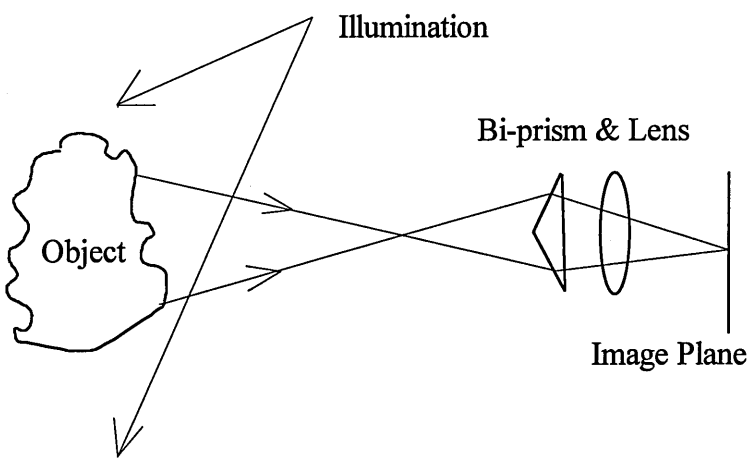

Fig. 2.8 Image shear generated by a bi-prism

2.5.1 Principles of shearography

In a shearography system, if the image shear is in the x direction by an amount δx, light reflected from a point P(x, y) on the object surface and light reflected from its neighbouring point P(x+δx, y) will be brought to interfere at the same point O(x_o, y_o) in the image plane. The wavefronts of the two sheared images can be expressed as

$$E_1(x,y) = e_1(x,y)\exp i\left[\phi_1(x,y) + \phi_{s1}\right] \tag{2.24}$$

$$E_2(x+\delta x,y) = e_2(x+\delta x,y)\exp i\left[\phi_2(x+\delta x,y) + \phi_{s2}\right] \tag{2.25}$$

where, e_1 and e_2 represent the amplitudes of the two image-sheared wavefronts, ϕ_1(x, y) and ϕ_2(x+δx, y) are phase angles of the wavefronts reflected from points P(x, y) and P(x+δx, y), and ϕ_{s1} and ϕ_{s2} are the randomly varying speckle phase terms.

The intensity at the camera is defined by

$$I(x_o,y_o) = \left\langle (E_1 + E_2)(E_1 + E_2)^* \right\rangle \tag{2.25a}$$

where (x_o, y_o) represents the conjugate position of (x, y) in the image plane, * implies a Hermitian conjugate and < > denotes a time average. The intensity in the image plane before object deformation, I_{bef}, becomes

$$I_{bef} = I_1 + I_2 + 2\sqrt{I_1 I_2}\cos(\phi + \phi_s) \tag{2.26}$$

where $I_1 = e_1^2$ and $I_2 = e_2^2$ are the intensities of the two image-sheared wavefronts respectively, $\phi = \phi_1 - \phi_2$ is the phase difference between these two beams, and $\phi_s = \phi_{s1} - \phi_{s2}$ is the difference of speckle phases.

When the object is deformed, a phase change is produced and the speckle pattern becomes

$$I_{aft} = I_1 + I_2 + 2\sqrt{I_1 I_2}\cos(\phi + \phi_s + \Delta\phi) \tag{2.27}$$

where, $\Delta\phi$ is the phase change due to the object deformation.

The subtraction of the image before object deformation from the image after object deformation is

$$I_{sub} = -4\sqrt{I_1 I_2}\sin(\phi + \phi_s + \Delta\phi/2)\sin(\Delta\phi/2) \tag{2.28}$$

The relationship between the optical phase change $\Delta\phi$ and the relative deformation on object surface has been well derived by Hung and Liang in 1979 [2.20] and is outlined below.

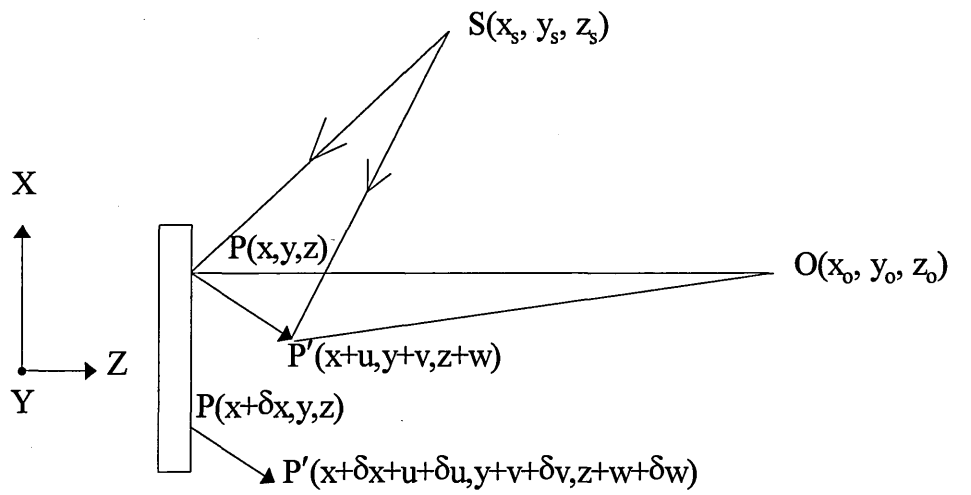

Fig. 2.9 Optical path diagram of shearography

A schematic diagram of the optical paths in shearography is shown in Fig. 2.9. The object is illuminated by a point source of laser light and the image shear is in the x

direction. An arbitrary point P(x, y, z) on the object surface is displaced to P'(x+u, y+v, z+w) after deformation. Similarly, a neighbouring point P(x+δx, y, z) which interferes with point P(x, y, z) in the image plane is displaced to P'(x+δx+u+δu, y+v+δv, z+w+δw).

The relative phase change $\Delta\phi_x$ is given by [2.20]

$$\Delta\phi_x = \frac{2\pi}{\lambda}\left(A\delta u + B\delta v + C\delta w\right) \tag{2.29}$$

where, (x_s, y_s, z_s) is the position of the point illumination, and (x_0, y_0, z_0) is the detection position and,

$$A = \left(\frac{x - x_0}{R_0} + \frac{x - x_s}{R_s}\right) \tag{2.30}$$

$$B = \left(\frac{y - y_0}{R_0} + \frac{y - y_s}{R_s}\right) \tag{2.31}$$

$$C = \left(\frac{z - z_0}{R_0} + \frac{z - z_s}{R_s}\right) \tag{2.32}$$

where, $R_o = (x_o^2 + y_o^2 + z_o^2)^{1/2}$, and $R_s = (x_s^2 + y_s^2 + z_s^2)^{1/2}$.

$\Delta\phi_x$ is a function of the relative displacements (δu, δv, δw) between point P(x, y, z) and P(x+δx, y, z). Equation (2.29) can be rewritten as

$$\Delta\phi_x = \frac{2\pi}{\lambda}\left(A\frac{\delta u}{\delta x} + B\frac{\delta v}{\delta x} + C\frac{\delta w}{\delta x}\right)\delta x \tag{2.33}$$

When the image shear is small, equation (2.33) becomes

$$\Delta\phi_x = \frac{2\pi}{\lambda}\left(A\frac{\partial u}{\partial x} + B\frac{\partial v}{\partial x} + C\frac{\partial w}{\partial x}\right)\delta x \tag{2.34}$$

Equation (2.34) reveals the relationship between the fringe phase and the gradients of surface displacements in the shearing direction. When the image shear is large, the fringes obtained just represent the relative displacements between the points on the surface separated by the distance δx, the amount of shearing.

When the image shear is in the y direction, the equation denoting phase change becomes

$$\Delta\phi_y = \frac{2\pi}{\lambda}\left(A\frac{\partial u}{\partial y} + B\frac{\partial v}{\partial y} + C\frac{\partial w}{\partial y}\right)\delta y \tag{2.35}$$

When the illumination and viewing directions are collinear, and the object size is small compared to the illumination and viewing distances (R_s and R_o), equations (2.34) and (2.35) are simplified to

$$\Delta\phi_x \cong -\frac{2\pi}{\lambda}\left[2\frac{\partial w}{\partial x}\right]\delta x \tag{2.36}$$

$$\Delta\phi_y \cong -\frac{2\pi}{\lambda}\left[2\frac{\partial w}{\partial y}\right]\delta y \tag{2.37}$$

As seen in these two equations, gradients of out-of-plane deformation can be detected directly without being effected by components of in-plane deformation.

For in-plane strain measurement, two fringe patterns recorded by different illuminating angles are required. Gradients of in-plane deformation can be calculated from the following equation (assuming the image shear is in the x direction) [2.20]

$$\frac{\partial u}{\partial x}=\left(\frac{\lambda}{2\pi}\right)\left[\frac{(1+\cos\theta_2)\Delta\phi_{x1}-(1+\cos\theta_1)\Delta\phi_{x2}}{(1+\cos\theta_1)\sin\theta_2-(1+\cos\theta_2)\sin\theta_1}\right] \tag{2.38}$$

where θ_1 and θ_2 are two different illuminating angles lying on the yz plane, and $\Delta\phi_{x1}$ and $\Delta\phi_{x2}$ are the phase changes in the fringe patterns associated with the illuminating angles θ_1 and θ_2 respectively.

In electronic shearography, the system resolution, the same as ESPI, also depends on the spatial resolution of the camera and the speckle size determined by the lens aperture setting. The fringe function in equation (2.28) is derived under the assumption that the speckle patterns before and after object deformation are perfectly correlated. Actually, speckle decorrelation occurs when the object is deformed or the phase of the illuminating wavefront is changed (e.g. generated by the wavelength change). Equations describe the shearing fringe pattern effected by speckle decorrelation was derived by Owner-Petersen [2.53]. A simplified equation describes the maximum tilt angle, γ_{max}, corresponding to the onset of complete decorrelation is given by [2.53]

$$\gamma_{\max}=\frac{A}{2U} \tag{2.39}$$

where, A is the diameter of a circular aperture, U is the distance between the object and the lens, and γ_{max} is the gradient of out-of-plane deformation in the x or y direction ($\gamma_y = \partial w/\partial x$ and $\gamma_x = \partial w/\partial y$). From this equation, as the aperture size is increased and the object distance decreased in the interferometer, the tolerance to speckle decorrelation becomes better.

2.5.2 Comparisons of ESPI and shearography

Although both ESPI and shearography are interferometric speckle techniques with the same electronic signal processing to generate correlation fringes, some of their differences are compared below and listed in Table 2.1.

Shearography, unlike smooth reference beam out-of-plane ESPI, is more similar to ESPI systems with two speckle beams, e.g. in-plane ESPI. Since the reference beam of shearography is a speckle pattern, normally the fringe visibility obtained by smooth reference beam out-of-plane ESPI is much clearer than those obtained by electronic shearography.

Correlation fringes in shearography represent the phase change due to the relative surface displacement of two neighbouring points on the object surface (or gradients of surface deformation in the shearing direction) when the object is deformed. However, fringes in ESPI represent the phase change due to the surface displacement at the same surface point.

Since the wavefronts in shearography have the same optical path before passing through the shearing device, it has much better robustness against the environment perturbation compared to ESPI, especially the tolerance to a certain rigid body displacement of the test object. However, when the image-shear increases to a certain amount, thermal effects that distort the fringe pattern might be observed since the sensitivity of the interferometer is greatly increased as well.

The optical path length difference in out-of-plane ESPI depends on the distance between the object and the detection optics. In contrast, the path length difference in shearography depends on the height variation between the image-sheared points on the object surface. This path length difference is normally negligible when the image shear is small.

System / Features	Out-of-plane ESPI (with a smooth reference beam)	In-plane ESPI	Shearography
Optical configuration	Separated two beams	Separated two beams	Common path
Fringe visibility	Good	Fair	Fair
Fringe representation	out-of-plane deformation	In-plane deformation	gradients of deformation
Mechanical stability required between object and optical system	Fair	Fair	Very good
Optical path length difference	Depends on the distance between the object and the detection optics	depends on surface height variation	depends on surface height variation
SOP adjustment	Necessary	Necessary	Not necessary
On-axis reference beam requirement	Yes	No	No

Table 2.1 The comparison of ESPI and shearography

In ESPI, the polarisation state of the reference and object beams must be kept as closely matched as possible to maintain high fringe visibility. This normally requires the use of polarisation state controllers in the reference arm. Components which are not of the same polarisation will not interfere but just raise the overall intensity level at the image sensor. Since the dynamic range of CCD cameras is restricted, this will reduce the possible modulation depth of the interference signals. In out-of-plane ESPI, an on-axis reference beam is required for the limited spatial resolution of CCD cameras. If the inclination of the reference beam with respect to the optical axis increases, the intensity variations of speckles due to the phase changes in the interferometer will be averaged within a pixel, i.e. the modulation in each pixel (or the signal-to-noise ratio) will be decreased. In electronic shearography, these two requirements are greatly released due to the common path optical configuration.

2.6 Fringe analysis

2.6.1 Introduction

Correlation fringes generated in ESPI and shearography are similar in appearance compared to conventional two-dimensional interferometric fringes, except that they appear very noisy due to the speckle effect. In ESPI, the measurement of physical quantities, e.g. deformation or shape, of object surface is actually the determination of phase variations of fringes across the object.

For qualitative analysis, the phase information can be evaluated by counting the number of fringes but without knowing the phase-changing direction unless some techniques, e.g. the fringe carrier method [2.54,2.55], have been applied. In non-destructive testing, areas of surface or subsurface defects also can be revealed through the observation of fringe distortion or concentration due to the in-homogeneous deformations or local strain concentration on the object surface.

In many spheres of engineering application , the results expressed by fringe patterns are normally not meaningful to engineers. Therefore, fringes need to be analysed so that the results can be presented in the required numerical or graphical form. Many methods have been developed for this purpose, including fringe tracking [2.56-2.58], Fourier transform [2.59-2.61], and temporal and spatial phase measurement [2.62-2.66] methods. Detailed description of these methods can be found in the literature [2.22,2.67,2.68]. A brief introduction to these methods is given below.

Fringe tracking methods

Fringe tracking is perhaps the most obvious approach to the analysis of fringe patterns. This involves identifying the fringe positions and following their track across the interferogram. Although these methods differ in detail, they usually involve the following steps [2.67]: (a) Filter the image. (b) Either fit curves to the intensity data with a view to interpolating between fringe centres or identify and track the intensity maxima and/or minima with a view to skeletonising the pattern and thereby minimising the amount of data which must subsequently be processed. (c) Number the fringe interactively or automatically. (d) Calculate the measurement parameter from the fringe pattern data.

To assign the fringe order number interactively, the operator need to have sufficient knowledge of the interferogram. In many circumstances, the ambiguity of fringe numbering can be overcome by introducing a sufficient tilt [2.54,2.55] so that the fringes become almost parallel and the fringe number can be determined from the straightness of the fringes. However, for more complicated interferograms, e.g. a fringe pattern with a gap existing between sections of the same fringe, the tilting method still can not guarantee a correct numbering [2.68].

For ESPI fringes [2.56], the speckle noise provides a great obstacle for fringe tracking, but for classical holograms the approach can be successful and is potentially the only way to analyse a fringe field when one image is available and closed fringes exist

[2.69]. In general, fringe tracking is not an automatic method for the analysis of interferograms except under highly controlled conditions.

Fourier transform (FTM) methods

In signal processing, any sequence of digitised data can be transformed into the frequency domain using a digital Fourier transform. To apply this method in fringe analysis, a high spatial carrier frequency is introduced by tilting or shifting the illumination. The desired phase information should change slowly compared to the variation introduced by the carrier frequency. The transformation of the fringe data then produces spectra in the frequency domain, of which the desired phase is separated from other frequency data, e.g. the background noise, by the carrier frequency. By isolating and translating one of the two spectra (side lobs) related to the desired phase toward the origin by the amount of carrier frequency and inverse transforming these data, the desired phase information is obtained. The phase data obtained using FTM is "wrapped" within a 2π range. A process called "phase unwrapping" is normally used to remove the phase discontinuity and integrate the phase data, which will be described later in section 2.6.3.

In ESPI, a spatial carrier fringe pattern can be obtained by subtracting the reference speckle image before object deformation, without tilting the object beam, from the speckle images after deformation, with a tilted object beam. If the frequency of the carrier is sufficiently separated from that of noise, e.g. speckle and background noise, the technique is extremely efficient at noise removal, making the identification of 2π ambiguities very easy. The disadvantage of the technique is the test object must be stable enough to allow the carrier to be applied [2.19].

Phase measurement methods

Phase measurement methods can be divided into two categories: temporal [2.62] and spatial [2.63]. In spatial phase measurement methods, all the information necessary to reduce the interferogram into a phase map is recorded simultaneously. The phase can be retrieved from one fringe pattern with a spatial carrier or from three or four, separated in space, phase shifted interferograms.

In temporal phase measurement methods, the phase data are retrieved from a number of phase shifted interferograms recorded sequentially. Many analytical algorithms have been published, including Carré, two step, three step and four step methods etc. Most of these algorithms are well summarised and described by Creath in a recent publication [2.62]. Some techniques that step the phase with a known amount between intensity measurements are called *phase stepping*. Others that integrate the intensity in each recording when the phase change is linearly ramped are called *integrating buckets*. The integrating bucket approach gives somewhat lower modulation as a result of integrating the sinusoidal intensity change over the recording period. This approach is not very suitable for ESPI fringes, since the modulation depth is already relatively low.

In this thesis, only temporal phase stepping (quasi-heterodyning) methods were used for the analysis of shearographic and ESPI fringes, since they are easier to implement and also produce accurate results. Two approaches of phase stepping methods commonly used in ESPI fringe analysis are described as follows.

2.6.2 Approaches of phase stepping method in ESPI

Temporal phase stepping is normally performed by stepping the phase of one arm of the interferometer with respect to the other, usually by moving a mirror mounted with a piezoelectric transducer. For automatic analysis of ESPI fringes using phase stepping methods, two different approaches were reported [2.64-2.66]. One approach is called

"temporal phase stepping speckle correlation" developed by Nakadate et al [2.64]. The other is called "digital phase stepping speckle interferometer" reported by Creath [2.65] and Robinson et al [6.66] respectively. To explain how they work, a three step algorithm with $2\pi/3$ steps is used as an example.

Digital phase stepping speckle interferometry (DiPSSI)

In this method, three phase-stepped speckle images before deformation are recorded which can be expressed as

$$I_{bef,k+1} = I_r + I_o + 2\sqrt{I_r I_o}\cos(\phi + \phi_s + 2k\pi/3) \qquad k = 0, 1, 2 \qquad (2.40)$$

The phase $\phi+\phi_s$ at each pixel is then calculated from the following equation [2.62] and a phase map related to the undeformed state is obtained.

$$\phi + \phi_s = \tan^{-1}\left(\sqrt{3}\cdot\frac{I_{E1} - I_{E3}}{2I_{E2} - I_{E1} - I_{E3}}\right) \qquad (2.41)$$

where, I_{E1}, I_{E2} and I_{E3} are the three step images. The object is then deformed and another three phase-stepped speckle images are recorded which can be expressed as

$$I_{aft,k+1} = I_r + I_o + 2\sqrt{I_r I_o}\cos(\phi + \phi_s + \Delta\phi + 2k\pi/3) \qquad k = 0, 1, 2 \qquad (2.42)$$

The phase $\phi+\phi_s+\Delta\phi$ at each pixel is again calculated using equation (2.41) and another phase map related to the deformation state is also obtained. Subtracting the two phase maps produces a phase fringe pattern that represent the phase change, $\Delta\phi$, induced by object deformation. The phase fringe pattern has a "saw-tooth" profile due to the nature of $\tan^{-1}$ function and the phase change varies within the range of 2π. Removing these discontinuities (phase unwrapping) gives the unambiguous information of surface displacement.

In the process of producing phase maps from speckle images, the phase at a pixel will not be accurately determined if that pixel is saturated or not sufficiently modulated. These pixels are masked to reduce the inaccuracy and displayed as a black point. The phase map is therefore "speckled" with points of unknown phase, and needs some pre-processing before phase unwrapping. Several methods have suggested to remove the masked pixels, e.g. by applying median filters [2.64], or substituting the masked pixel by a phase value determined from a set of neighbouring pixels [2.65].

Temporal phase stepping speckle correlation (TPSSC)

To perform this method, a speckle image before deformation, I_{bef}, is recorded as a reference frame. After object deformation, three phase-stepped speckle images, $I_{aft,k}$, are then recorded. The three speckle images are subtracted from the reference frame to generate three phase-stepped correlation fringes which can be expressed as

$$I_{k+1} = I_{aft,k+1} - I_{bef} = 2\sqrt{I_r I_o}\left[\cos(\phi + \phi_s + \Delta\phi + 2k\pi/3) - \cos(\phi + \phi_s)\right] \quad \text{k} = 0,1,2 \quad (2.43)$$

The speckle fringe patterns are noisy and need some pre-processing, e.g. by low pass filtering, to reduce the speckle noise before passing to the phase calculation algorithm. The phase change, $\Delta\phi$, due to object deformation is then calculated using equation (2.41).

Since the speckle fringe patterns have been pre-processed, e.g. low pass or convolution filtered, before the phase calculation, each pixel is no longer the original interferometer and consequently the measurement accuracy is reduced. For out-of-plane deformation measurement, the accuracy of using this method was evaluated as 1/13 λ [2.63], however the accuracy using DiPSSI was reported as 1/20~1/40 λ [2.64]. However, this method is still attractive, because it requires less image acquisition and processing time compared to DiPSSI. Correlation fringes produced also make the measurement more visible and predictable.

Summary

There are also different approaches of using phase stepping in ESPI. Most of them are the modification of the above two methods. One modification of TPSSC is to take several phase stepped images before deformation instead of after deformation, which is suitable for the measurement of slowly varying deformation [2.70]. Another modification of TPSSC is by taking two phase stepped images before deformation and another two after deformation [2.71]. Vikhagen has reported a max-min scanning technique based on the characteristics of temporal phase drift in the interferometer (or purposely generated by piezoelectric transducer) to calculate the phase data [2.72].

In ESPI, an existed error source, among other errors (e.g. electronics error) is speckle decorrelation, i.e. the speckle phase ϕ_s assumed as a constant after small object deformation actually changes slightly. A method of calculating the phase error was recently published [2.73].

2.6.3 Phase unwrapping

The phase data obtained by phase stepping and Fourier transform methods are wrapped phase maps, i.e. discontinuities occurs every time the phase angle changes by 2π. The wrapped phase map is normally displayed in a normalised form using a grey scale to represent phase. For each phase fringe, the intensity ranges from black representing a fringe phase of zero to intense white representing a phase of 2π, as shown in Fig. 2.10. *Phase unwrapping* is a process that can unwrap or integrate these phase discontinuities. The basic processing technique involves the counting of 2π discontinuities by line scanning, and adding 2π each time the phase angle jumps from 2π to zero or subtracting 2π if the change is from zero to 2π. Fig. 2.11 shows the difference of wrapped and unwrapped phase data.

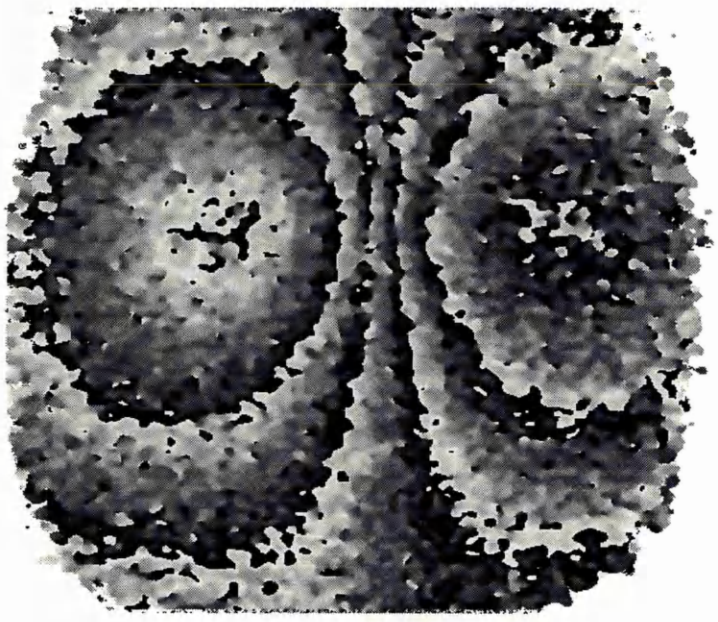

Fig. 2.10 Wrapped phase map of deformation gradient fringes measured using shearography

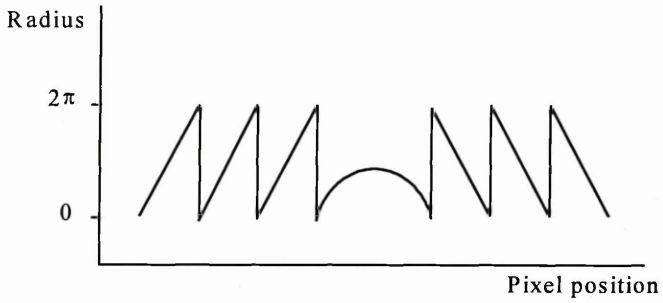

(a) Wrapped phase data

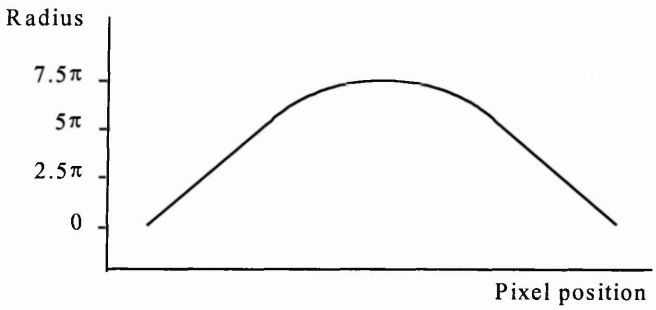

(b) Unwrapped phase data

Fig. 2.11 Schematic diagram of the phase unwrapping process

Wrapped phase maps calculated from ESPI fringes are inherently noisy and sometimes even have holes, broken fringes and masked pixels on them. The basic processing method normally can not correctly unwrap this kind of phase map. Many phase unwrapping algorithms for resolving these problems have been developed. Each algorithm varies in computing efficiency, accuracy and the ability to handle discontinuities and noisy data. These methods are well reviewed in some recent publications [2.68,2.74].

The phase unwrapping program we used was provided by Dr. P. J. Bryanston-Cross. The noise tolerant algorithm is based on minimising phase changes between pixels via minimum spanning trees [2.61,2.75-2.78]. The technique utilises the fundamental principle that adjoining areas of the phase map should produce the same unwrapped phase solution along their common boundary, unless an error is present.

In the method, the phase map is divided into square tiles. The phase data in each tile is unwrapped independently, by the path scanning technique. The phase data at the edge of adjacent tiles are then compared to ascertain the integer fringe order difference between tiles, based on the difference value that most edge pixels agree on. Tiles with large areas of low modulation or noisy pixels can be masked out and eliminated from the tile assembly process. The advantage of this approach is that a phase discontinuity is limited to a region within one tile.

When the tiles have been processed, they are arranged into order according to the confidence attached to the accuracy and consistency of the phase data. The tiles are re-assembled under a priority scheme according to a minimum spanning tree connected path, i.e. segments which seem to have solved unambiguously (the tiles with higher degree of confidence) are employed in advance of less consistent ones.

The advantage of this method is that it combines the speed of simple phase unwrapping procedures with the reliability of pixel ordering techniques. However, the choice of tile

size is very important. Optimal performance will occur when the size is chosen so that on average there are one or two fringes crossing each tile.

References

2.1 Archbold, E., Burch, J. M. and Ennos, A. E., Recording of in-plane surface displacement by double-exposure speckle photography. *Opt. Acta*, **17** (1970) 883-898.

2.2 Leendertz, J. A., Interferometric displacement measurement on scattering surfaces utilising speckle effect. *J. Phys. E: Sci. Instrum.*, **3** (1970) 214-218.

2.3 Yamaguchi, I., Real-time measurement of in-plane translation and tilt by electronic speckle correlation. *Jpn. J. Appl. Phys.*, **19** (1980) L133.

2.4 Archbold, E., Burch, J. M., Ennos, A. E., Taylor, P. A., Visual observation of surface vibration nodal patterns. *Nature*, **222** (1969) 263-265.

2.5 Butters, J. N., Leendertz, J. A., Holographic and video techniques applied to engineering measurements. *J. Meas. Control*, **4** (1971) 349-354.

2.6 Macovski, A., Ramsey, D., Schaefer, L. F., Time lapse interferometry and contouring using television systems. *Appl. Opt.*, **10** (1971) 2722-27.

2.7 Schwomma, O., German Pat. 298830 (1972); see also: Forschung und Technik, *Neuer ZÜricher Beilage,* (1975) 257.

2.8 VIDISPEC ESPI system, Ealing Electro-Optics Plc, Greycaine Road, Watford, WD2 4PW, U.K.

2.9 SD 800-ESPI system, Spectradata GmbH, Uferstrasse 74, D-2900 Oldenburg, Germany.

2.10 HC-4000 ESPI system, Newport, 4320 First Avenue, Newbury Business Park, London Road, Newbury RG 132, U.K.

2.11 RETRA TV-Holography system, Conspec As, PO Box 658, N-7001 Trondheim, Norway.

2.12 Ettemeyer Qualitatssicherung, Memminger Str. 72/207, D-89231 Neu-Ulm, Germany.

2.13 Leendertz, J. A. & Butters, J. N., An image-shearing speckle pattern interferometer for measuring bending moments. *J. Phys. E: Sci. Instrum.*, **6** (1973) 1107-10.

2.14 Hung, Y. Y., Taylor, C. E., Speckle-shearing interferometric camera - a tool for measurement of derivatives of surface displacements. *SPIE*, Vol. 41 (1973) 169-175.

2.15 Nakadate, S., Yatagai, T., Saito, H., Digital speckle-pattern shearing interferometry. *Appl. Opt.*, **19** (24) (1980) 4241-46.

2.16 Goodman, J. W., Statistical properties of laser speckle patterns. *Laser speckle and related phenomena*, ed. Dainty, J. C., Springer-Verlag, Berlin, (1975) 9-76.

2.17 Jones, R. & Wykes, C., *Holographic and Speckle Interferometry*. Cambridge University Press, Cambridge, 2nd ed., (1989).

2.18 Løkberg, O. J., Recent developments in video speckle interferometry. *Speckle metrology*, ed. Sirohi, R. S., Marcel Dekker Inc., New York, (1993) 157-193.

2.19 Davies, J. C. and Buckberry, C. H., Television holography and its applications. *Optical Methods in Engineering Metrology*, ed. Williams, D. C., Chapman & Hall, London, 1993.

2.20 Hung, Y. Y. and Liang, C. Y., Image-shearing camera for direct measurement of surface strains. *Appl. Opt.*, **18** (7) (1979) 1046-51.

2.21 Owner-Petersen, M., Digital speckle pattern shearing interferometry: limitations and prospects. *Appl. Opt.*, **30** (19) (1991) 2730-38.

2.22 Robinson, D. W. and Reid, G. T. (ed.), *Interferogram Analysis - Digital Fringe Pattern Measurement Techniques*, ed. IOP Publishing Ltd, Bristol, (1993).

2.23 Sirohi, R. S. (ed.), *Speckle metrology*. Marcel Dekker Inc., New York, (1993).

2.24 Ennos, A. E., Speckle interferometry. *Laser speckle and related phenomena*, ed. Dainty, J. C., Spriger-Verlag, Berling, (1975) 203-253.

2.25 Ennos, A. E., Speckle interferometry. *Coherent Optical Engineering*. ed. Arecchi, F. T. and Degiorgio, V., North-Holland Publishing Company, (1977) 129-149.

2.26 Denby, D. and Leendertz, J. A., Plane-surface strain examination by speckle-pattern interferometry using electronic processing. *J. Strain Analysis*, **9** (1) (1974) 17-24.

2.27 Moore, A. J. and Tyrer, J. R., Surface strain measurement with ESPI applied to fracture mechanics. *Proc. SEM, Hologram Interferometry and Speckle Metrology*, Bethel, Conn. USA, (1990) 192-198.

2.28 Creath, K. and Slettemmoen, G. A., Vibration-observation techniques for digital speckle-pattern interferometry. *J. Opt. Soc. Am.*, 2 (10) (1985) 1629-1636.

2.29 Høgmoen, K. and Pedersen, H. M., Measurement of small vibrations using electronic speckle pattern interferometry: Theory. *J. Opt. Soc. Am.*, 67 (11) (1977) 1578-83.

2.30 Spooren, R., TV-holography using a double pulsed single oscillator Nd: YAG laser; restrictions and possibilities. *Proc. SEM, Hologram Interferometry and Speckle Metrology*, Bethel, Conn. USA, (1990) 260-267.

2.31 Moore, A. J., Santoyo, F. M. and Tyrer, J. R., Algorithm for calculating phase from ESPI addition fringes. *SPIE*, Vol. 2003 (1993) 135-146.

2.32 Shellabear, M. C., Santoyo, F. M. and Tyrer, J. R., Processing of addition and subtraction fringes from pulse ESPI for study of vibrations. *Proc. SEM, Hologram Interferometry and Speckle Metrology*, Bethel, Conn. USA, (1990) 238-244.

2.33 Santoyo, F. M., Shellabear, M. C. and Tyrer, J. R., Four cases of engineering studies using pulsed ESPI. *SPIE*, Vol. 1508 (1991) 143-152.

2.34 Preater, R. W. T. and Swain, R. C., In-plane strain measurement on high speed rotating components using pulsed laser ESPI. *Proc. SEM, Hologram Interferometry and Speckle Metrology*, Bethel, Conn. USA, (1990) 288-293.

2.35 Stetson, K., An electronic system for real-time display and quantitative analysis of hologram interference fringes. *Proc. Optical Sensing and Measurement, ICALEO* '89, Vol. 70 (1989) 78-85.

2.36 Stetson, K., Brohinsky, W. R., Wahid, J. and Bushman, T., An electro-optic holography system with real-time arithmetic processing. *J. Nondestructive Evaluation*, **8** (2) (1989) 69-76.

2.37 Wykes, P. V., Smoothing of speckle and moire fringes by computer processing. *Optics. and Lasers in Eng.*, **3** (1982) 87-100.

2.38 Crennell, K. M. and Bowler, I. W., The smoothing of electronic speckle pattern interferometric images. *Optics. and Lasers in Eng.*, **7** (1986/87) 163-173.

2.39 Slettemoen, G. A., Electronic speckle pattern interferometric system based on a speckle reference beam. *Appl. Opt.*, **19** (4) (1980) 616-623.

2.40 Løkberg, O. J. and Slettemoen, G. A., Improved fringe definition by speckle averaging in ESPI. *Proc. ICO* (1984) 116-117.

2.41 Davies, J. C., Jones, J. D. C. and Pannell, C. N., Development and application of a fibre optic electronic speckle pattern interferometry. *SPIE*, Vol. 863 (1987) 194-207.

2.42 Ganesan, A. R., Sharma, D. K. and Kothiyal, M. P., Universal digital speckle shearing interferometer. *Appl. Opt.*, **27** (22) (1988) 4731-34.

2.43 Kothiyal, M. P. and Delisle, C., Shearing interferometer for phase shifting interferometry with polarisation shifter. *Appl. Opt.*, **24** (1985) 4439.

2.44 Velera, J. D. and Jones, J. D. C., Phase stepping in fibre-based speckle shearing interferometry. *Opt. Lett.*, **19** (15) (1994) 1161-63.

2.45 Mohan, N. K., Saldner, H. O. and Molin, N. E., Electronic shearography applied to static and vibrating objects. *Opt. Commun.*, **108** (1994) 197-202.

2.46 Bryanston-Cross, P. J., Chan, P. H. and Judge, T. R., Analysis of lateral shearing interferogram using 2-D DFT techniques. *One-day Meeting, Engineering applications of optical diagnostic techniques*, SME Cranfield University, 7th Dec. (1994) 1-4.

2.47 Denby, D. and Leendertz, J. A., Plane-surface strain examination by speckle-pattern interferometry using electronic processing. *J. Strain Analysis*, **9** (1) (1974) 17-25.

2.48 Løkberg, O. J., Electronic speckle pattern interferometry. *Phys. Technol.*, **11** (1980) 16-22.

2.49 Moran, S. E., Law R. L., Craig, P. N. and Goldberg, W. M., Optically phase-locked electronic speckle pattern interferometer. *Appl. Opt.*, **26** (1986) 475-491.

2.50 Ng, T. W. and Chau, F. S., Automated linear shear measurements in digital shearing speckle interferometry. *Opt. Eng.*, **33** (5) (1994) 1728-29.

2.51 Ng, T. W. and Chau, F. S., Moire technique for linear shear measurement in photographic speckle shearing interferometry. *Opt. Eng.*, **33** (5) (1994) 1726-27

2.52 Ng, T. W., Shear measurement in digital speckle shearing interferometry using digital correlation. *Opt. Commun.*, **115** (1995) 241-244.

2.53 Owner-Petersen, M., Digital speckle pattern shearing interferometry (DSPSI): limitations and prospects. *Proc. SEM, Hologram Interferometry and Speckle Metrology*, Bethel, Conn. USA, (1990) 150-157.

2.54 Yatagai, T., Nakadate, S., Idesawa, M. and Saito, H., Automatic fringe analysis using digital image processing techniques. *Opt. Eng.*, **21** (1982) 432-5.

2.55 Hung, Y. Y., Hovanesian, J. D. and Takezaki, J., A fringe carrier technique for unambiquous determination of fringe orders in shearography. *Optics. and Lasers in Eng.*, **8** (1988) 73-81.

2.56 Button, B. L., Cutts, J., Dobbins, B. N., Moxon, C. J. and Wykes, C., The identification of fringe positions in speckle patterns. *Opt. and Laser Technol.*, **17** (1985) 189-192.

2.57 Funnell, W. R. J., Image processing applied to the interactive analysis of interferometric fringes. *Appl. Opt.*, **20** (1981) 3245-49.

2.58 Nakadate, S., Yatagai, T. and Saito, H., Computer aided speckle pattern interferometry. *Appl. Opt.*, **22** (1983) 237-243.

2.59 Takeda, M., Ina, H. and Kobayashi, S., Fourier-transform method of fringe-pattern analysis for computer-based topography and interferometry. *J. Opt. Soc. Am.*, **72** (1981) 156-160.

2.60 Kujawinska, M. and Wojciak, J., High accuracy Fourier transform fringe pattern analysis. *Appl. Opt. digest*, 17th-20th Sep. (1990) 257-258.

2.61 Judge, T. R., Quan, C. and Bryanston-Cross, P. J., Holographic deformation measurements by Fourier transform technique with automatic phase unwrapping. *Opt. Eng.*, **31** (3) (1992) 533-543.

2.62 Creath, K., Temporal Phase Measurement Methods. *Interferogram Analysis - Digital Fringe Pattern Measurement Techniques*, ed. Robinson, D. W. and Reid, G. T., IOP Publishing Ltd, Bristol, (1993) 94-140.

2.63 Kujawinska, M., Spatial phase measurement methods. *Interferogram Analysis - Digital Fringe Pattern Measurement Techniques*, ed. Robinson, D. W. and Reid, G. T., IOP Publishing Ltd, Bristol, (1993) 141-193.

2.64 Nakadate, S. and Saito, H., Fringe scanning speckle-pattern interferometry. *Appl. Opt.*, **24** (14) (1985) 2172-2180.

2.65 Creath, K., Phase-shifting speckle interferometry. *Appl. Opt.*, **24** (18) (1985) 3053-58.

2.66 Robinson, D. W. and Williams, D. C., Digital phase stepping speckle interferometry. *Opt. Commun.*, **57** (1) (1986) 26-30.

2.67 Reid, G. T., Automatic fringe pattern analysis: a review. *Optics. and Lasers in Eng.*, **7** (1986/7) 37-68.

2.68 Judge, T. R. and Bryanston-Cross, P. J., A review of phase unwrapping techniques in fringe analysis. *Optics. and Lasers in Eng.*, **21** (1994) 199-239.

2.69 Hunter, J. C., Assessment of some image-enhancement routines for use with an automatic fringe tracking program. *SPIE*, Vol. 1163 (1989) 83-94.

2.70 Kujawinska, M, Spik, A. and Robinson, D. W., Analysis of ESPI interferograms by phase stepping techniques. *FASIG* (1989).

2.71 Owner-Petersen, M. and Jensen, P. D., Computer-aided electronic speckle pattern interferometry (ESPI): Deformation analysis by fringe manipulation. *NDT International*, **21** (6) (1988) 422-426.

2.72 Vikhagen, E., Vibration measurement using phase shifting TV-holography and digital image processing. *Opt. Commun.*, **69** (1989) 214-218.

2.73 Huntley, J. M., Random phase measurement errors in digital speckle pattern interferometry. *SPIE*, Vol. 2544 (1995) 246-257.

2.74 Robinson, D. W., Phase unwrapping methods. *Interferogram Analysis - Digital Fringe Pattern Measurement Techniques*, ed. Robinson, D. W. and Reid, G. T., IOP Publishing Ltd, Bristol, (1993) 194-229.

2.75 Towers, D. P., Judge, T. R. and Bryanston-Cross, P. J., A quasi-heterodyne holographic technique and automatic algorithms for phase unwrapping. *SPIE*, Vol. 1163, 1989.

2.76 Towers, D. P., Judge, T. R. and Bryanston-Cross, P. J., Analysis of holographic fringe data using the dual reference approach. *Opt. Eng.*, **30** (4) (1991) 452-460.

2.77 Towers, D. P., Judge, T. R. and Bryanston-Cross, P. J., Automatic Interferogram Analysis Techniques Applied to Quasi Heterodyne Holography and ESPI. *Optics and Lasers in Eng.*, **14** (1991) 239-282.

2.78 Ettemeyer, A., Neupert, U., Rottenkolber, H. and Winter, Schnelle und robuste bildanalyse von streifenmustern–ein wichtiger schritt der automation von holografischen profprozessen. *Proc. 1st Int. Workshop on Automatic Processing of Fringe Patterns*, (1989) 23-31.

3. COMPONENTS AND SYSTEM DESCRIPTION

This chapter presents the basic principles and operations of components and devices used in electronic shearography and ESPI systems. The experimental set-ups of electronic shearography and existing ESPI systems utilised in this work are introduced. At the end of this chapter, the written program which integrate the electronic shearography and ESPI systems in a PC is described.

3.1 Optoelectronic components

The fundamental components of ESPI and electronic shearography include laser sources, optical components (e.g. beamsplitters, mirrors, optical fibres, and zoom lens etc.), CCD cameras, and frame grabbers. In this section, laser diodes [3.1-3.3], optical fibres [3.3], CCD cameras [3.4-3.6] and frame grabbers [3.7,3.8] are introduced. Detailed description of these devices can be found in the literature.

3.1.1 Laser diodes

Since ESPI and shearographic fringes are generated from the correlation of interferometrically encoded speckle images (interferograms), the coherence of the light source is an important consideration for the implementation of ESPI. In the past, He-Ne lasers were commonly used in ESPI systems. However, the limitation of optical power output and coherence length of He-Ne lasers restricts the application range of these systems.

Laser diodes, as cheap and reliable light sources, have replaced gas lasers in many interferometric systems. These lasers are very compact and require only relatively low

voltages (~15V) as compared with voltages (~ kV) required to power gas lasers. In addition, they are compatible with optical fibres, i.e. optical fibres can be permanently mounted (pigtailed) with the laser. The coherence length of laser diodes can be several meters which is especially suitable for interferometric measurements with a large optical path-length difference. The tunability of laser diode emission wavelengths, either by changing the injection current or junction temperature, is a useful property which has been used to implement many enhanced signal processing techniques in ESPI and electronic shearography (these will be described in chapters 4 ~ 6). Some important operating characteristics of laser diodes are described below.

One characteristic of laser diodes is their elliptical and rapidly divergent output beam profile. This arises because the diode cross-sectional emitting area (aperture) is typically of the order less than 1 μm × a few micrometers. The light output is seriously diffracted by this aperture, especially across the narrow stripe width direction. Generally, the divergent beam can be collimated using a microscope objective lens or specially designed micro lens located close to the diode emitting facet, and the ellipticity can be adjusted using an anamorphic prism pair.

The nature of the diode cavity is to produce operation in the TEM_{00} mode, and in general the output is plane polarised parallel to the plane of the junction. Laser diodes can operate on a single longitudinal mode or on multiple modes. When the operating current is tuned to just above threshold, the output will contain several longitudinal modes. As the current is increased, a single mode starts to dominate and extracts most of the available gain.

At the moment, the output power for single stripe diode devices is limited to approximately 200 mW. This limit is imposed by the heat dissipation, since the small dimensions of the active area produce very high intensities (power per unit area). Overheating can cause melting of the facet, or can make dislocations in the material mobile initiating crack propagating through the active area and resulting in catastrophic damage.

The dependence of the laser output power upon the injection current is shown schematically in Fig. 3.1. The start of laser action at the threshold current density is detected by an abrupt increase in the radiance of the emitting region. When the injection current is below threshold, the output is due to spontaneous emission, and the diode acts as an LED.

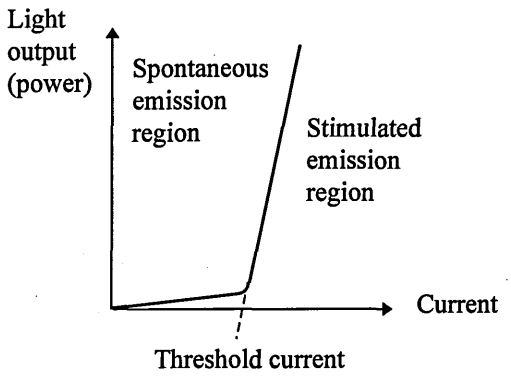

Fig. 3.1 Light output versus current variation of an ideal laser diode

The output wavelength of laser diodes is a sensitive function of temperature because the energy gap of the semiconductor and the refractive index of the cavity are both dependent on temperature. The change in wavelength is typically 0.3 nm/°C. Temperature stabilisation is therefore necessary for a stable operating wavelength. The wavelength also can be modulated via the injection current [3.10-3.12], due to the dependence of the laser temperature on injection current. The magnitude of this dependence is typically 0.05 K/mA. The current also controls the charge carrier concentration, and consequently affects the cavity refractive index. Equations for the modulation of the laser diode wavelength are described below [3.9]. The laser cavity condition can be expressed as [3.9]

$$\lambda = \frac{2nL}{m} \tag{3.1}$$

where n is the refractive index, L is the cavity length and m is an integer. When the injection current varies linearly with time t, as $\Delta i = \alpha t$, the wavelength changes slightly by $\Delta\lambda$, expressed as

$$\Delta\lambda = \beta\Delta i = \beta \cdot \alpha \cdot t \tag{3.2}$$

where Δi is the change of injection current, and α and β are proportionality constants. When the injection current is modulated slightly, a small amount of temperature change ΔT_m takes place and is given by

$$\Delta T_m = R\Delta i \tag{3.3}$$

where R is the thermal resistance. The wavelength change $\Delta\lambda$ is derived from the differentiation of equation (3.1) and becomes

$$\Delta\lambda = \frac{2}{m}\left(L\frac{\partial n}{\partial T_m} + n\frac{\partial L}{\partial T_m}\right)\Delta T_m \tag{3.4}$$

Since the cavity length change is negligibly small compared with that of the refractive index change, equation (3.4) reduces to

$$\Delta\lambda = \frac{2}{m} \cdot L \cdot \frac{\partial n}{\partial T_m} \cdot \Delta T_m \tag{3.5}$$

Substituting ΔT_m as expressed in equation (3.3) and m in equation (3.1) into equation (3.5) results in

$$\Delta\lambda = \frac{\lambda}{n} \cdot \frac{\partial n}{\partial T_m} \cdot R \cdot \Delta i \tag{3.6}$$

By equating equations (3.6) and (3.2), the proportional constant β can be calculated from the refractive index, refractive index differential and the thermal resistance. For example, for $\lambda = 780$ nm, n = 3.5, $\partial n/\partial T_m = 10^{-3}$/°C and R = 25 °C/A [3.9], then

$$\beta = \frac{\lambda}{n} \cdot \frac{\partial n}{\partial T_m} \cdot R = 6 \times 10^{-3} (nm/mA) \tag{3.7}$$

Frequency modulation of laser diodes through the change of injection current has been widely used for signal processing in many interferometric applications [3.9,3.13,3.14]. However, large current modulation, e.g. down to the threshold, of a single longitudinal mode laser diode also can cause a dynamic shift of the peak wavelength emitted from the device [3.15]. The phenomenon, which results in dynamic linewidth broadening, is referred to as frequency chirping. It arises from the gain-induced variations in the laser refractive index due to the strong coupling between the free carrier density and the index of refraction which is present in any semiconductor structure [3.3]. Hence, even small changes in carrier density result in a phase shift of the optical field, giving an associated change in the resonance frequency within the laser structures.

Several techniques have been developed to reduce frequency chirping. One approach is to bias the laser sufficiently above threshold so that the modulation current does not drive below the threshold where the rate of change of optical output power varies rapidly with time. Unfortunately, this strategy also gives a poor extinction ratio at the output. Another method involves the damping of the relaxation oscillations that can occur at turn-on and turn-off states which result in large power fluctuations. This has been achieved, for instance, by shaping the electrical drive pulses [3.16,3.17]. The injection current pulse can be conditioned by a high pass filter, e.g. a pulse shaping circuit, that compensates for the laser diode thermal time-constants, hence providing a stable wavelength during the period of the pulse [3.17].

The linewidth of a single frequency laser diode is typically 30 MHz, limited by the phase noise induced by fluctuations in the current supply and temperature control.

Optical feedback from unwanted external reflections can also seriously degrade the linewidth of the laser output [3.2,3.18]. This is a major problem when these devices are used with optical fibres. Therefore, an optical isolator, which use Faraday effect to isolate the back reflection, may be required to provide reliable singlemode operation. An alternative and less expensive technique of reducing back-reflections is to cleave or polish the fibre ends at an angle of ~ 8° [3.19].

Mode hopping is another specific characteristic of all single-mode laser diodes. The phenomenon is a consequence of increases in temperature of the device junction. The transition (hopping) from one mode to another is not a continuous function of the drive current but occurs suddenly over only 1 to 2 mA. Mode hopping alters the light output against current characteristics of the laser, and is responsible for the kinks observed in the characteristics of many single-mode devices. A schematic diagram of laser diode spectrum representing the combined effect of wavelength modulation and mode hopping is shown in Fig. 3.1-1. Stabilisation against mode hopping and mode shift may be obtained with adequate heat sinking or thermoelectric cooling. However, at constant heat sink temperature, shifts due to thermal increases can only be fully controlled by the use of feedback from external or internal grating structures [3.3].

3.1.2 Optical fibres

In recent years, single mode optical fibres are increasingly used in interferometric applications. They provide a means of steering coherent wavefronts around complex optical paths whilst retaining the smooth phase and intensity distribution. In out-of-plane ESPI, a reference beam with a high degree of spatial coherence is required to obtain good quality fringes. Single-mode optical fibres with a typical core diameter of a few μm, acting as a very good spatial filter that provides a uniform illumination profile, just fulfils this requirement.

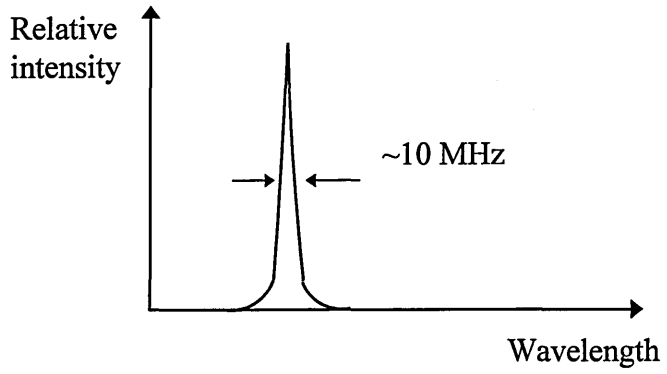

(a) The spectrum of a single longitudinal mode laser diode

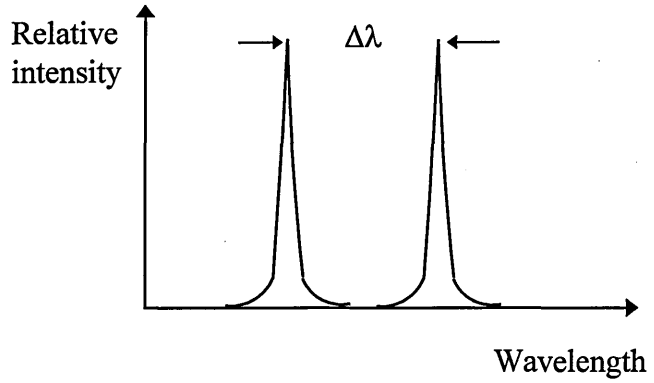

(b) The spectrum of the single mode diode injection current modulated to produce two sequential wavelengths separated by $\Delta\lambda$

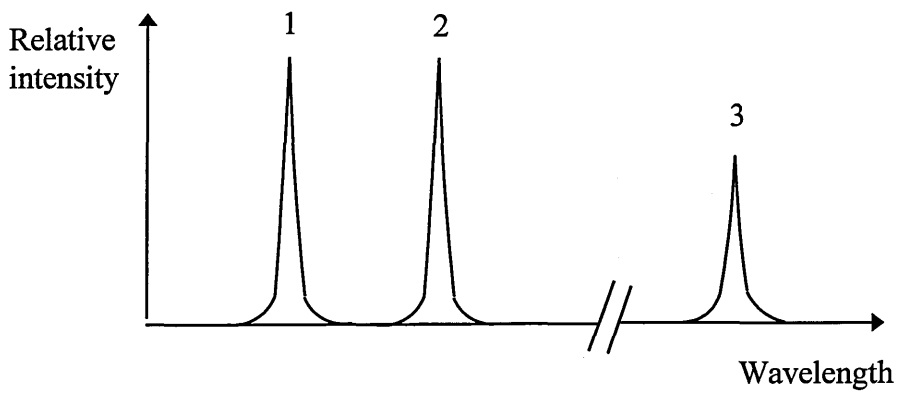

(c) The spectrum of the single mode diode with injection current modulated to produce two sequential wavelengths and simultaneous mode hopping (Peak 1 and 2 are separated by $\Delta\lambda$ and have approximately equal intensity. Peaks 1, 2 and 3 are separated by 0.3 ~ 3 nm depending on laser characteristic and have in general unequal intensities

Fig. 3.1-1 The schematic diagram of laser diode spectrum related to the combined effect of wavelength modulation and mode hopping

The use of single-mode optical fibres in ESPI systems has simplified their optical design and made them more compact and portable compared to traditional bulk systems. They are immune to the dust ingress which occurs in bulk arrangements. Beam-splitting elements can be replaced with their optical equivalent, directional couplers, which are available in a range of splitting ratios. Consequently, these fibres provide extra flexibility for delivering the light beam and optical components are reduced. The characteristics of single-mode optical fibres are described below.

Single mode optical fibres are designed to allow the propagation of the LP_{01} (Gausian intensity profile) mode and guide the input laser beam efficiently without the degradation of its coherence properties. However, the state of polarisation (SOP) of light propagating through a single mode fibre is modified due to the birefringence induced by mechanical and thermal strains, or the anisotropic variation of refractive index and core shape etc. For interferometric systems with two separated optical paths, the consistency of the SOP between the two beams becomes unpredictable, and is in general different causing a reduction in fringe visibility.

A means of overcoming this problem is to use highly birefringent fibres [3.20,3.21]. These fibres are often called polarisation preserving but this is something of a misnomer. Such fibres preserves only the two special polarisation eigenstates. It is therefore essential to ensure that only the correct SOP is launched into the fibre. Special highly birefringent fibre was also reported [3.22], in which one of the eigenmodes is suppressed so that such fibre can be used as a polariser (polarising fibres).

Alternatively, polarisation state controllers [3.23] can be used to adjust the SOP of light emerging from single-mode fibres, instead of using the costly highly birefringent fibres. These devices are the fibre optic equivalent of conventional waveplates and are constructed by choosing appropriate coil diameters, lengths of fibre, and tension of the coiled fibres. Using this controller, the SOP of light propagating through the fibre can be adjusted.

For shifting the phase of light propagating in an optical fibre, a hollow cylindrical piezoelectric transducer (PZT) is commonly used [3.24-3.26]. A sufficient length of the fibre is first wrapped tightly around the device. Voltage applied accross the cylinder then expands the diameter of the PZT and stretches the fibres. This causes an optical phase change in the light beam propagating through the fibre via the change of length and refractive index of the fibre. The phase change can be expressed as

$$\Delta\phi = \beta_1 \Delta L + L\frac{d\beta_1}{dn}\Delta n \tag{3.8}$$

where, β_1 is the propagation coefficient, ΔL is the length change of the fibre, $d\beta_1/dn$ is the variation of propagating coefficient with respect to the refractive index change, and Δn is the refractive index change of the fibre.

A major disadvantage of using fibres in ESPI is the phase drift due to the temperature change. This effect can be greatly reduced by using thermal isolation sleeves or by applying some active compensation techniques [3.27-3.29].

3.1.3 CCD cameras

During the past two decades, imaging technology has undergone considerable development and the charge-coupled device (CCD) is one of the major innovations [3.30]. The high sensitivity of CCD cameras to low light levels and the accuracy of the pixel location along with the broad range of spectral response have stimulated the use of CCDs in many applications. Nowadays, nearly all newly developed ESPI and electronic shearography systems use CCD cameras as the image detector. The features of CCD cameras and their relevance to the performance of ESPI systems are well explored by Spooren [3.6] and are briefly outlined below.

A CCD consists mainly of a series of metal-oxide semiconductor (MOS) capacitors. The capacitor has three-layer structure, a metal electrode, a silicon-oxide insulating

layer and a semiconductor substrate of p-type silicon. A simplified schematic cross section through a CCD is shown in Fig. 3.2. When a positive voltage is applied between an electrode and the silicon substrate, the majority carriers (holes in p-type Si) are repelled from the interface between the semiconductor and isolator, creating a region free from mobile carriers directly underneath the electrode. This region is known as the depletion region and has a typical thickness of the order of a few micrometers .

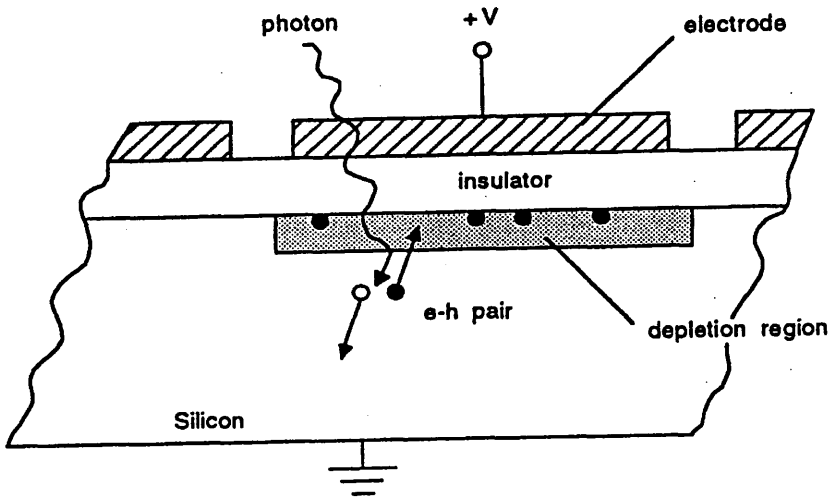

Fig. 3.2 A simplified diagram of the cross section of a CCD [3.6]

The metal electrodes (usually made of polysilicon) are transparent for wavelengths greater than about 400 nm. If an incident photon has sufficiently large energy ($h\nu >$ bandgap in silicon), it can create an electron-hole pair in the semiconductor. When this creation occurs in or near the depletion region, the photon generated electron is attracted towards the potential well, which is formed under the positively charged electrode. In this way, a charge packet is formed, consisting of photon-electrons that were created in the vicinity of a specific electrode. These charge packets can be transferred to neighbouring electrodes by proper control of the electrode potentials. Finally, the charge packets are sensed at the output of the shift register.

Since the invention of the CCD device, three detecting architectures have been developed, which include linear array, interline transfer and frame transfer sensors.

Interline transfer and frame transfer CCDs are full-image sensors with different image read-out process. In an interline CCD, the photo-electrons are transferred to vertical shift registers located near by each linear array, then transported simultaneously into horizontal shift registers, and read out line by line. A frame transfer CCD has two identical areas: an image section and a storage section. All charge packets are rapidly transferred from the image section to the storage section, and then are read out by a horizontal shift registers.

To choose a CCD camera for an ESPI system, the camera specifications should be compared carefully to decide which device most closely matches the requirement. Attention should be paid especially to spectral response, dynamic range, sensitivity, output linearity, and desired control options such as gain adjustment and integration time control etc.

The spectral response of CCD cameras is an important feature that effects the system sensitivity. For an ESPI system, a camera with a better response to the wavelength of the light source is normally selected. The dynamic range of cameras is another important parameter in ESPI as it represents the best achievable signal-to-noise ratio. In general, frame transfer CCDs offer a larger dynamic range than interline transfer CCDs because the structure of frame transfer CCDs possess a larger integration area in each pixel, thus more electrons can be stored. For in-plane ESPI and shearography, the light reflected from the object is usually very low. A camera with a better sensitivity to the low light level and a convenient gain adjustment is preferred. To perform an accurate phase measurement, e.g. using phase stepping methods, a camera with a linear response is required. Normally, a linear response of CCD cameras can be obtained by setting the internal gain (Gamma value) into 1. The integration time control enables some special applications in ESPI. The signal-to-noise ratio may be improved for the measurement with low light level by increasing the integration time. However, stroboscopic measurement can be implemented by shuttering the light instead of chopping the light source.

3.1.4 Frame grabbers

Frame grabbers are image processing devices that convert analog video signals to the form of digital "picture elements" or "pixels". These data are stored and processed in the same device, which can then be displayed on a TV monitor. Nowadays, there are a number of PC based frame grabbers available for developing ESPI and shearography systems. Depending on the cost and the version, these devices can have different amounts of frame memory, different numbers of pixels in each frame, and also different grey levels (bits) per pixel. In choosing a frame grabber, the number of pixels per frame is normally matched to the resolution of the camera. The typical operations and functions of frame grabbers are discussed as follows.

The electronic sampling of video signals, performed by frame grabbers, is normally called image acquisition. This function converts an image into an array of data points, which can be stored digitally in the frame memory. The video inputs and outputs of most frame grabbers are compatible with a number of video standards in the world, e.g. the CCIR (Comite Consultatif International Radio, an international standards organisation) standard which is commonly used in northern Europe. The CCIR standard has a signal update rate of 50 Hz with interlaced display between two image fields (odd and even fields) and as a whole has 25 Hz image frame update rate.

Standard video signals are actually complex waveforms, and contain information about the brightness of each region of the display, along with timing pulses which indicate the end of each display line (horizontal synchronisation) and the end of each display field (vertical synchronisation). The horizontal and vertical synchronisation signals within the video input are then used to control the timing of the frame grabber. Most frame grabbers allow the user to select the source of synchronisation signals, either extracted from the video input, from a separate synchronisation device, or from an on-board clock.

For a typical monochrome frame grabber, each image frame has 512 × 512 pixels, and each pixel has 8 bits for the grey level of brightness, i.e. the intensity variation from total black to total white is $2^8 = 256$. If there are other bits in the pixel, they are normally used for colouring or signal processing etc. In colour frame grabbers, three A/D converters are used to simultaneously sample the red, green and blue components of the colour signals. The colour resolution of each pixel is then determined by the sum bits of the three converters, i.e. if each colour has 8 bit resolution, colour levels are $2^{24} =$ 16,777,216.

For most frame grabbers, there are various types of high-speed buffers named look-up-tables (LUT) for the quick processing of image signals. Input LUT can map the acquired signals to other data in real time, and also can be used to process with the data fed back from the frame memory etc. The pixel values stored in the frame memory is transformed using output LUTs. If output LUTs for colour operation exist, they can be used to colour monochrome images.

Digital image processing, e.g. image subtraction, addition and transformation etc., can be performed either by the host CPU or by dedicated processing hardware. The addition of an on-board Arithmetic Logic Unit (ALU) even enables multi-frame operations in real time. The display interface in the frame grabber receives digital data from the output LUTs and converts the data to an analog CCIR or other standard signals for use by a TV monitor.

3.2 System description

3.2.1 Electronic shearography

The optical configuration of the electronic shearography system used in this work is shown in Fig 3.3. A 100 mW single longitudinal mode laser diode (Spectra Diode Labs, SDL-5411-G1) emitting at 827 nm was coupled into a single mode optical fibre to

illuminate the test object. Temperature stability better than 0.005°C (for which $\Delta\lambda <$ 0.0015 nm) was achieved using a thermoelectric temperature controller. Optical feedback was minimised using a Faraday isolator (isolation level of 30 dB). The single mode optical fibre was used to provide a flexible illumination for the experiment. It also acts as a very good spatial filter to provide a uniform beam profile.

Light scattered from the object surface is divided by a Michelson interferometer arrangement into two beams. The image shear is generated by tilting one of the mirrors, and these two sheared images are recombined onto a CCD camera (Pearpoint P176 MK2 monochrome camera). One mirror is mounted with a piezoelectric transducer (Bimorph P-286) for performing phase stepping and dithering in some measurements.

Speckle images detected by the camera are digitised and stored in a frame grabber to facilitate the image processing, e.g. real-time image subtraction. Correlation fringes are obtained when the phase changes on the object surface are detected.

Light efficiency is an important concern in a shearography system. The CCD has been selected to have high response to the infra-red wavelengths. However, the measured light efficiency of the zoom lens is around 50%, which is very poor. The laser diode originally used was 30 mW, but was later upgraded to 100 mW to improve the fringe visibility. The replacement of ordinary aluminium mirrors (75~80% reflection) to high reflection mirrors (95~99%) also helps to improve the light efficiency. The gain adjustment in the CCD camera sometimes helps to increase the fringe visibility, but it also proportionally increase the electronic noise which can be observed from the displayed images. This is not suitable when phase stepping measurements are required.

3.2.2 Existing ESPI system

The existing out-of-plane ESPI system used in this work is a fibre based portable device developed by a previous PhD student [3.31]. A schematic diagram of the system is

shown in Fig 3.4. Laser light emitted from a 30 mW laser diode (Sharp LT024MD) pigtailed to a single mode optical fibre is split by a directional coupler (the splitting ratio is 90/10) into an object beam and a reference beam. The light propagating through the reference and object beams can be modulated by stretching the fibre wrapped around each hollow cylindrical piezoelectric transducer.

The object beam emerging from the fibre end is expanded to illuminate the object surface, and the back scattered wavefronts are imaged by a zoom lens and combined with the reference beam (by a beamsplitter) onto a CCD camera. The image processing in this system is the same as that in the electronic shearography system.

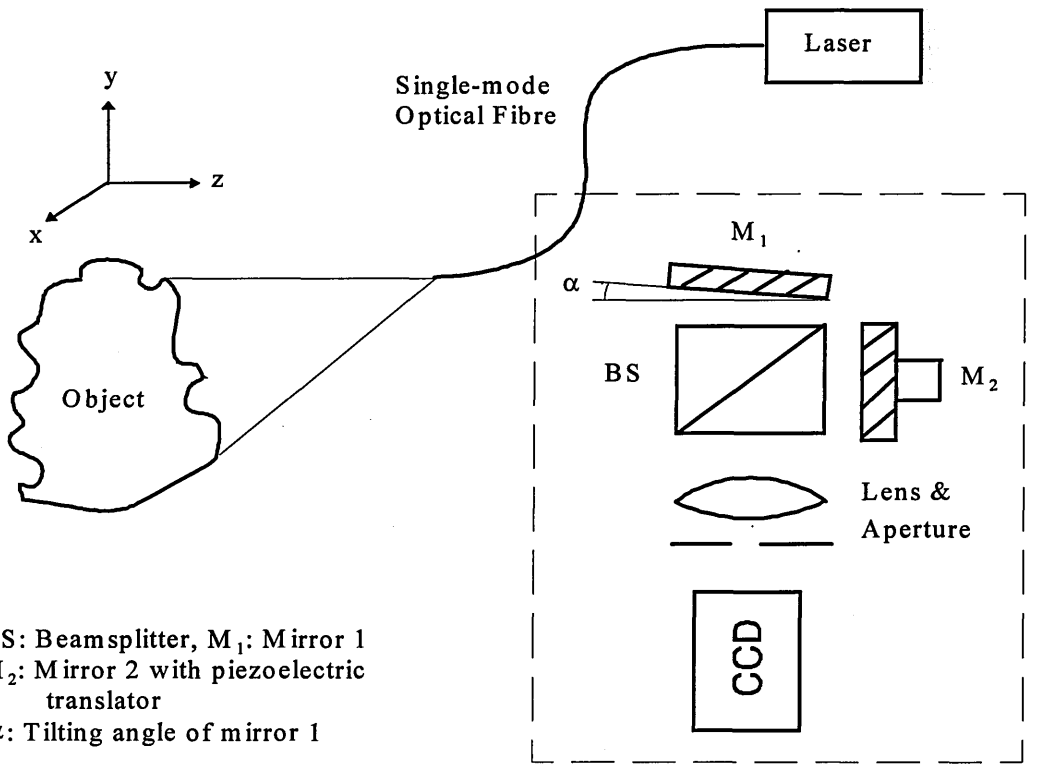

Fig. 3.3 Optical configuration of the electronic shearography system (the components inside the dashed-line box have to be mounted together)

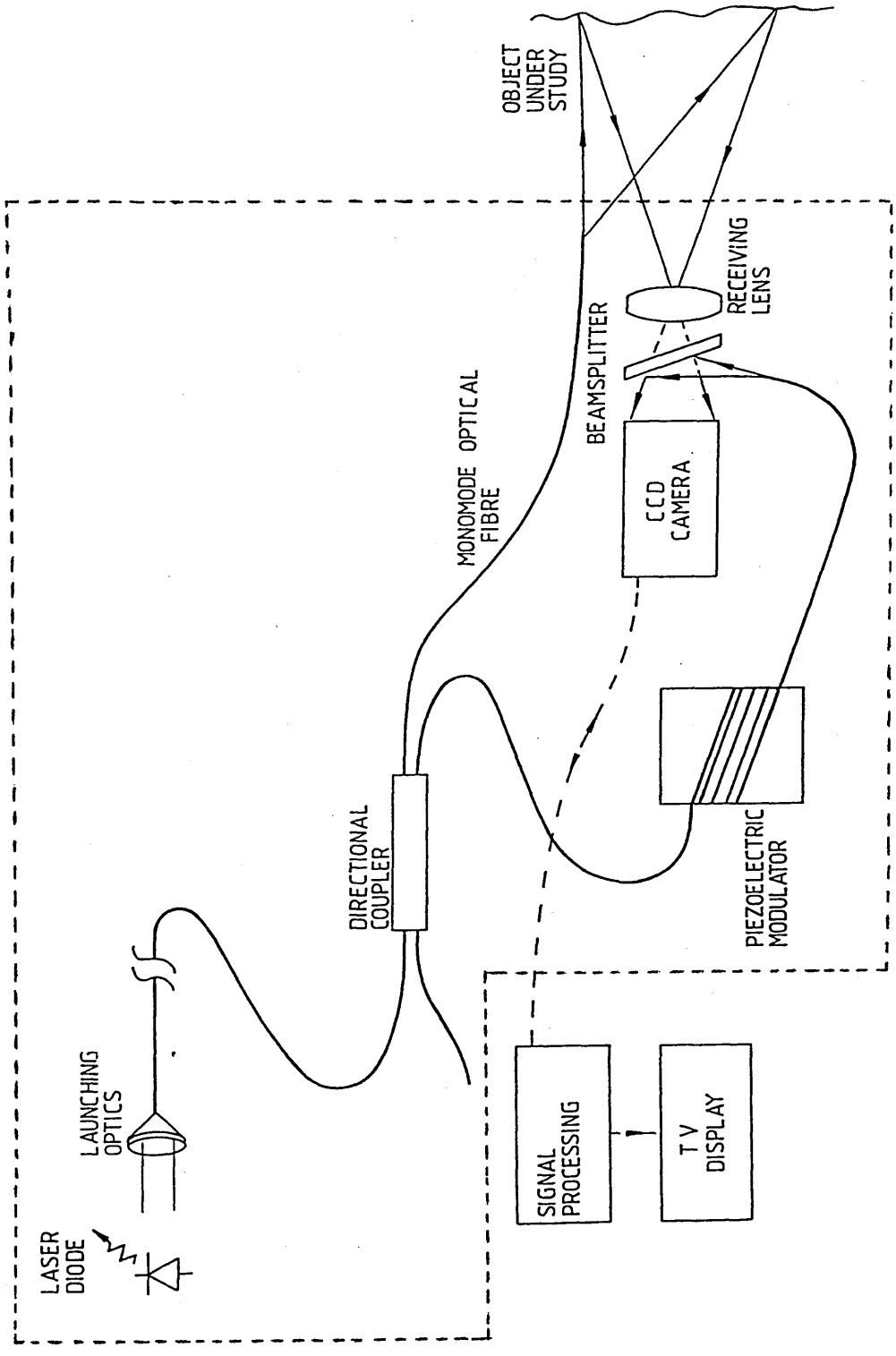

Fig. 3.4 The out-of plane ESPI system (the components inside the dashed-line box have to be mounted together)

3.3 Software programming

The program that integrates the electronic shearography and ESPI systems with a PC is called "DSPI". In DSPI, all the functions (subroutines) were written using Microsoft C version 6.0. Since the frame grabber we used is not compatible with the Windows environment, all the facilities provided by Windows are therefore not applicable. The program is therefore run under the DOS environment and driven by a pull down menu to select the functions interactively. Two kinds of pull down menu have been used. One is modified from the demonstration program provided by the Microsoft C 6.0 compiler. The other is modified from a C programming book [3.32]. The functions are described below and listed in appendix B.

Select a camera: To select the input camera from CAM 1 ~ CAM 3 and the default setting is CAM 1.

Reset 100 board: This function provides a hardware and software reset for the frame grabber. All the registers and LUTs are initialised to the default data. The function is used during the following situation: (1) When entering this program (2) To return from the real time processing modes back to the normal acquisition mode. (3) Every time when the grabber malfunctions, e.g. register overflow, and image shaking etc.

Continuous grab: Continuously acquire images from the selected CCD camera.

Snap an image: To freeze (or snap) an incoming image.

Static SUB: To perform static subtraction, an image is first snapped as a reference frame, e.g. before loading the object, and the incoming images are then subtracted continuously from the reference frame.

Sequential SUB: To perform sequential subtraction, as described in section 2.4.3. In this function, the dithering signal (the π phase shift) between frames need to be provided

by a function generator with a square wave at 12.5 Hz. Image flickering is observed because the image acquisition and the dithering signals are not well synchronised.

Sequential SUB 2: In this function, the dithering signal is provided by a D/A board and synchronised with the image update rate. More stable images can be obtained using this function.

Swap 2 bits: The snapped image from static subtraction and sequential subtraction is a 6 bit image. Before saving the image, perform this function to transform it to become an 8 bit image.

Save a page: Save the snapped image into a floppy or hard disk.

Read an image: Read a stored image from disk into the frame memory.

View all pages: The data in the four image frames are contracted into one image frame and displayed on the active page.

Clear active page: To clear the data stored in the acquisition frame.

Clear all pages: To clear all the data stored in the four frame memory.

Enhance an image: To linearly enhance the image by multiplying a factor.

Nonlinear enhance: To enhance the image nonlinearly by the power of the input enhance number *en*, i.e. the original intensity I_{org} will be enhanced to become $(I_{org})^{en}$.

Log Image: This function is used to improve the TV monitor visibility of time-averaged vibration fringes by reducing the intensity difference of the Bessel fringe pattern using the log function.

Histogram: To observe the intensity distribution of the image.

Read pixel value: This function can read a horizontal or vertical line of pixel data. It is normally used to check the modulation range of the speckle fringe pattern.

Electronic Noise: To continuously monitor the intensity variation of different pixel and evaluate the amplitude of noise.

Convol filter: The 5x5 convolution filter can be used to smooth the speckle fringe data before the phase calculation.

Low pass filter: This is a 3x3 low pass filter for smoothing the speckle image.

PZT/Diode calibration: The function is used to decide the required voltage number for generating 2π phase shift, either by modulating the PZT input voltage or the diode injection current.

Dual Grab: The function is used to store four images into the frame memory in the image frame update rate.

Contr-fast-p1: The function is to generate contour/slope fringes by modulating the diode injection current with a certain high frequency (larger than 1 kHz) using sequential subtraction (will be discussed in section 4.3.2). Before the processing, the diode operating current and the modulation voltage number need to be carefully decided.

Static Mod p0~p5: These D/A signals can be used for the diode wavelength modulation and PZT phase stepping.

References

3.1 Yariv, A., Optical Electronics. 4th ed., Saunders College Publishing, (1991) 552-591.

3.2 Buus, J., Single frequency semiconductor lasers. Tutorial Texts in Optical Eng., Vol. TT5, SPIE Optical Eng. Press, (1991).

3.3 Senior, J., Optical fibre communications. Prentice-Hall, (1985).

3.4 Kim, C. K., The physics of charge coupled devices. in *Charge Coupled Devices and Systems*, ed. Howes, M. J. and Morgan, D. V., John Wiley and Sons, Chichester, (1979).

3.5 Beynon, J. D. E. and Lamb, D. R., Charge coupled devices and their applications. McGraw-Hill, Maidenhead, (1980).

3.6 Spooren, R., Standard charge-coupled device cameras for video speckle interferometry. Opt. Eng., 33 (3) (1994) 889-896.

3.7 Baxes, G. A., Digital image processing - A practical primer. Prentice-Hall, (1984).

3.8 VS-100-AT Frame Grabber User Manual, Imaging Technology Inc., (1990).

3.9 Tatsuno, K. and Tsunoda, Y., Diode laser direct modulation heterodyne interferometer. *Appl. Opt.*, **26** (1) (1987) 37-40.

3.10 Dandridge, A. and Goldberg, L., Current induced frequency modulation in diode lasers. *Electron. Lett.*, **18** (1982) 302.

3.11 Kobayashi, S., Yoshihisa, Y., Ito, M. and Kimura, T., Direct frequency modulation in AlGaAs semiconductor lasers. *IEEE J. Quantum Electron.*, QE-18, (1982) 582.

3.12 Giles, I. P., Uttamchandani, D., Culshaw, B. and Davies, D. E., Coherent optical-fibre sensors with modulated laser sources. *Electron. Lett.*, **19** (1) (1983) 14.

3.13 Tatam, R. P., Davies, J. C., Buckberry, C. H. & Jones, J. D. C., Holographic surface contouring using wavelength modulation of laser diodes. *Optics & Laser Technology*, 22 (5) (1990) 317-321.

3.14 Kersey, A. D., Jackson, D. A. and Corke, M., Demodulation scheme for interferometric sensors employing laser frequency switching. *Electron. Lett.*, **19** (1983) 102.

3.15 Linke, R. A., Modulation induced transient chirping in single frequency lasers. *IEEE J. Quantum Electron.*, **QE-21**, (1985) 593-597.

3.16 Bickers, L. and Westbrook, L. P., Reduction in laser chirp in 1.5 μm DFB lasers by modulation pulse shaping. *Electron. Lett.*, **21** (1985) 103-104.

3.17 Anderson, D. J., Jones, J. D. C., Sinha, P. G., Kidd, S. P. and Barton, J. S., Scheme for extending the bandwidth of injection-current-induced laser diode optical frequency modulation. *J. Modern Optics*, **38** (1991) 2459.

3.18 Henry, C. H. and Kazarinov, R. F., Instability of semiconductor lasers due to optical feedback from distant reflectors. *IEEE J. Quantum Electron.*, **QE-22**, (1986) 294.

3.19 Groot, P. D., Fibre-coupled laser diode mount for interferometry. *Eng. Lab. Notes*, Supplement to Appl. Opt., (1993) 7122-23.

3.20 Payne, D. N., Barlow, A. J. and Hansen, J. J. R., Development of low and high birefringence optical fibres. *IEEE*, J. Quantum Electron., QE 18 (1982) 477.

3.21 Birch, R. D., Fabrication and characterisation of circularly birefringent helical fibres. *Electron. Lett.*, **23** (1987) 150.

3.22 Varnham, M. P., Payne, D. N., Barlow, A. J. and Tarbox, E. J., Coiled-birefringent-fibre polarisers. *Opt. Lett.*, **9** (1984) 306.

3.23 Lefevre, H. C., Single-mode fibre fractional wave devices and polarisation controllers. *Electron. Lett.*, **16** (20) (1980) 778-780.

3.24 Davies, D. E. and Kingsley, S., Method of phase modulating signals in optical fibres: application to optical telemetry systems. *Electron. Lett.*, **10** (21) (1974) 21.

3.25 Kingsley, S., Optical-fibre phase modulator. *Electron. Lett.*, **11** (1974) 453.

3.26 Martini, G., Analysis of a single-mode optical fibre piezoelectric phase modulator. *Opt. & Quantum Electron.*, **19** (1987) 179.

3.27 Santos, J. L., Newson, T. P. and Jackson, D. A., Electronic speckle pattern interferometry using single-mode fibres and active fringe stabilisation. Opt. Lett., **15** (1990) 573-575.

3.28 Valera J D, Harvey D and Jones J D C: "Automatic heterodyning of fibre optic speckle pattern interferometry", SPIE, Vol 1508 (1991) 170-179.

3.29 Dupont, C., Optoelectronic stabilisation for electronic speckle pattern interferometry. MSc thesis, Cranfield University, (1992).

3.30 Rose, A. and Weimer, P. K., Physical limits to the performance of imaging systems. *Phys. Today*, **42** (1989) 24-32.

3.31 Atcha H: "Optoelectronic Speckle Pattern Interferometry", PhD thesis, Cranfield University, (1995).

3.32 Jones, B. and Guntle, G., Teach yourself advanced C in 21 days. SAMS Publishing, (1994).

4. TWO-WAVELENGTH SLOPE MEASUREMENT

4.1 Introduction

The measurement of surface profile and gradients of surface profile is a requirement for many engineering applications, e.g. on-line quality control, solid modelling (the transfer of contour information from prototypes to CNC machines), biomedical applications, and the measurement of mechanical wear. Although in practice, coordinate measuring machines with contact probes (or some with optical triangulation heads) are commonly used, these point-detection schemes are very time-consuming and have a number of limitations. Test objects should be compact and portable enough to be brought in and positioned on the measuring table, and for some fragile materials or in some biomedical applications, the contact probe might damage or deform the surface under test.

Various full-field optical techniques have been developed for contour and slope measurements, such as moire techniques, holographic interferometry, speckle interferometry and shearography. With the characteristics of non-contact detection and extended field of view, these methods have been applied successfully in many engineering applications.

Electronic speckle pattern interferometry (ESPI) and shearography systems are full-field optical techniques that can be used for out-of-plane contour and slope measurements respectively [4.1,4.2]. ESPI measures surface profiles or shape directly, while shearography measures surface gradients (slopes). For objects with non-planar shapes, contours and slopes are required for a complete surface strain analysis [4.3]. For the study of stress distribution in a hydroformed axisymmetrical shell, accurate measurements of the local curvatures of the object surface are required, i.e. the membrane stresses are directly related to the local principal curvatures [4.4]. These curvatures are determined by the second-order derivatives (d^2z/dx^2) and the slopes

(dz/dx) of the object surface, and shearography becomes a more straightforward approach in this work [4.5].

In this chapter, a two-wavelength slope measurement technique using an electronic shearography system is presented. Fringe patterns representing the slope variation of the object surface are compared with contour fringes generated by a fibre-based ESPI system using the same two-wavelength technique.

4.2 Review of full field optical techniques

Contouring using full field optical techniques is made by generating fringes over the surface of interest, where each fringe represents a constant depth variation determined by the specific technique as well as the illumination and viewing directions. In contrast, by using shearography, each fringe represents a constant slope variation along the image-sheared direction.

In this section, full-field optical methods for contour/slope measurements including moire techniques, holographic interferometry, speckle interferometry, and shearography are reviewed and compared. Comparisons of different techniques are also listed in Table 4.1 (on page 80-1).

4.2.1 Moire techniques

A moire fringe pattern is observed when two gratings (geometric arrays or regularly repeated structures with nearly the same spacing) are superimposed. The moire effect is often termed "mechanical interference" of two grid image [4.6] and can be formed by different types of gratings, e.g. parallel line gratings, circular gratings and radial gratings etc. The moire technique is one of the popular full-field optical methods for stress/strain and contour measurements (vibration measurement is not as popular). Detailed

description of moire methods and their applications can be found in some of the recent publications [4.7,4.8]. In contour measurements, projection moire (including fringe projection methods) and shadow moire are commonly used.

Contouring by fringe projection methods were first reported by Rowe and Welford in 1967 [4.9], and Brooks and Heflinger two years later [4.10]. When an object is illuminated by two nearly parallel and mutually coherent plane waves, the two waves interfere and generate fringes which are projected onto the object surface. A camera positioned at an angle to the projection axis is used to image the surface. The projected fringes deformed by the height variation of the object surface are recorded. A moire fringe pattern, which depicts the contour difference, can be obtained by recording projection fringes on two different objects by double exposure. The surface topography also can be determined by measuring the phase of projected fringes on the object surface and comparing the phase distribution to that of a flat surface [4.11]. In this method, the maximum sensitivity and accuracy is obtained when the angle between the illumination and the viewing directions approaches 90°. In practice, shadow effects occur when objects with non-planar shapes are measured. Another disadvantage of the method is that the recorded images are degraded by laser speckles when small apertures are used.

An equivalent technique to the fringe projection method, termed projection moire, was reported by Hovanesian and Hung, and by others [4.12-4.14], in which incoherent illumination and a grating was used to generate the projected fringes. Instead of recording projection fringes on two different objects by double exposures, moire fringe pattern, which represents the shape of the object surface, also can be directly observed by imaging the object through a reference grating [4.14]. Recently in the bio-mechanical application, projection moire has been used to study the changes in topography of human scapula induced by muscle contraction [4.15,4.55].

Contouring by shadow moire was proposed by Takasaki [4.16,4.17] and Meadows et al [18], in which a grating was placed in front of the object surface. Moire fringes are formed between the grating and its own shadow, which represent the topographic map

over the surface. It has been successfully implemented to contour the shape of a human body [4.17].

The main concern of using moire techniques in contouring, is how to obtain high resolution and accuracy. Phase shifting techniques has been applied to improve the situation [4.19-4.21], of which the sensitivity up to 1/100 of a fringe has been reported. Moire techniques have much less stability requirements compared to holographic and speckle interferometry, however the depth of field is limited by diffraction effect.

4.2.2 Holographic interferometry

In holographic interferometry, contouring has been reported using two-wavelength illumination [4.22,4.23,4.54], two refractive index [4.24-4.27], two source method [4.23] and translating the observation points (including sandwich holography) [4.28,4.29].

Two-wavelength contouring in holographic interferometry was first proposed by Haines and Hildebrand [4.22]. The object under test is recorded holographically using two different wavelengths, λ_1 and λ_2 either simultaneously or by double exposure. Reconstruction of the hologram yields two superimposed images on the object surface. Under suitable viewing conditions, these two wavefronts will interfere and generate contour fringes of the object [4.1]. This technique is similar to the use of beats between two laser wavefronts with a small wavelength difference. The contour fringe interval is in the order of the effective wavelength $\lambda_{eff} = \lambda_1\lambda_2 / |\lambda_1-\lambda_2|$. In 1985, two-wavelength holographic contouring was also implemented using laser diode emission wavelength modulation [4.54].

The two refractive index method was first reported by Tsuruta et al [4.24]. The technique is similar to the two wavelength method. It requires the object to be immersed in a liquid or gas bath with a slight refractive index change in between the

exposures. Using materials with different refractive index, contour fringe intervals in the range of a few μm to several millimetres can be obtained [4.25,4.26]. Although this technique is simpler to perform compared to the two wavelength method, it is very slow and inconvenient, and not practically applicable in many applications.

The two source method, which is analogous to the fringe projection method in moire techniques, was also proposed by Hildebrand and Haines [4.23]. In this technique, the laser source is laterally displaced between exposures to generate contour fringes. The interference of wavefronts reconstructed from the two-source holograms produces a hyperboloid fringe pattern in space with foci at the sources. Simplification of the method was also achieved by the use of singlemode optical fibres in the system [4.30]. The same as fringe projection method, shadow effect might occur in the measurement of convoluted objects using the two source method.

In sandwich holography [4.28], the hologram, recorded using two source method, is tilted through a small angle during reconstruction. The reconstructed fringe pattern can be rotated by the tilt to become parallel to any required orientation. Therefore, the interpretation of the contour fringes can be simplified.

Compared with moire techniques in contouring, holographic methods generally achieve better sensitivity in the order of the illumination wavelength. However, the stability requirement of these methods is much higher than that of moire techniques.

4.2.3 Speckle interferometry and ESPI

Almost all the processing techniques for contouring in holographic interferometry have been extended to speckle interferometry or ESPI, e.g. two-wavelength illumination [4.31-4.36], refractive index change of the medium surrounding the object [4.37], tilting the object [4.38,4.39] and shifting or tilting the illumination [4.40-4.43].

Two wavelength contouring in ESPI can be performed by illuminating the object at two wavelengths, λ_1 and λ_2 , either simultaneously or sequentially. Correlation of two speckle interferograms by image subtraction then generates a fringe pattern, which represents a contour map of the object surface. This method is similar to two wavelength holography. The implementation of two wavelength contouring by modulating a laser diode source in an ESPI system was reported by Tatam et al and others [4.33-4.36]. The same technique has been extended to slope measurements using a wavelength modulated laser diode based shearography system [4.44, 4.45], and will be detailed later in this chapter.

Shifting the illumination position for contouring was first reported by Winther and Slettemoen [4.40], and by Bergquist and Montgomery [4.41]. In Winther's method, the object illuminating beam of an out-of-plane ESPI system was laterally displaced, i.e. orthogonal to the illumination axis, between image frames and the subtraction process was used to generate contour fringes. The correlation fringes are analogous to those in two source holography [4.23,4.30], and the fringe sensitivity is controlled by the translation of the illuminating beam and the angle between the illumination and viewing axis.

In Bergquist's method [4.41], the object illuminating beam of an out-of-plane ESPI system was rotated to generate contour fringes. By rotating the wavefront at TV frame rate, and using sequential subtraction processing, contour fringes, which are less affected by environmental disturbance, were obtained. Since then, similar techniques extended to dual-beam illuminating configuration (in-plane ESPI) and different ways of shifting, e.g. by moving the illuminating beam or by tilting the object, has been thoroughly explored theoretically and experimentally [4.46,4.39,4.42,4.43]. The technique was also given a new name [4.46] as "electronic speckle contouring".

Contour measurements using ESPI systems have the same sensitivity as using holographic methods, but with less stability requirements. However, the disadvantage

of using this method is that speckle noise degrades the fringe visibility and affects the accuracy of the phase measurement.

4.2.4 Shearography

In shearography, two refractive index [4.2], two source (or shifting the illumination position) [4.47-4.49], tilting the object [4.50] and two-wavelength [4.44,4.45] methods have been reported for slope measurements.

Two refractive index and two source methods were all first demonstrated by Hung et al in 1978 [4.2,4.47]. The implementation of slope measurement, by shifting the illumination position, were theoretically detailed and reported by Tay et al [4.48,4.49]. Recently, tilting the object [4.50] and two wavelength [4.44,4.45] methods were reported.

Although most of the contouring techniques can be extended to shearography for slope measurement, illumination-shifting and object-tilting method normally need to record speckle interferograms by photographic films and use Fourier filtering to generate slope fringes. This is due to the obvious speckle-decorrelation effect, which will degrade the fringe visibility imaged by a CCD camera, when the illumination beam or the object is moved. Photographic films have larger dynamic range (or grey levels) compared with CCD cameras (normally 8 bits, 256 grey levels), and Fourier filtering can enhance the fringe visibility.

Slope measurements by two wavelength method have been found to give better fringe visibility compared to shifting techniques in electronic shearography, due to less speckle decorrelation effect. This will be demonstrated experimentally later in this work.

Optical techniques	Methods	Sensitivity (fringe spacing)	Max. resolution
Moire techniques (shape)	Fringe projection	25 μm ~ a few mm	1/100 of a fringe (by phase stepping)
	projection moire		
	shadow moire		
Holographic interferometry (shape)	Two-wavelength	3 μm ~ a few mm	1/1000 × λ (by heterodyning)
	Two refractive index	3 μm ~ a few mm	
	Two source	14 μm ~ a few mm	
ESPI (shape)	Two-wavelength	30 μm ~ a few mm	1/100 × λ (by phase stepping)
	Two refractive index	10 μm ~ a few mm	
	Illumination shifting (or object tilting)	0.75 mm ~ a few mm	
Shearography (slope)	Two-wavelength	0.5 mm ~ a few mm	1/100 × λ (by phase stepping)
	Two refractive index	0.3 mm ~ a few mm	
	Illumination shifting (or object tilting)	0.3 mm ~ a few mm (recorded by photograph)	

Table 4.1 Full field optical techniques for shape and slope measurements

4.2.5 Summary

The processing techniques for contouring in holography, speckle interferometry and shearography can be divided into two main categories. One is two wavelength illumination (including two index method) and the other is two source method (including shifting and tilting methods, either in the illumination beam or the object). Both these methods are analogous to the projection moire technique. Two wavelength methods can be regarded as projecting two gratings (interferograms of λ_1 and λ_2) with a small pitch difference, and the two source method can be seen as projecting two gratings with the same pitch but slightly displaced with respect to each other.

The advantages of two source methods are its simplicity of implementation and the wide contour range that can be obtained. However, The main drawback of these methods is the inherent shadow effect which is caused by the sensitivity requirement. Other disadvantages include the requirement of some form of calibration in the measurement and the complexity of the equations describing the contour/slope fringes [4.41,4.49].

The advantages of two wavelength methods are they can be performed in a mechanical passive manner, the fringe interpretation is much simpler compared to two source methods, and less speckle decorrelation occurs when applied in speckle interferometry. However, the wavelength modulation needs to be calibrated and the laser source needs to be well characterised.

4.3 Theory of two wavelength technique

Contour and slope measurements using two wavelength technique can be performed by illuminating the object at two wavelengths, λ_1 and λ_2 , either simultaneously or sequentially. When the object is illuminated simultaneously with two wavelengths in each image frame, the sequential-subtraction processing mode, as described in section 2.4.3, can be used to generate the correlation fringes. In contrast, when the object is

illuminated sequentially between image frames, the static subtraction mode, as described in section 2.4.1, is used to generate the correlation fringes. In this section, the equations that describe slope fringes in shearography and contour fringes in ESPI using the two wavelength method are derived. To demonstrate the similarity and difference of using the two processing modes, sequential illumination is used in the derivation of equations of slope fringes, and simultaneous illumination is used in the derivation of equations of contour fringes.

4.3.1 Slope measurement

A schematic diagram of the optical path in shearography is shown in Fig. 4.1. A test object is illuminated by a point coherent light source at the position $S(x_s, y_s, z_s)$. If the image shearing is in the x direction by an amount δx, light reflected from a point P(x, y, z) and light reflected from its neighbouring point $P'(x+\delta x, y, z+\delta z)$ will be brought to interfere at the same point $O(x_o, y_o, z_o)$ in the image plane, where δz represents the height variation between point P and P'.

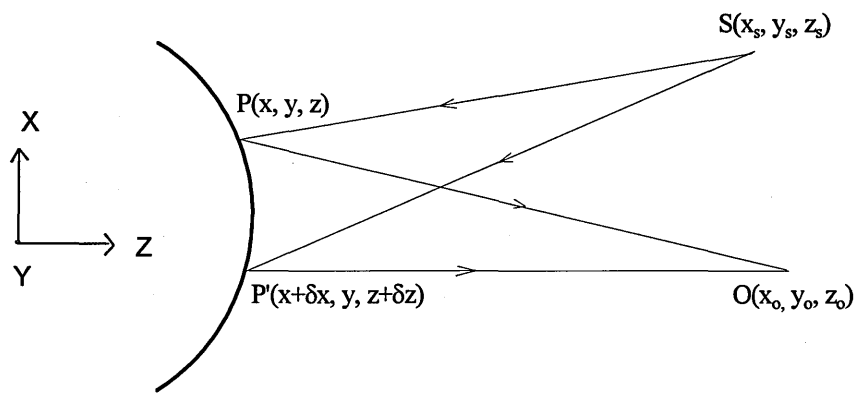

Fig. 4.1 Schematic diagram of the optical path in shearography

The intensity of the resulting speckle image is represented by

$$I(x_o, y_o) = e_1^2(x,y) + e_2^2(x+\delta x, y) + 2e_1(x,y)e_2(x+\delta x, y)\cos[\phi + \phi_s] \tag{4.1}$$

where, $e_1(x, y)$ and $e_2(x+\delta x, y)$ are the electric field amplitudes of light reflected from point P and P', ϕ is the phase difference between these two beams, ϕ_s is the randomly varying phase term due to speckle noise and (x, y) and (x_o, y_o) are conjugate points on the object and the image plane. The optical path difference between these two beams is given by

$$\delta\ell = (SP + PO) - (SP' + P'O) = (SP - SP') + (PO - P'O)$$

$$= \frac{(SP)^2 - (SP')^2}{SP + SP'} + \frac{(PO)^2 - (P'O)^2}{PO + P'O} \tag{4.2}$$

where,

$$SP = \left[(x - x_s)^2 + (y - y_s)^2 + (z - z_s)^2\right]^{1/2} \tag{4.3a}$$

$$SP' = \left[(x + \delta x - x_s)^2 + (y - y_s)^2 + (z + \delta z - z_s)^2\right]^{1/2} \tag{4.3b}$$

$$PO = \left[(x - x_0)^2 + (y - y_0)^2 + (z - z_0)^2\right]^{1/2} \tag{4.3c}$$

$$P'O = \left[(x + \delta x - x_0)^2 + (y - y_0)^2 + (z + \delta z - z_0)^2\right]^{1/2} \tag{4.3d}$$

Since δx and δz are small, we can assume

$$SP' \cong SP = R_s \text{ and } P'O \cong PO = R_o \tag{4.3e}$$

R_s and R_o are the illumination and the viewing distances for point P. Substituting equations (4.3a)-(4.3e) into equation (4.2) and rearranging yields

$$\delta\ell = C_x\delta x + C_z\delta z \tag{4.4}$$

where,

$$C_x = -\left[R_o\left(x - x_s + \delta x/2\right) + R_s\left(x - x_o + \delta x/2\right)\right]/R_sR_o \tag{4.5a}$$

$$C_z = -\left[R_o\left(z - z_s + \delta z/2\right) + R_s\left(z - z_o + \delta z/2\right)\right]/R_sR_o \tag{4.5b}$$

The phase difference between these two beams is

$$\phi = \frac{2\pi}{\lambda}\delta\ell = \frac{2\pi}{\lambda}\left(C_x\delta x + C_z\delta z\right) \tag{4.6}$$

When the object is sequentially illuminated at two wavelengths, the first image is recorded at λ_1 and then subtracted from the second image recorded at λ_2 . Subtracting the two images leads to

$$\Delta I(x_o, y_o) = -4e_1e_2\sin\left[\frac{2\pi}{\lambda_1}\left(C_x + C_z\frac{\delta z}{\delta x}\right)\delta x + \phi_s\right]\sin\left[\frac{\pi}{\lambda_{eff}}\left(C_x + C_z\frac{\delta z}{\delta x}\right)\delta x\right] \tag{4.7}$$

where, $\lambda_{eff} = \lambda_1\lambda_2 / (\lambda_1 - \lambda_2) = c / \Delta\nu$, $\Delta\nu$ is the optical frequency difference, and c is the free space velocity of light. The randomly varying speckle phase term, ϕ_s , prevents the first term in square brackets from producing slope fringes even for very small slope variations. Rectification of equation (4.7) therefore produces speckle correlation fringes periodic in the order of λ_{eff} .

From equation (4.7), it can be seen that C_x and C_z need to approach constants to carry out the slope measurement with maximum accuracy. This means that the illumination distance (the distance between the light source and the object) and the viewing distance (the distance between the camera faceplate and the object) should be large compared with the object size.

When the illumination and the viewing directions are collinear, and the object size is small compared with the illumination and viewing distances, we obtain $C_x \cong 0$, $C_z \cong 2$, and equation (4.7) can be simplified to become

$$\Delta I(x_o, y_o) = -4e_1 e_2 \sin\left[\frac{4\pi}{\lambda_1}\left(\frac{\delta z}{\delta x}\right)\delta x + \phi_s\right]\sin\left[\frac{2\pi}{\lambda_{eff}}\left(\frac{\delta z}{\delta x}\right)\delta x\right] \tag{4.8}$$

As indicated in equation (4.8), the fringe spacing depends on the shearing amount δx, the effective wavelength λ_{eff} and the slope variation $\delta z/\delta x$. The larger δx and $\delta z/\delta x$, and the smaller λ_{eff}, the more closely spaced will be the slope contour fringes generated on the object surface.

If the image shearing is in the y direction by an amount δy, equation (4.7) is modified to become

$$\Delta I(x_o, y_o) = -4e_1 e_2 \sin\left[\frac{2\pi}{\lambda_1}\left(C_y + C_z\frac{\delta z}{\delta y}\right)\delta y + \phi_s\right]\sin\left[\frac{\pi}{\lambda_{eff}}\left(C_y + C_z\frac{\delta z}{\delta y}\right)\delta y\right] \tag{4.9}$$

where,

$$C_y = -\left[R_o\left(y - y_s + \delta y/2\right) + R_s\left(y - y_o + \delta y/2\right)\right]/R_s R_o \tag{4.10}$$

When the illumination and the viewing directions are collinear, and the object size is small compared with the illumination and viewing distances, equation (4.10) simplifies to

$$\Delta I(x_o, y_o) = -4e_1e_2 \sin\left[\frac{4\pi}{\lambda_1}\left(\frac{\delta z}{\delta y}\right)\delta y + \phi_s\right]\sin\left[\frac{2\pi}{\lambda_{eff}}\left(\frac{\delta z}{\delta y}\right)\delta y\right] \tag{4.11}$$

As indicated in equations (4.5a), (4.5b) and (4.10), the parameters of slope fringes C_x, C_y and C_z, are expressed by very simple functions. When the slope variation in the x direction is measured, only the x dimension of the object will affect the accuracy of measurement. Similarly, only the y dimension of the object will affect the accuracy of slope measurement in the y direction. Since the magnification of the imaging system can be evaluated easily, a point (x, y) on the object can then be determined by the equivalent image point. The height of the object (z) is the only variable still left in these equations, which can be assumed to be half of the object height as long as the height of the object is reasonably small compared to the illumination and viewing distances. C_x, C_y and C_z can be easily calculated to calibrate the phase obtained from the slope fringes and improve the accuracy of the slope measurement.

4.3.2 Contour measurement

To perform two-wavelength contouring under a pseudo-simultaneous illuminating condition, the test object is illuminated by a laser diode of which the emission wavelength is modulated between λ_1 and λ_2 during each image frame. When the wavelength modulation frequency is much greater than the image frame update rate, the object and reference wavefronts are expressed as

$$E_{o1,2} = e_o \exp i\left(\frac{2\pi}{\lambda_{1,2}} l_o + \phi_s\right) \tag{4.12a}$$

$$E_{r1,2} = e_r \exp i\left(\frac{2\pi}{\lambda_{1,2}} l_r\right) \tag{4.12b}$$

where, $\lambda_{1,2}$ represents λ_1 and λ_2 within one image frame, e_o is the electric field amplitude of light reflected from the object, e_r is the amplitude of reference beam, l_o is the object beam path length, l_r is the reference beam path length, and ϕ_s represents the randomly varying speckle phase. The interference wavefront, E_{tot}, is

$$E_{tot} = E_{o1,2} + E_{r1,2} \tag{4.13}$$

Here, we can assume that each wavelength occurs equally within the exposure period, T, of one image frame, the intensity at a point on the image plane is then given by

$$I_{1,2} = \frac{1}{T}\int_0^T E_{tot} E_{tot}^*$$

$$= e_o^2 + e_r^2 + e_o e_r \cos\left[\frac{2\pi}{\lambda_1}(l_o - l_r) + \phi_s\right] + e_o e_r \cos\left[\frac{2\pi}{\lambda_2}(l_o - l_r) + \phi_s\right] \tag{4.14}$$

If one arm of the interferometer is modulated by a π phase shift in between image frames, and the incoming frame is subtracted with the previous frame sequentially (sequential subtraction mode) as described in section 2.4.3, the subtracted image signals are given by

$$\Delta I = 2e_o e_r \cos\left[\frac{2\pi}{\lambda_1}(l_o - l_r) + \phi_s\right] + 2e_o e_r \cos\left[\frac{2\pi}{\lambda_2}(l_o - l_r) + \phi_s\right] \tag{4.15}$$

When the illumination and the viewing directions are collinear, and the object size is small compared with the illumination and viewing distances, the path-length difference between the object beam and the reference beam can be denoted as

$$l_o - l_r = 2h + \delta l \tag{4.16}$$

where, h is the height variation of the object surface, and δl is the path-length difference between the object and reference beams, but without the height variation of the object.

Under these conditions, equation (4.15) simplifies to

$$\Delta I = 4e_o e_r \cos\left[\frac{2\pi}{\lambda_1}(2h + \delta l) + \phi_s\right] \cos\left[\frac{\pi}{\lambda_{eff}}(2h + \delta l)\right] \tag{4.17}$$

where, $\lambda_{eff} = \lambda_1\lambda_2 / (\lambda_1 - \lambda_2)$. The randomly varying speckle phase term, ϕ_s, prevents the first term in square brackets from producing contour fringes even for very small height variations. Rectification of equation (4.17) therefore produces speckle correlation fringes periodic in the order of λ_{eff}. As indicated in the equation, each fringe interval represents the height variation of $\lambda_{eff}/2$.

For contouring using simultaneous two-wavelength illumination, the speckle pattern produced by the wavelength λ_1 is superimposed (correlated) with the speckle pattern produced by λ_2 in the same image frame, as seen from equations (4.14). Contour fringes can be obtained by subtracting two speckle images with a certain phase shift. The phase change between image frames only affect the fringe visibility and a π phase shift generates the best contrast. To apply phase stepping, the phase change must be introduced between the two wavelengths and synchronised with the diode modulation frequency. If a phase step ψ_i is added into one arm of the interferometer when the illumination is in the wavelength λ_1 and reset to zero in the wavelength λ_2, the intensity of the phase stepped images, $I_{i,0}$, can be expressed as

$$I_{i,0} = e_o^2 + e_r^2 + e_o e_r \cos\left[\frac{2\pi}{\lambda_1}(l_o - l_r) + \phi_s + \psi_i\right] + e_o e_r \cos\left[\frac{2\pi}{\lambda_2}(l_o - l_r) + \phi_s\right] \tag{4.18}$$

where i = *1, 2, ...n*, depends on the applied phase stepping algorithm. If using sequential subtraction to generate correlation fringes, the intensity of the phase stepped images with an additional π phase shift, $I_{i,\pi}$, can be expressed as

$$I_{i,\pi} = e_o^2 + e_r^2 + e_o e_r \cos\left[\frac{2\pi}{\lambda_1}(l_o - l_r) + \phi_s + \psi_i + \pi\right] + e_o e_r \cos\left[\frac{2\pi}{\lambda_2}(l_o - l_r) + \phi_s + \pi\right] \tag{4.19}$$

The subtracted image signals are then given by

$$\Delta I_i = 2e_o e_r \left\{\cos\left[\frac{2\pi}{\lambda_1}(l_o - l_r) + \phi_s + \psi_i\right] + \cos\left[\frac{2\pi}{\lambda_2}(l_o - l_r) + \phi_s\right]\right\} \tag{4.20}$$

Equation (4.20) represents phase-stepped contour fringes performed by adding the required phase steps which synchronise with the wavelength modulation.

Equations of contouring using the two-wavelength technique was also theoretically detailed and reported by Tatam et al [4.28]. In their method, the object is sequentially illuminated. The first image is recorded at λ_1 as a reference frame and then subtracted with the other images recorded at λ_2. The transfer function of contour fringes under sequential illumination [4.28] is analogous to equation (4.17), which is derived under a pseudo-simultaneous illuminating condition (i.e. λ_1 and λ_2 appear equally in one image frame).

4.4 Experimental verification

The optical configurations of the electronic shearography and ESPI systems, used for slope and contour measurements, are shown in Fig. 3.3 (page 66) and Fig. 3.4 (page 66-1). In slope measurements, the laser diode was first operated at a wavelength λ_1, and an image was collected at this wavelength. The diode was then tuned to a second wavelength λ_2, and a second image collected. Subtracting these two images and rectifying, generates correlation fringes that depict slope variations of the object surface.

In slope measurement, wavelength modulation was achieved by adjusting the working temperature of the laser, because the phase change due to the slope variation is normally much smaller than that due to the height variation. The image shear was also set to a small amount (4 mm) to ensure the accuracy of slope measurement. By adjusting the working temperature of the diode, a broader wavelength change with less intensity variation can be obtained to produce better fringe visibility.

However in contour measurement, the wavelength change was obtained by modulating the injection current of the laser. The injection current of a laser diode can be modulated much faster than its working temperature. Therefore, this enables the correlation of two speckle patterns generated by two wavelengths in the same image frame in a fibre based ESPI system. In this measurement, the laser diode emission wavelength was modulated, between λ_1 and λ_2 , at a frequency much greater than the image frame update rate (at least 1 kHz due to the software limitation). Correlation fringes obtained by sequential subtraction were more stable since the thermal drift was greatly reduced.

The wavelength difference was measured using a scanning Fabry-Pérot interferometer for which the free spectral range had been set to $1 \pm 0.2\%$ nm using a monochromator and a broad band light source.

Three simple geometric objects and a gas turbine blade were used as test objects, Fig. 4.2 and Fig. 4.3 (page 95-1), to evaluate the techniques. The three simple objects are a conical test object (with 12.5 cm base diameter and 17.2 cm high), a cylindrical tin can (9.5 cm diameter and 13 cm high), and a spherical plastic ball (with 6.2 cm radius). The gas turbine blade is approximately 170 mm in height, 110 mm in width and has an overall depth of approximately 40 mm. In slope measurements, the viewing and observation distances were approximately 1200 mm, and the x direction image shear was $\delta x = 4$ mm.

For quantitative analysis of slope variations on the object, a three-step phase stepping technique [4.51] was implemented by moving one of the mirrors which is mounted on a PZT actuator. The 2π phase shift of the PZT was calibrated to $\pm 0.5\%$ by a simple program (will be described in chapter 5). The phase stepped fringe patterns were stored in the frame grabber and low pass filtered by a 3x3 convolution filter. These three fringes were then processed by a fringe analysis program [4.52], provided by Dr. P. J. Bryanston-Cross at Warwick University, to get the wrapped and unwrapped phase maps which represent the slope variation of the test objects.

4.5 Results and discussion

4.5.1 Results (figures in this section are shown on pages 95-2 ~ 95-11)

Fig 4.4 shows the contour fringes of the conical object when the wavelength change is 0.076 nm ($\Delta\nu$= 37.5 GHz), corresponding to an effective wavelength of 8 mm. Since the object is inclined from the base to the top, the fringe patterns intrinsically show sections of equal heights on the object.

Fig. 4.5 and Fig. 4.6 show slope fringes of the conical object when the laser diode was modulated to generate wavelength changes of 0.2 nm ($\Delta\nu$=88 GHz) and 0.3 nm ($\Delta\nu$=132 GHz) which correspond to effective wavelengths of 3.4 mm and 2.3 mm

respectively. As expected, the slope variation is more rapid toward the top of the cone, and the larger frequency modulation produces closer spaced fringes on the object surface which demonstrates the tuneable sensitivity of this technique in slope measurement.

Fig. 4.7 and Fig 4.8 show the contour fringes ($\Delta\lambda$ = 0.13 nm, $\Delta\nu$ = 64 GHz, λ_{eff} = 4.6 mm) and slope fringes ($\Delta\lambda$ = 0.45 nm, $\Delta\nu$ = 198 GHz, λ_{eff} = 1.5 mm) of the cylindrical object. These two pictures have the similar fringe patterns, which means the height variation of the object is similar to the slope variation in the x (horizontal) direction.

Fig. 4.9 shows the contour fringes ($\Delta\lambda$ = 0.05 nm, $\Delta\nu$ = 24.6 GHz, λ_{eff} = 12 mm) of the spherical object, and the fringe patterns are concentric circles. Fig. 4.10 shows slope fringes of the spherical objects respectively when the wavelength change is 0.45 nm ($\Delta\nu$=198 GHz), corresponding to an effective wavelength of 1.5 mm. The fringe pattern in Fig. 4.10 is slightly asymmetric due to the effect that the viewing axis did not pass through the centre of the spherical object.

Figures 4.11-4.13 show the theoretical slopes dz/dx of the test objects compared with the experimental results obtained by counting fringes on the horizontal centre line across each image in Figs. 4.6, 4.8 and 4.10. Slope variations were determined from equation (4.8). Although there is a certain error in locating fringe centres due to the coarseness of the fringes, good agreement between the theoretical and measured slopes is still obtained as may be seen in Figs. 4.11-4.13.

The error between the experimental and the theoretical values is increased in the area that is away from the centre of the object due to the variation of C_x and C_z as expected from equation (4.7). Using equation (4.5), the maximum variation of C_x / C_z in the measurement of the conical, cylindrical and spherical objects is 6.24 %, 4.8 % and 6.2 % respectively, when the viewing and observation distances are 1000 mm. If these distances are increased to 2000 mm, the maximum variation of C_x / C_z in the above measurements is reduced by a factor of two.

Figs. 4.14-4.19 show the wrapped and unwrapped phase maps of slope variation dz/dx of the cylindrical, spherical and conical objects. This data represents the three dimensional slope contour measurement and could be integrated to provide direct shape information. As seen in Fig. 4.19, the phase unwrapping for slope fringes of the conical object seems to be unsuccessful. A possible reason is that the slope variation of the conical structure is increased rapidly from the bottom to the top, which makes the fringes more noisy. Fig. 4.20 shows the 3D plot of slope variation of the cylindrical object.

Figs 4.21-4.22 show the contour fringes of the turbine blade, viewed from different angles. In these contour measurements, the contour fringe visibility is greatly effected by the path-length difference between the object and reference beams. This effect is caused by the multi-wavelength operation in one image frame due to the feedback of light, when the diode was modulated. Since the laser diode is directly pigtailed to launch into the fibre, the isolation of the diode from the feedback light might be poor. The fringe visibility of Fig. 4.22 is not as good as that of Fig 4.21, because the speckle decorrelation is more obvious when the wavelength modulation is greater. Fig.4.23 shows the slope fringes of the turbine blade measured by x shear of 20 mm and the optical frequency modulation of 42 GHz. The image shear used was very big due to the small slope variation of the blade structure.

4.5.2 Discussion

In two wavelength slope and contour measurements, the wavelength change ($\Delta\lambda$) is measured using a scanning Fabry-Pérot interferometer for which the free spectral range had been accurately calibrated using a monochromator. Error sources in the phase calculation include the measurement of $\Delta\lambda$, the setting of the free spectral range, and a very small change of speckle phase term ϕ_s, as seen in equation (4.1), due to the speckle decorrelation effect induced by the wavelength change.

In a fibre based ESPI system, contouring by modulating the wavelengths of a laser diode with a certain frequency (e.g. 1 kHz which is much higher than the image update rate) in each image frame generates more stable fringes. The distortion of contour fringes due to the thermal drift between the reference and object beams is not noticeable. However, there is a small phase step calibration error (either calibrated in the wavelength of λ_1 or λ_2) when phase stepping techniques are applied. The maximum phase error is about 0.13° (0.0023 rad) when 3 step technique with 120° phase difference and the wavelength change $\Delta\lambda = 0.45$ nm are applied.

The intensity variation of subtracted images is always very low because half of the dynamic range of the CCD camera is occupied by the non-interference terms (I_r and I_o) and the image speckles also have the tendency of approaching the lower intensity as described in section 2.2.1. Essentially, these images were normalised and filtered before the calculation of the wrapped phase map and the processing of phase unwrapping.

In slope measurement, if the magnitude of image shear is large, the observed correlation fringes will not represent the real slope of the object, but just imply the phase change induced by the variation of the relative height difference between neighbouring points separated by the shearing distance. As seen from the images of slope variations of conical, spherical and cylindrical objects, the fringes at the horizontal edges are very unclear. The reason is that the slope variations of these area are very deep, thus the generated fringes are too fine to be resolved by the CCD camera.

The wavelength modulation range of a laser diode is limited in each operating mode. When mode hopping was used for the measurement, the wavelength is sometimes not so repeatable. An external cavity diode laser [4.53] with a stable and narrow linewidth output would provide more continuous and controllable wavelength modulation.

Theoretically, the unwrapped phase map of the slope variation can be integrated to get a contour map of the test object. However, speckle noise residues in the phase map

normally generate cusps within the map, which could be smoothed out by some curve fitting methods. Fig. 4.24 shows the Contour of the cylindrical object obtained by the integration of the measured slope data (see Fig. 4.12). As seen from this figure, the measured contour data has a certain offset error with respect to the theoretical data, which is generated by the accumulation of the measured slope errors (especially at the edge of the object) during the integration.

4.6 Summary

We have presented a slope measurement technique based on the wavelength modulation of a laser diode in an electronic shearography system. This technique does not require shifting or tilting of the illuminating beam, and thus generates better fringe visibility as speckle decorrelation is reduced.

It has been used to characterise conical, cylindrical and spherical objects, and the experimental results are presented. Comparisons of experimental results with theoretical data are in good agreement, and it has been shown that the error can be reduced by increasing the illumination and viewing distances. The accuracy of phase measurements can be improved by calculating the related parameters C_x , C_y and C_z in the fringe function. As we have demonstrated, this technique is useful for the measurement of objects with different slope variations due to its variable sensitivity that can be achieved in a mechanically passive manner by varying the wavelength change.

When phase stepping methods are combined with this technique, an accurate measurement may be achieved provided that the test object has continuous and limited slope variations across the entire object surface. This technique offers the advantage, compared to illumination-shifting and object-tilting techniques, of no mechanical movement of any of the components required to produce the fringes combined with variable sensitivity and robustness to environmental perturbations compared to ESPI configurations.

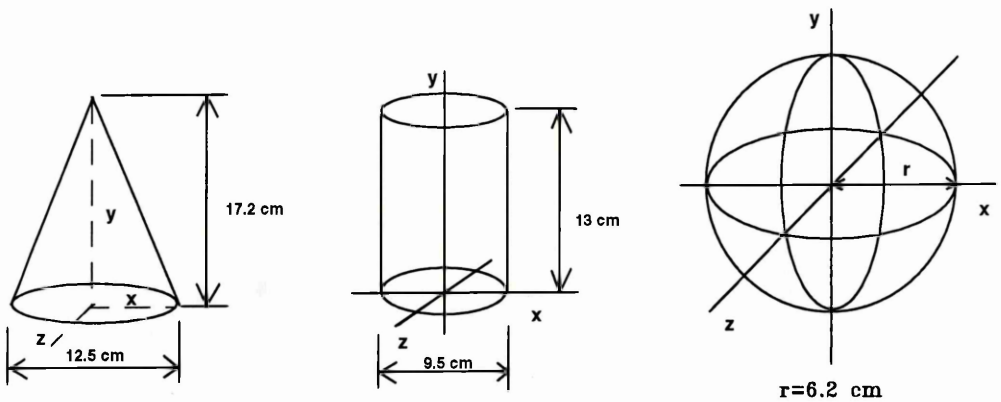

(a) conical (b) cylindrical (c) spherical

Fig. 4.2 Dimensions of conical, cylindrical and spherical test objects

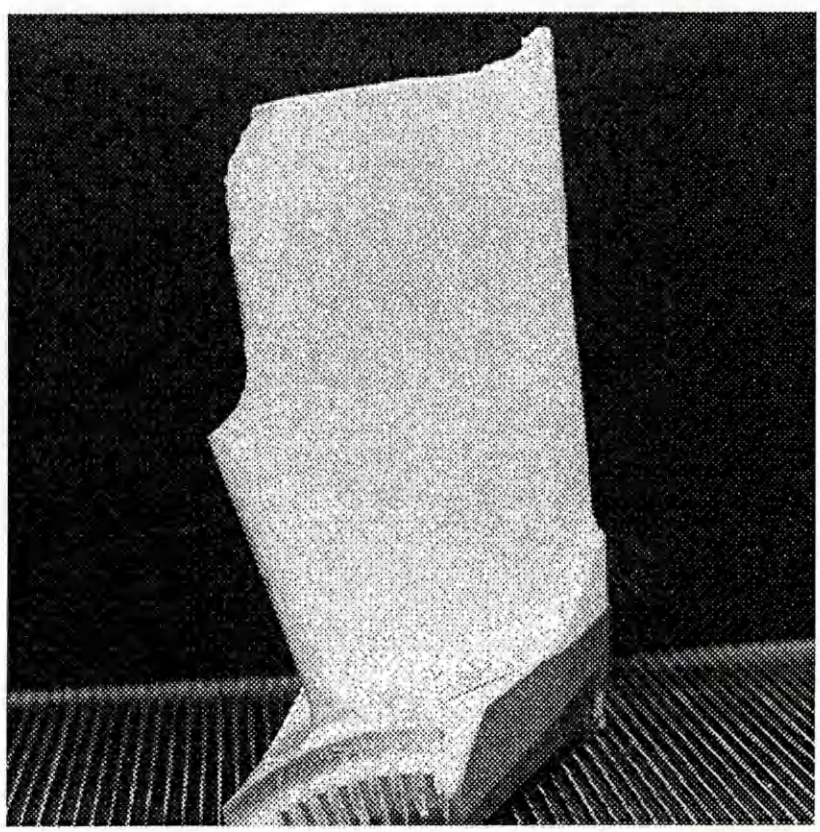

Fig. 4.3 Image of the turbine blade.

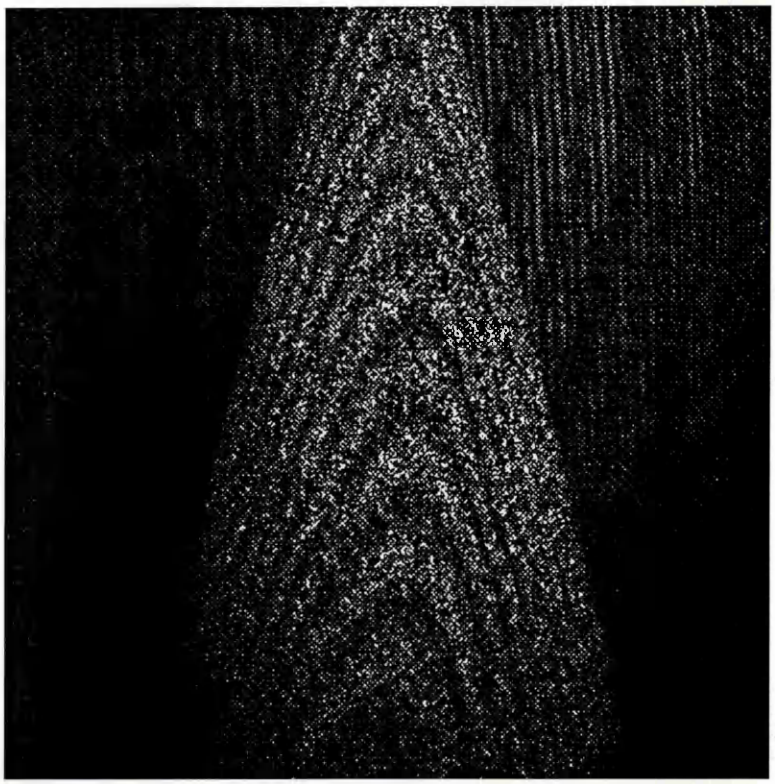

Fig 4.4 Contour fringes of the conical object ($\Delta\lambda = 0.076$ nm, $\lambda_{eff} = 8$ mm)

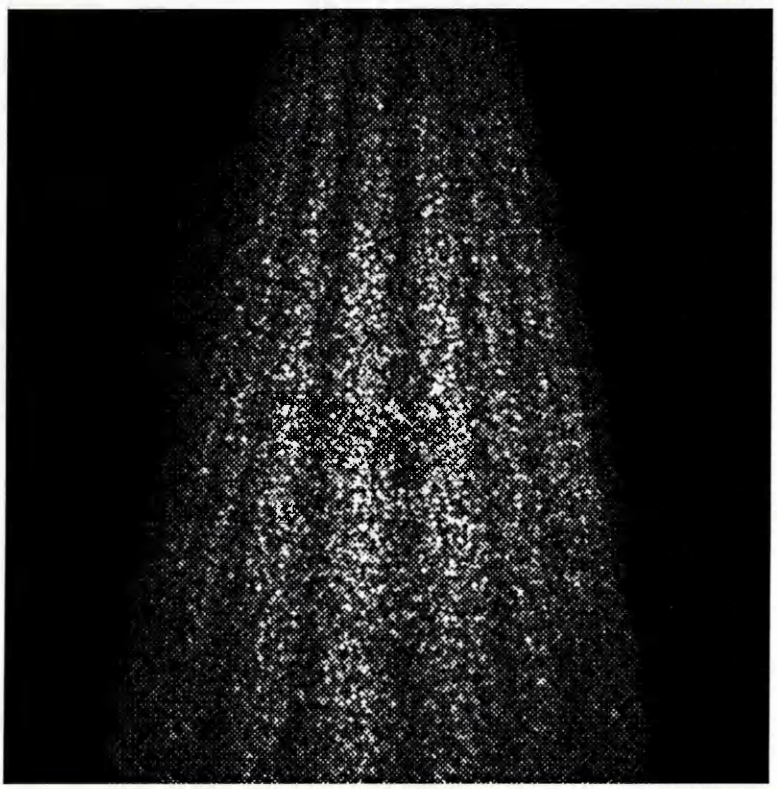

Fig. 4.5 Slope fringes of the conical object ($\delta x = 4$ mm, $\Delta\lambda = 0.2$ nm)

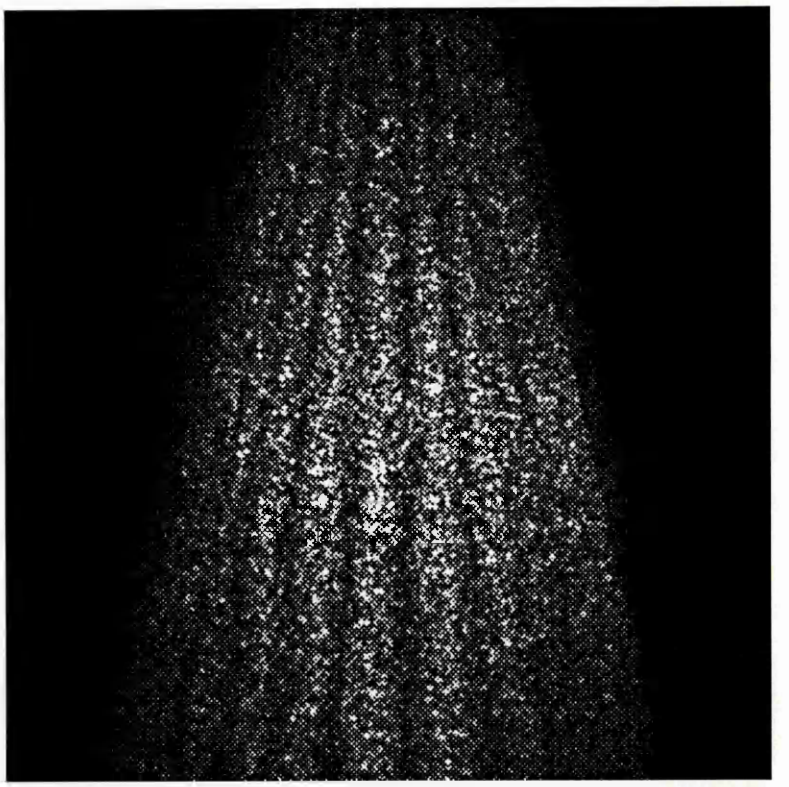

Fig. 4.6 Slope fringes of the conical object ($\delta x = 4$ mm, $\Delta\lambda = 0.3$ nm)

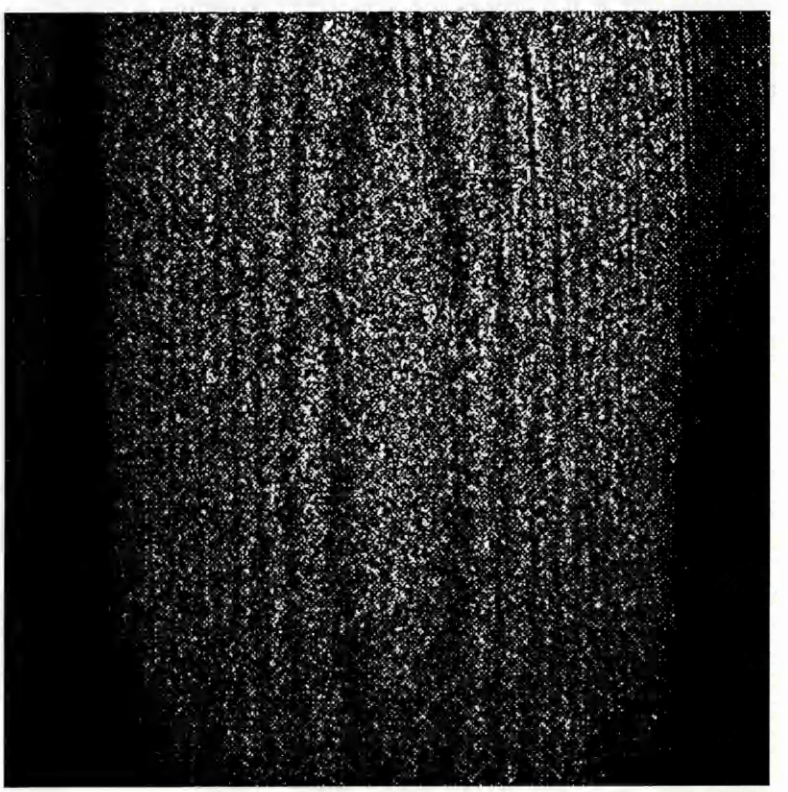

Fig 4.7 Contour fringes of the cylindrical object ($\Delta\lambda = 0.13$ nm, $\lambda_{eff} = 4.6$ mm)

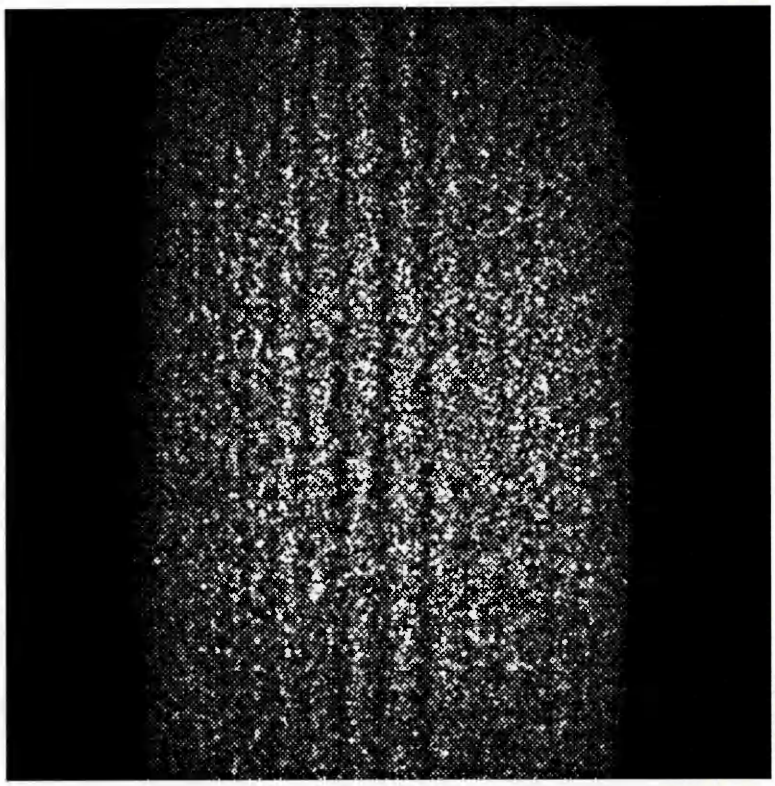

Fig. 4.8 Slope fringes of the cylindrical object ($\delta x = 4$ mm, $\Delta\lambda = 0.45$ nm)

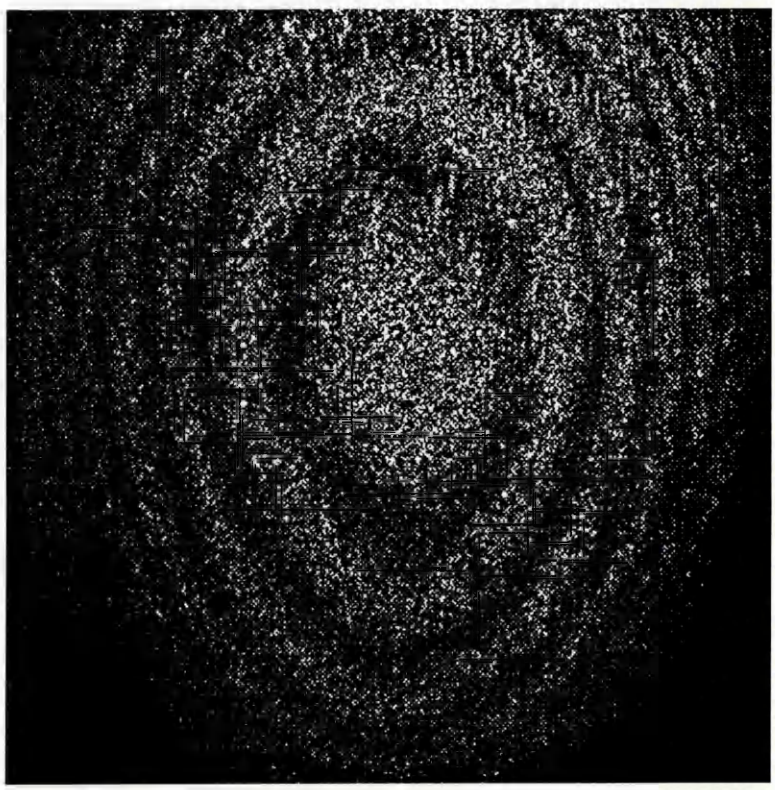

Fig. 4.9 Contour fringes of the spherical object ($\Delta\lambda = 0.05$ nm $\lambda_{eff} = 12$ mm)

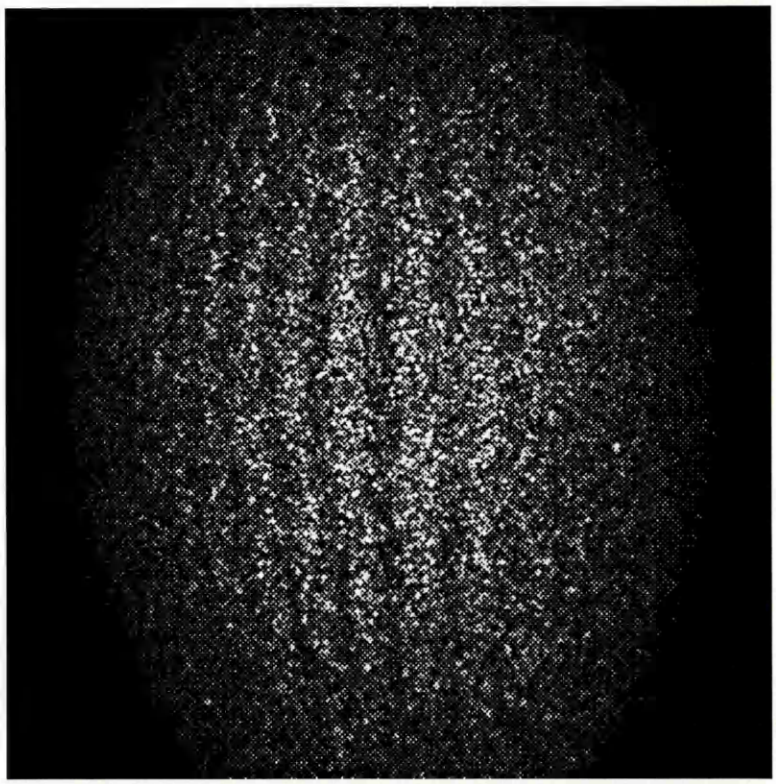

Fig. 4.10 Slope fringes of the spherical object ($\delta x = 4$ mm, $\Delta\lambda = 0.45$ nm)

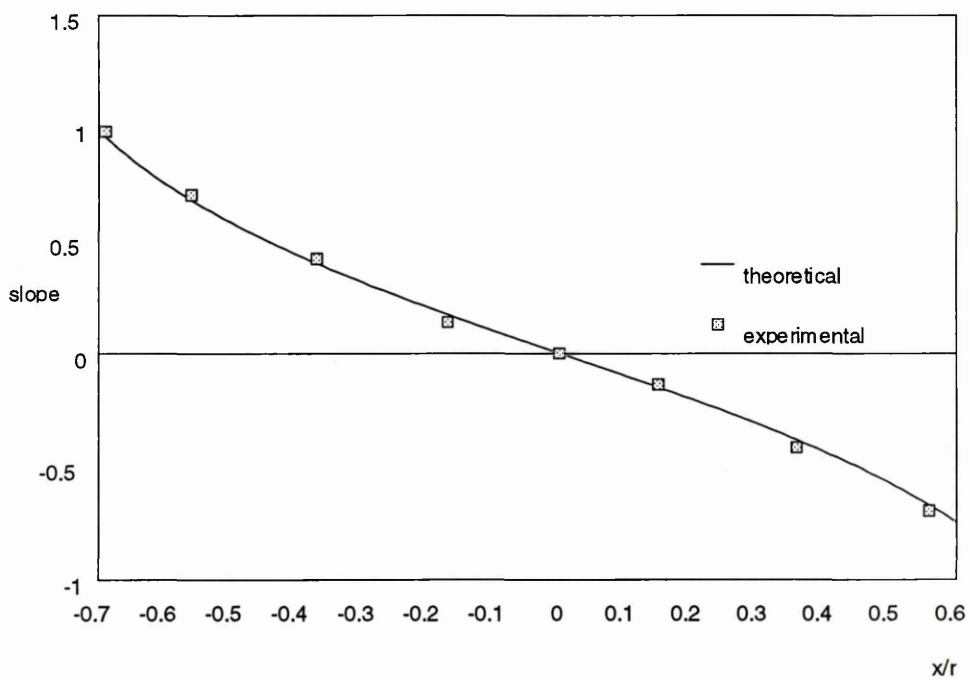

Fig. 4.11 Comparison of theoretical and measured slopes of the conical object

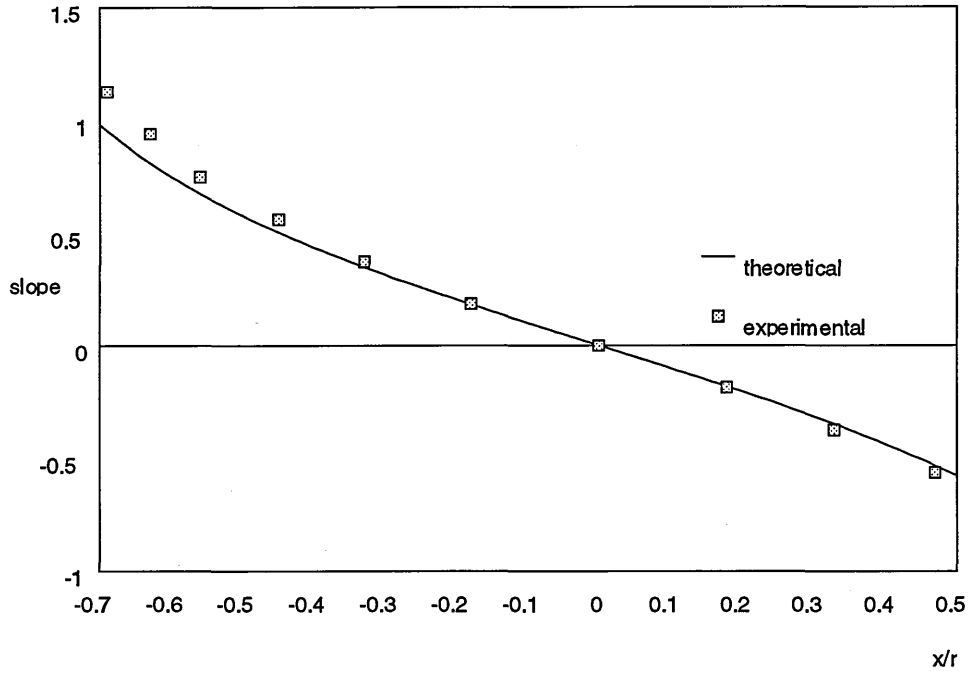

Fig. 4.12 Comparison of theoretical and measured slopes of the cylindrical object

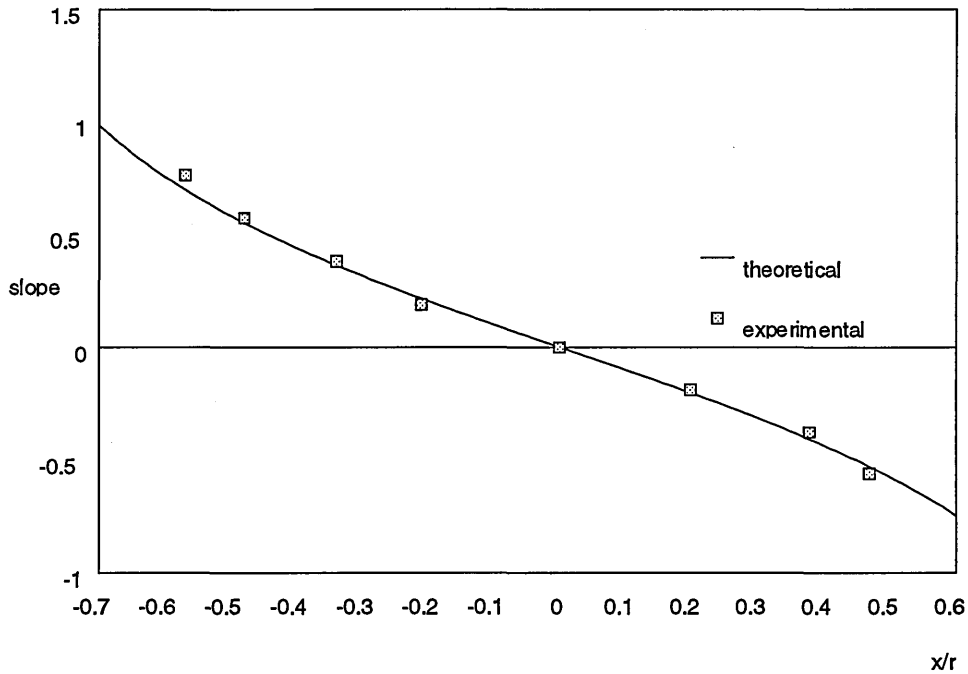

Fig. 4.13 Comparison of theoretical and measured slopes of the spherical object

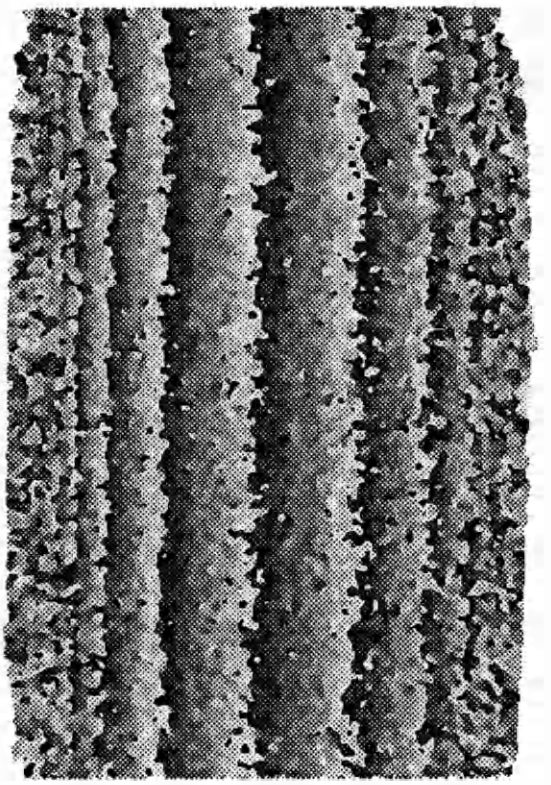

Fig. 4.14 wrapped phase map of slope variation of the cylindrical object.

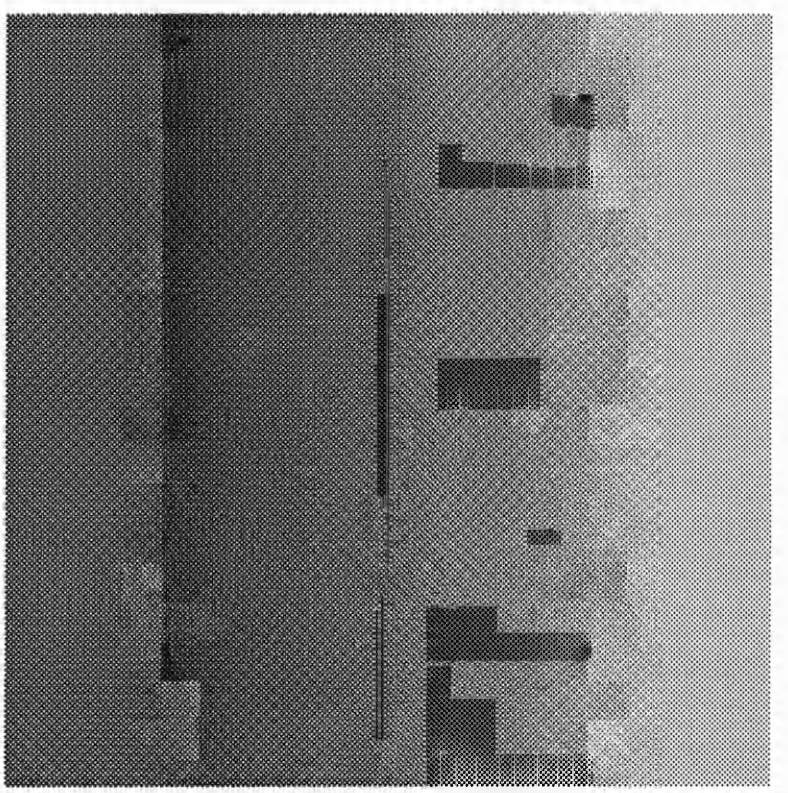

Fig. 4.15 Unwrapped phase map of slope variation of the cylindrical object

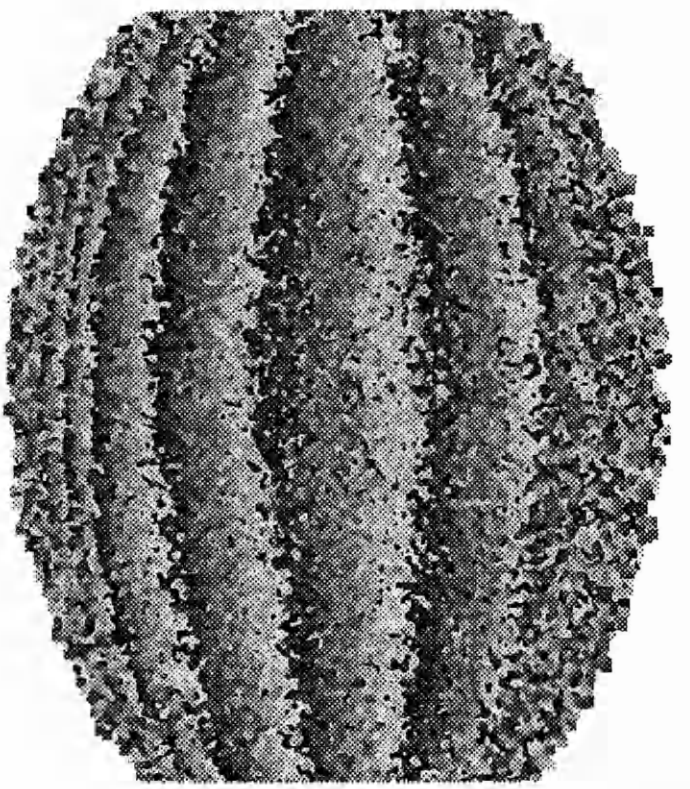

Fig. 4.16 Wrapped phase map of slope variation of the spherical object

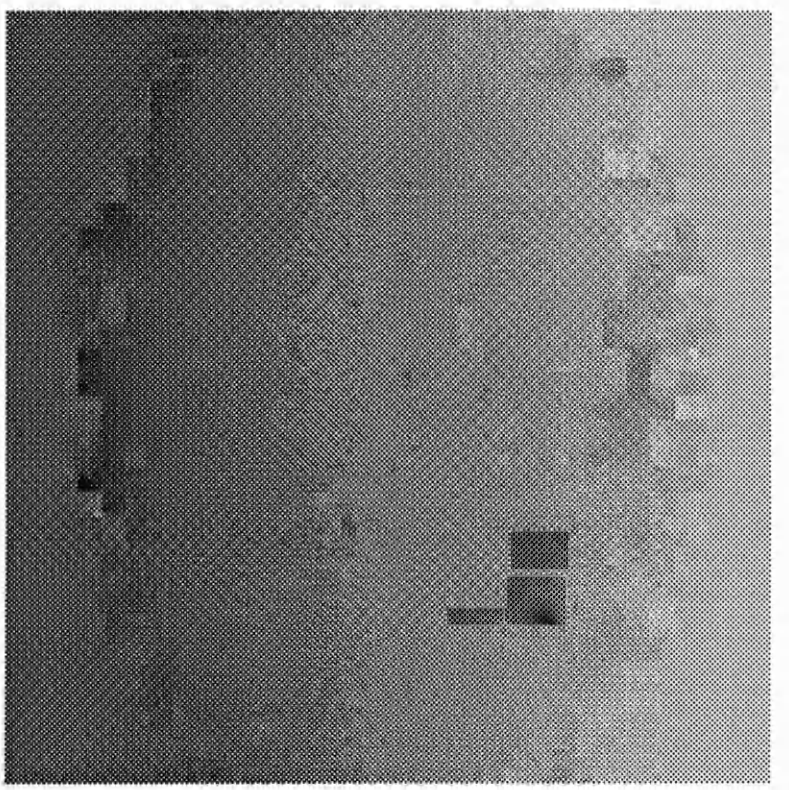

Fig. 4.17 Unwrapped phase map of slope variation of the spherical object

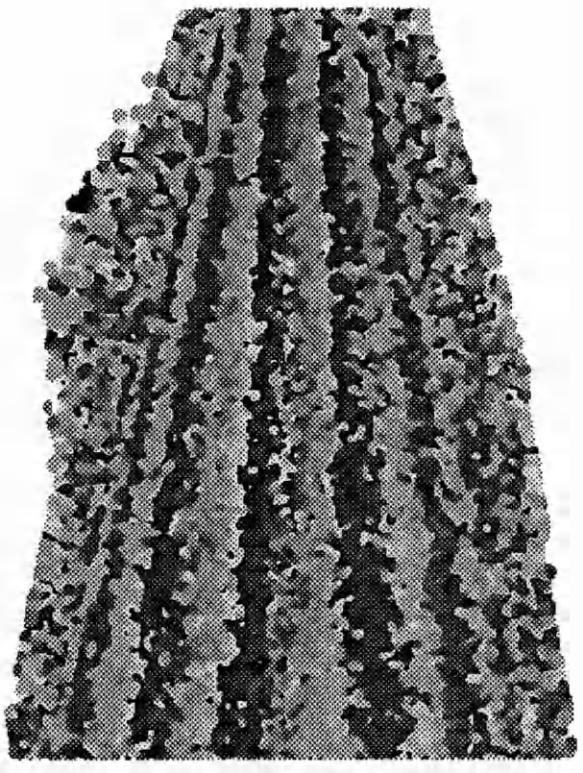

Fig. 4.18 Wrapped phase map of slope variation of the conical object

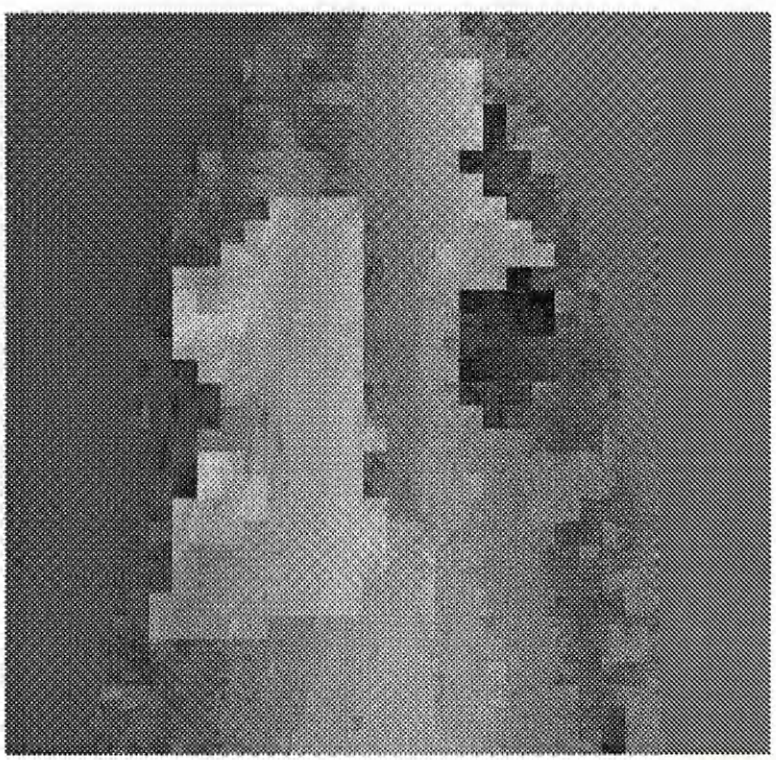

Fig. 4.19 Unwrapped phase map of slope variation of the conical object

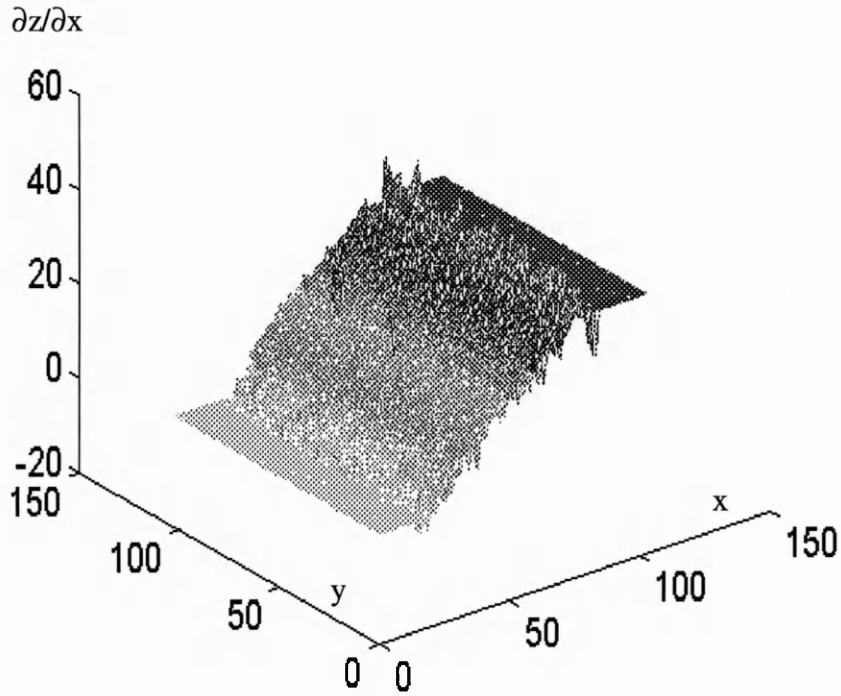

Fig. 4.20 Mesh plot of slope variation in x direction of the cylindrical object (the numbers in x and y axis represent the grid number and each grid is separated by 5 pixels)

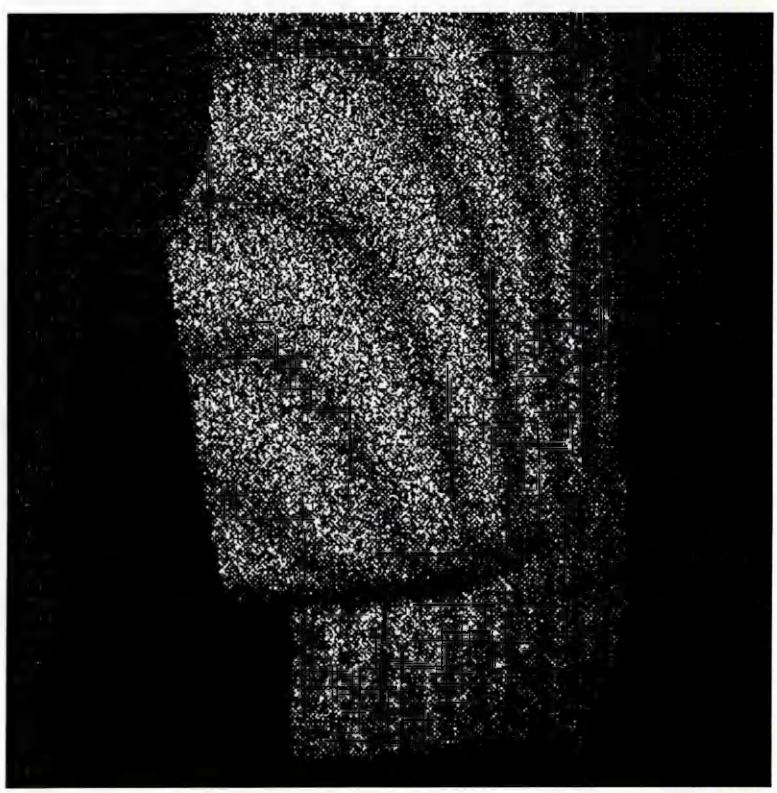

Fig. 4.21 Contour fringes of the turbine blade (view 1)

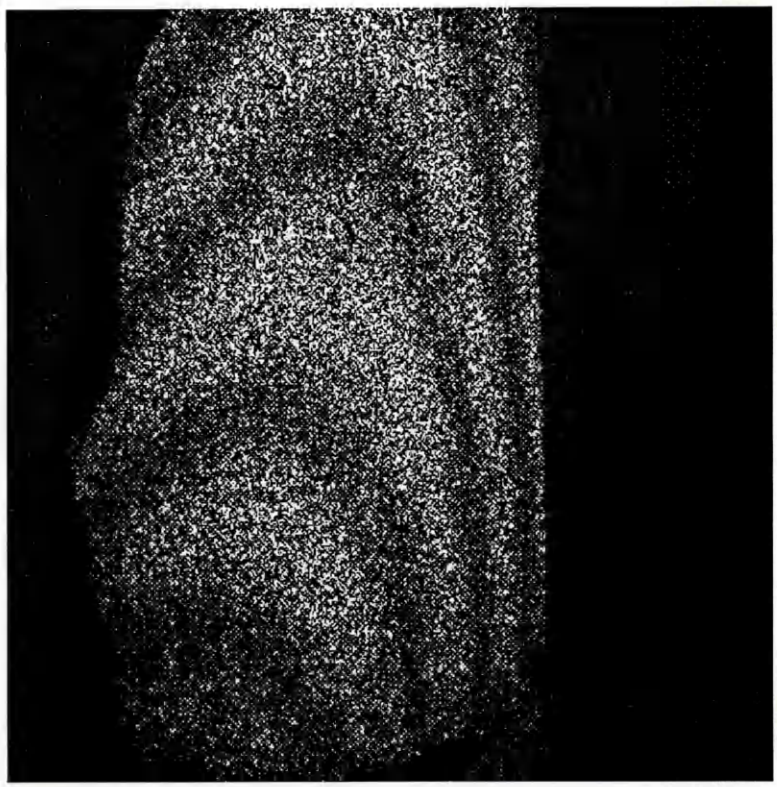

Fig. 4.22 Contour fringes of the turbine blade (view 2)

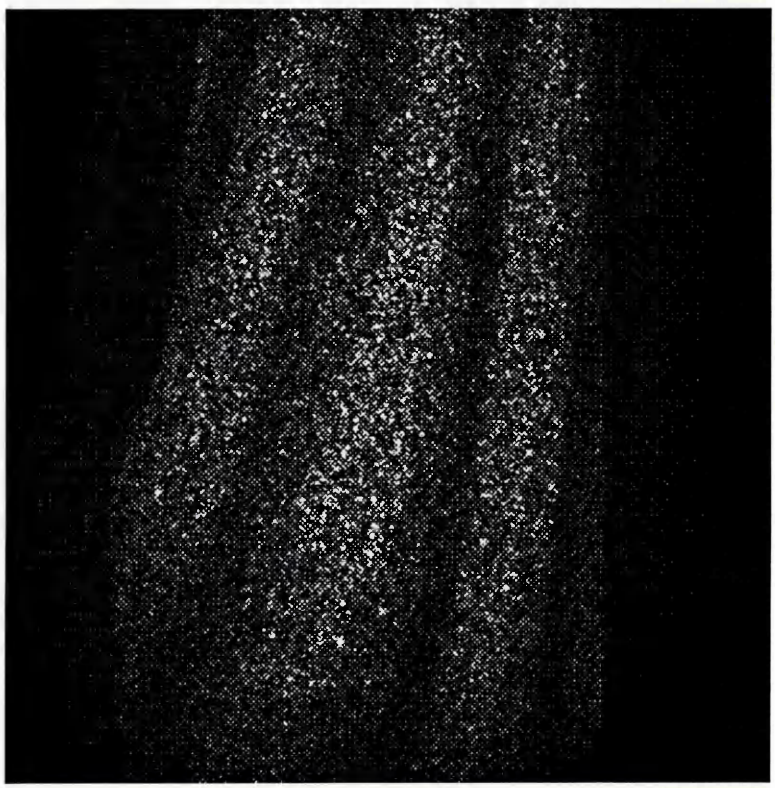

Fig. 4.23 Slope fringes of the turbine blade (δx=20 mm, $\Delta\nu$=42 GHz)

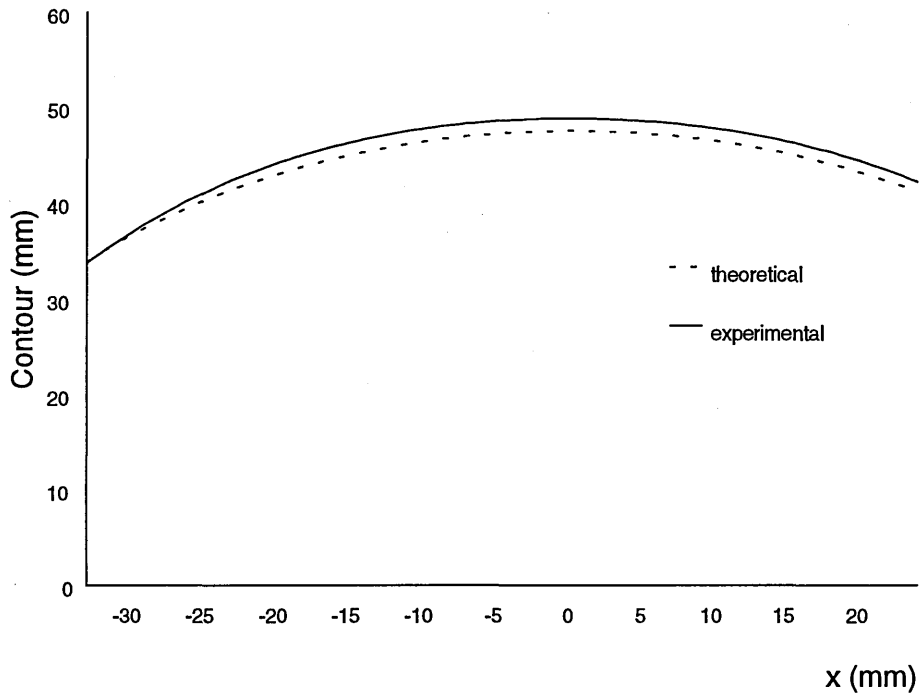

Fig. 4.24 Contour of the cylindrical object obtained by the integration of the measured slope data (see Fig. 4.12)

References

4.1 Jones, R. and Wykes, C., *Holographic and Speckle Interferometry*. Cambridge University Press, Cambridge, 2nd ed., (1989) 197-238.

4.2 Hung, Y. Y., Turner, J. L., Tafralian, M., Hovanesian, J. D. and Taylor, C. E., Optical method for measuring contour slopes of an object. *Appl. Opt.*, **17** (1) (1978) 128-131.

4.3 Hung, Y. Y. and Hovanesian, J. D., Full-field Surface-strain and Displacement Analysis of Three-dimensional Objects by Speckle Interferometry. *Exp. Mechanics*, **12** (10) (1972) 454-460.

4.4 Hsu, T. C., Shang, H. M., Lee, T. C. and Lee, S. Y., Flow stresses in sheet material formed into nearly spherical shapes. *J. Eng. Materials Technol., Trans. ASME*, **97** (1975) 57-65.

4.5 Tay, C. J., Shang, H. M., Chau, F. S. and Toh, S. L., Curvature measurement of hydroformed axisymmetrical shells using shearography. *Exp. Techniques*, **17** (6) (1993) 27-29.

4.6 Gasvik, K. J., Moire technique. Optical Metrology, Chap. 5, John Wiley & Sons, (1987) 117-144.

4.7 Patorski, K., Handbook of the moire fringe technique. Elsevier, Amsterdam, (1993).

4.8 Post, D., Han, B. T. and Ifju, P., High sensitivity moire: experimental analysis for mechanics and materials. Springer-Verlag, New York, (1994).

4.9 Rowe, S. H., Welford, W. T., Surface topography of non-optical surfaces by projected interference fringes. *Nature*, **216** (1967) 786-787.

4.10 Brooks, R. E., Heflinger, L. O., Moire gauging using optical interference patterns. *Appl. Opt.*, **8** (5) (1969) 935-939.

4.11 Srinivasan, V., Liu, H. C. and Halioua, M., Automated phase-measuring profilometry of a 3-D diffuse objects. *Appl. Opt.*, **23** (1984) 3105-08.

4.12 Hovanesian, J. D., Hung, Y. Y., Moire contour-sum, contour-difference, and vibration analysis of arbitrary objects. *Appl. Opt.*, **10** (1971) 2734-38.

4.13 Dessus, B., Leblance, M., Fringe method and its application to the measurement of deformation, vibrations, contour lines, and differences of objects. *Opt. Elect.*, **5** (1973) 369-391.

4.14 Benoit, P., Mathieu, E., Hormiere, J., Thomas, A., Characterisation and control of three dimensional objects using fringe projection techniques. *Nouv. Rev.*, **6** (1975) 67-86.

4.15 Moga, P. J. and Cloud, G. L., A study of scapular displacement by differential moire methods. Proc. Conference on Experimental Mechanics, Bethel, CT: Society for Experimental Mechanics, (1991) 736-750.

4.16 Takasaki, H., Moire topology. *Appl. Opt.*, **9** (6) (1970) 1457-72.

4.17 Takasaki, H., Moire topology. *Appl. Opt.*, **12** (4) (1973) 845-850.

4.18 Meadows, D. M., Johnson, W. O. and Allen, J. B., Generation of surface contours by moire patterns. *Appl. Opt.*, **9** (4) (1970) 942-947.

4.19 Reid, G. T., Rixon, R. C., Messer, H. I., Absolute and comparative measurements of three dimensional shape by phase measuring moire topography. *Opt. and Laser Technol.*, **16** (6) (1984) 315-319.

4.20 Kakunai, S., Iwata, K., Hasegawa, M. and Sakamoto, T., Profile measurement by projecting phase-shifted interference fringes. *SPIE*, Vol. 1163 (1989) 128-137.

4.21 Mercer, C. R. and Beheim, G., Fibre-optic projected-fringe digital interferometry. *SPIE*, Vol (1990) 210-216.

4.22 Haines, K. and Hilderbrand, B. P., Contour generation by wavefront reconstruction. *Phys. Lett.*, **19** (1) (1965) 10-11.

4.23 Hilderbrand, B. P. and Haines, K., Multiple-wavelength and multiple-source holography applied to contour generation. *J. Opt. Soc. Am.*, **57** (2) (1967) 155-162.

4.24 Tsuruta, T., Shiotake, N., Tsujinchi, J. and Matsuda, K., Holographic generation of contour map of diffusely reflecting surface by using immersion method. *Jap. J. Appl. Phys.*, **6** (1967) 661-662.

4.25 Zalenka, J. S. and Varner, J. R., Multi-index holographic contouring. *Appl. Opt.*, **8** (7) (1969) 1431-34.

4.26 Marrone, E. S. and Ribbens, Dual index holographic contour mapping over a large range of contour spacing. *Appl. Opt.*, **14** (1) (1975) 23-24.

4.27 Hariharan, P. and Oreb, B. F., Two-index holographic contouring - applications of digital techniques. *Opt. Commun.*, **51** (3) (1984) 142-144.

4.28 Abramson, N., Sandwich hologram interferometry 3: contouring. *Appl. Opt.*, **15** (1) (1976) 200.

4.29 Abramson, N., Holographic contouring by translation. *Appl. Opt.*, **15** (1976) 1018.

4.30 Quan, C. and Bryanston-Cross, P. J., Double source holographic contouring using fibre optics. *Opt. & Laser Technol.*, 22 (4) (1990) 255-259.

4.31 Denby, D., Quintanilla, G. E. and Butters, J. N., The Engineering uses of coherent optics. ed. Robertson, E. R., Cambridge University Press, Cambridge, (1975) 171-197.

4.32 Fercher, A. F., Hugh, Z. and Vry, U., Rough surface interferometry with a two-wavelength heterodyne speckle interferometer. *Appl. Opt.*, 24 (1985) 2181-88.

4.33 Tatam, R. P., Davies, J. C., Buckberry, C. H. & Jones, J. D. C., Holographic surface contouring using wavelength modulation of laser diodes. *Optics & Laser Technology*, **22** (5) (1990) 317-321.

4.34 Atcha, H., Tatam, R. P., Buckberry, C. H., Davies, J. C. & Jones, J. D. C., Surface contouring using TV holography. *SPIE*, Vol. 1504 (1991) 221-232.

4.35 Atcha, H. & Tatam, R. P., The use of laser diodes and monomode optical fibre in electronic speckle pattern interferometry. *SPIE*, Vol. 1584 (1991) 425-434.

4.36 Diao, H. Y., Peng, X., Zou, Y. L., Tiziani H. J. & Chen, C., Contouring using two-wavelength electronic speckle pattern interferometry employing dual-beam illuminations. *Optik*, **91** (1) (1992) 19-23.

4.37 Rastogi, P. K., Displacement and deformations. ed. Sirohi, R. S., *Speckle metrology*. Marcel Dekker Inc., New York, (1993) 85-87.

4.38 Jaisingh, G. K. & Chiang, F. P., Contouring by laser speckle. *Appl. Opt.*, **20** (19) (1981) 3385-87.

4.39 Ganesan, A. R. & Sirohi, R. S., New method of contouring using digital speckle pattern interferometry (DSPI). *SPIE*, Vol. 954 (1988) 327-332.

4.40 Winther, S. and Slettemoen, G. A., An ESPI contouring technique in strain analysis. *SPIE*, Vol. 473 (1984) 44-47.

4.41 Bergquist, B. D. and Montgomery, P., Contouring by electronic speckle pattern interferometry (ESPI). *SPIE*, Vol. 599 (1985) 189-195.

4.42 Rodriguez-Vera, R., Kerr, D. & Mendoza-Santoyo, F., Electronic Speckle Contouring. *J. Opt. Soc. Am.*, **A9** (1992) 2000-2008.

4.43 Peng, X., Diao, H. Y., Zou, Y. L. & Tiziani H., Contouring by modified dual-beam ESPI based on tilting illumination beams. *Optik*, **90** (2) (1992) 61-64.

4.44 Huang, J-R. and Tatam, R. P., Optoelectronic shearography: two wavelength slope measurement. *SPIE*, Vol. 2544 (1995) 300-308.

4.45 Huang, J-R., Ford, H. D. and Tatam, R. P., Slope measurement by two-wavelength electronic shearography. Accepted for publication in *Optics. and Lasers in Eng.*

4.46 Montgomery, P. C., Forward looking in electronic speckle pattern interferometry. PhD thesis, Loughborough University of Technology, (1987) 127-158.

4.47 Hung, Y. Y., Displacement and strain measurement. *Speckle metrology*, ed. Erf, R. K., Academic Press, London (1978) 68-70.

4.48 Tay, C. J., Chau, F. S., Shang, H. M., Shim, V. P. W. & Toh, S. L., The Measurement of Slope Using Shearography. *Optics and Lasers in Eng,* **14** (1991) 13-24.

4.49 Tay, C. J., Shang, H. M., Poo, A. N. & Luo, M., On the determination of slope by shearography. *Optics and Lasers in Eng*, **20** (1994) 207-217.

4.50 Rastogi, P. K., Measurement of the derivatives of curved surfaces using speckle interferometry. *J. Modern Optics*, **41** (4) (1994) 659-661.

4.51 Creath, K., Temporal Phase Measurement Methods. *Interferogram Analysis - Digital Fringe Pattern Measurement Techniques*, ed. Robinson, D. W. and Reid, G. T., IOP Publishing Ltd, Bristol, (1993) 94-140.

4.52 Towers, D. P., Judge, T. R. and Bryanston-Cross, P. J., Automatic Interferogram Analysis Techniques Applied to Quasi Heterodyne Holography and ESPI. *Optics and Lasers in Eng*, **14** (1991) 239-282.

4.53 Environmental Optical Sensors Inc., 2395 Gunpark Drive, Boulder, Colorado, 80301-3376, USA.

4.54 Yonemura, M., Wavelength-change characteristics of semiconductor lasers and their application to holographic contouring. *Opt. Lett.*, **10** (1985) 1-3.

4.55 Kujawinska, M. and Patorski, K., Application of moire techniques in biomedicine. *SPIE*, Vol. 1647 (1992).

5. PHASE STEPPING USING LASER DIODE WAVELENGTH MODULATION

Phase stepping is an efficient and accurate method for the determination of phase distributions in interferograms. It has been applied in almost all types of interferometer especially in full field optical techniques, e.g. holographic interferometry [5.1,5.2], ESPI [5.3-5.5], moire topography [5.6,5.7], and photoelasticity [5.8].

Practically, phase stepping is performed by shifting the phase of one arm of the interferometer with respect to the other. The phase shift can be generated in different ways, e.g. by moving a mirror mounted on a piezoelectric transducer (PZT) [5.3], tilting a glass plate [5.9,5.10], modulating liquid crystals [5.11-5.13], translating a diffraction grating [5.14], rotating a polariser or wave plate [5.15,5.16], stretching an optical fibre [5.17,5.18], or modulating the wavelength of light source in an unbalanced interferometer [5.19-5.21].

In shearography, phase stepping has been reported using polarisation phase shifters [5.16], liquid-crystal phase shifters [5.11,5.12] and piezoelectric transducers [5.18,5.22]. This chapter presents another phase stepping for shearography, using diode wavelength changes via injection current modulation.

5.1 The principle

In a two beam interferometer, the phase difference between two optical paths can be expressed as

$$\phi = \frac{2\pi}{\lambda}\Delta l = \frac{2\pi\nu}{c}\Delta l \qquad (5.1)$$

where, λ and ν are the wavelength and frequency of the light source respectively, and Δl is the optical path length difference. When the wavelength (or optical frequency) of the light source is changed, the resulting phase change $\Delta\phi$ is given by

$$\Delta\phi = -\frac{2\pi}{\lambda^2}\cdot\Delta l\cdot\Delta\lambda = \frac{2\pi\cdot\Delta l\cdot\Delta\nu}{c} \tag{5.2}$$

where, $\Delta\lambda$ and $\Delta\nu$ are the wavelength and frequency changes of the light respectively. For diode laser sources, the application of a ramp modulation signal to the injection current produces a concomitant linear variation in the optical frequency of the output light [5.23,5.24], and hence provides the phase shift in an unbalanced interferometer.

To perform phase stepping in shearography using laser diode wavelength modulation, a certain path length imbalance is required. With the Michelson interferometer arrangement, as shown in Fig. 3.3, the path lengths of the two sheared images can be easily unbalanced by adjusting the distances of the mirrors to the beamsplitter. However, two potential difficulties arise since the path-length difference between the image-sheared wavefronts results in two images with different image magnification and focal distances.

The problem can be overcome by inserting a parallel-sided block of high refractive-index material, e.g. a perspex block, into the longer interferometer arm [5.25] adjacent to the mirror, Fig. 5.1. The block acts as a lens of zero power which changes the apparent position of the object without altering its apparent size.

As shown in Fig. 5.1, the physical path-length difference in the interferometer is $2(l_2 - l_1)$. For a perspex block with a refractive index of n_b, the required thickness l of the block is given by [5.25]

$$l = \frac{n_b}{n_b - 1}(l_2 - l_1) \tag{5.3}$$

The perspex block can correct the difference of magnifications and focal distances between the two sheared images. It also helps to increase the optical path-length imbalance. The optical path-length difference, ΔL, generated in the Michelson interferometer arrangement is given by

$$\Delta L = 2(l_2 - l_1) + 2(n_b - 1)l = 2(1 + n_b)(l_2 - l_1) \tag{5.4}$$

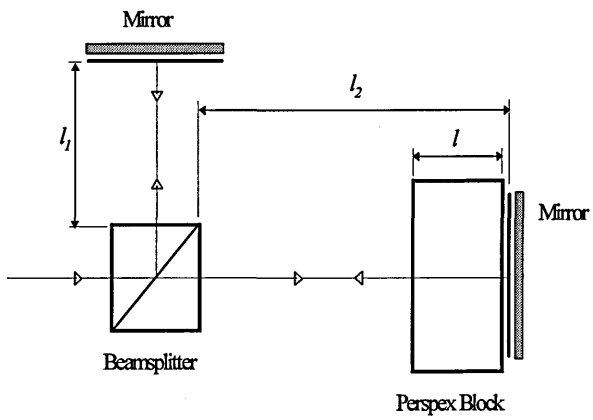

Fig 5.1 Details of unbalanced interferometer

In shearography, if the image shear is in the x direction by an amount δx, light reflected from two neighbouring points P(x, y) and P(x+δx, y) will be brought to interfere at the same point O(x_o, y_o) in the image plane. The intensity of the speckle image (interferogram) can be expressed as

$$I(x_o, y_o) = I_1 + I_2 + 2\sqrt{I_1 I_2}\cos(\phi + \phi_s) \tag{5.5}$$

where I_1 and I_2 are the intensities of the two image-sheared wavefronts respectively, ϕ_s is the speckle phase, and ϕ is the phase difference between these two beams. In the unbalanced optical arrangement, ϕ is given by

$$\phi = \frac{2\pi}{\lambda}(\Delta L + \delta l) = \frac{2\pi}{\lambda}\left[\Delta L + (C_x \delta x + C_z \delta z)\right] \tag{5.6}$$

where, $\delta l = (C_x\delta x + C_z\delta z)$ is the path length difference induced by the image shear and object height variation, as derived in equation (4.6). When the illumination and the viewing directions are collinear, and the object size is small compared with the illumination and viewing distances, $\delta l = 2\delta z$. The phase change due to the wavelength change of light becomes

$$\Delta\phi = -\frac{2\pi}{\lambda^2}(\Delta L + 2\delta z)\Delta\lambda = \frac{2\pi}{c}(\Delta L + 2\delta z)\Delta\nu \tag{5.7}$$

As seen from equation (5.7), the phase change in the interferogram is effected by the height variation between the neighbouring points on the object. To reduce this effect, a relatively large path-length imbalance (compared to the height variation) is required. If $\Delta L >> \delta z$, equation (5.7) can be simplified to become

$$\Delta\phi = -\frac{2\pi}{\lambda^2} \cdot \Delta L \cdot \Delta\lambda = \frac{2\pi}{c} \cdot \Delta L \cdot \Delta\nu \tag{5.8}$$

5.2 Experimental

This phase stepping method has been applied in the measurement of static deformation. A flat aluminium plate, 150 mm wide and 100 mm high, was used as a test object. The plate was clamped around the edge and mechanically loaded at the centre of the back surface. The thickness of the perspex block is 25 mm with a refractive index of 1.495, which can compensate the image magnification difference for a physical path length imbalance of 16.7 mm. The total path length imbalance in this arrangement is 41.7 mm. Thus for a 2π phase shift, an optical frequency change of 7.25 GHz is required.

The laser diode was modulated by applying a voltage from a D/A board housed in the same PC as the frame grabber (the voltage is digitised to a 12 bit integer number, i.e. the resolution is 4095) to its injection current. The phase change in the interferogram with respect to the applied voltage was calibrated by a simple program. The procedure of this program is described below.

(1) The voltage level for the diode injection current modulation is set via the D/A board to a minimum value (normally zero). (2) A speckle image is stored in an image frame on the frame grabber. (3) After increasing the voltage input from the D/A board (the voltage increment, V_{inc}, is 0.00122 V), another image is stored. (4) The images are subtracted and rectified. (5) The intensity of a small window of image pixels (from 10x10 ~ 50x50 pixels) are summed and stored in an integer array. (6) The procedure from step (1) to step (5) is repeated N times with the voltage level increased, i.e. $V = (N+1)V_{inc}$, until the required modulation range ($V > V_{max}$) has reached, e.g. at least more than 2π phase shift has been generated. (7) The summed intensities stored in the array are normalised and graphically displayed. The 2π phase shift is then evaluated by fitting the intensity curve manually.

A flow chart of this procedure is shown in Fig. 5.2. In this program, the speckle images acquired are real-time processed by the sequential subtraction mode (see section 2.4.3). This is especially suitable for the phase shift calibration in a fibre based ESPI system, because the reference image is obtained when the modulation voltage is reset to zero and hence the phase change is less susceptible to thermal drift. To suppress the noise effect (e.g. speckle and electronic noise), the biggest window (50x50 pixels) was normally used. The voltage for a 2π phase shift was measured as 0.26 V$\pm$ 0.5%. This program has also been used for the calibration of the PZT transducer, e.g. in slope and contour measurement.

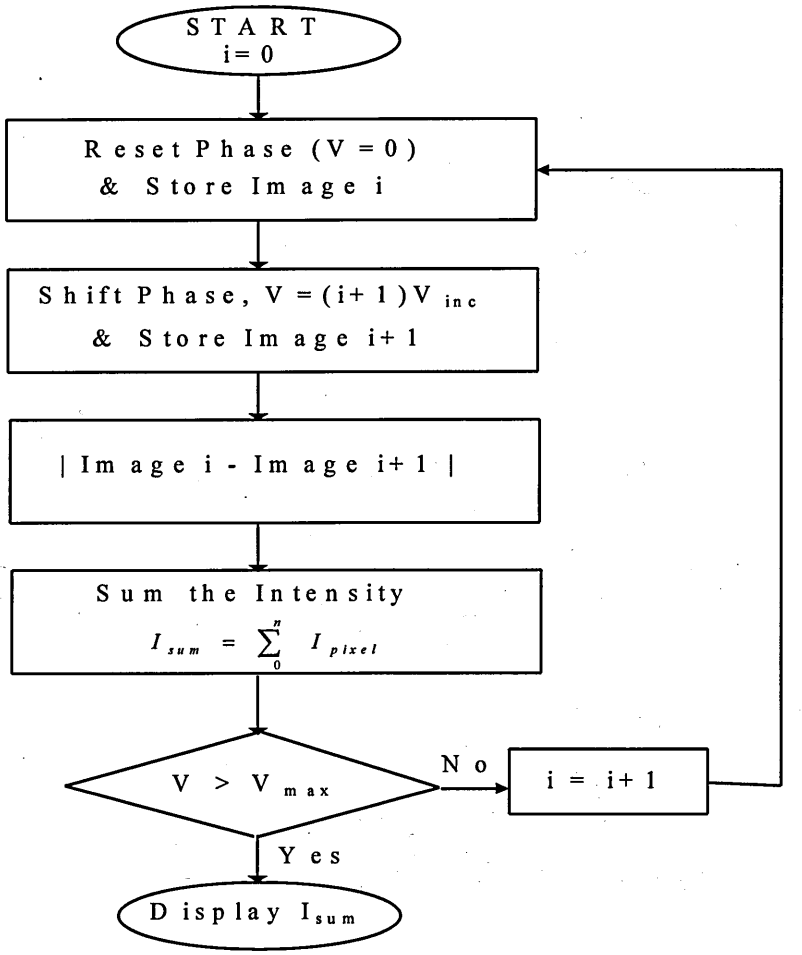

Fig. 5.2 The procedure of phase shift calibration

The optical frequency change of the laser diode was measured using a confocal Fabry-Pérot interferometer with 2 GHz free spectral range and a finesse of ~200. The injection current of the laser diode was modulated by different amounts (from 1 mA to 8 mA with a step of 0.5 mA). The ratio of the optical frequency change to the injection current change was measured to be 1.433 GHz/mA with an error of ±1% (the diode temperature is 18.01°C and the initial current is 100.01 mA). The optical frequency change required for a 2π phase change is 7.453 GHz, which is slightly (2.7%) bigger than the calculated value of 7.25 GHz. The difference might be generated by the deviation of the refractive index and the measured physical path length imbalance, however, this does not effect the measurement accuracy.

A three-step (each step = $2\pi/3$) phase stepping method [5.26] was used. The phase stepped fringes were normalised and low pass filtered by a 5x5 convolution filter, and then processed by a fringe analysis program [5.27] provided by Dr. P. J. Bryanston-Cross at Warwick University to get the wrapped and unwrapped phase maps which represent gradients of deformation on the object surface.

5.3 Results and discussion

Figs. 5.3-5.5 show three phase stepped fringes, of which the shear amount is 6 mm in the x (horizontal) direction. Fig. 5.6 and Fig. 5.7 show the wrapped and unwrapped phase maps calculated from the phase stepped images. Fig. 5.8 shows the 3D plot of the deformation gradients on the object. It can be seen from Fig. 5.8 that the gradient of deformation is positive on the left of the object, and negative on the right.

To achieve an accurate phase measurement, the potential error sources and their effect must be reduced. The stepped phase angles should be well calibrated since they could generate quite significant error in the phase calculation. For phase stepping using wavelength modulation in shearography, the phase shift in each pixel is effected by the height variation of the object surface, as seen from equation (5.7). In this work, the test object is a flat surface located perpendicular to the viewing axis, and also measured from a long distance (1.2 m), therefore this effect is negligible. However, if the object is curved, the error will become more obvious. To evaluate the phase shift error, an unbalanced shearography system with 167 mm path length imbalance (the thickness of the perspex block is now assumed 100 mm) and 6 mm shear is assumed to measure a flat surface at different tilted angles with respect to the viewing axis. The phase shift error is calculated and shown in Fig. 5.9. If a smaller perspex block, e.g. 50 mm, is used, the phase shift error is double that of using 100 mm block.

Other error sources, including the electronic noise which is related to the gain setting of CCD camera, the frame grabbers and its sensitivity to DC voltage supplied by the PC, and the linearity of the CCD camera also should be calibrated or optimised.

For phase stepping techniques using laser injection current modulation, the output power of the laser is effected by the current modulation [5.28]. This violates the assumption of constant intensity in most of the phase extraction algorithms [5.26]. The problem can be overcome by normalising the intensity of the phase stepped images with a factor obtained by monitoring the intensity variation of the laser light using a photodetector [5.29]. Alternatively, a six step phase extraction algorithm which is insensitive to the changes of laser power [5.30] or the use of a constant amplitude laser diode source [5.31] are also feasible solutions.

5.4 Summary

A novel phase stepping technique using laser diode injection current modulation has been demonstrated, which provides additional phase shifting method in electronic shearography. An unbalanced Michelson-interferometer arrangement, with a thick perspex block inserted into the longer arm of the interferometer, was used to accomplish the task. Advantages of this technique include the removal of an active phase-shifting component for phase stepping which reduces electrical signals in the detection head and a greater linearity in the phase shifts through the wavelength modulation of laser diodes.

However the main disadvantage of this technique is that the phase shift accuracy is effected by the error induced by the height variation on the object surface. This is an inherent characteristic of phase stepping methods using wavelength modulation. In principle, a greater path length imbalance can be applied to make this error negligible. For the shearing device in this work, a perspex or glass block with a larger thickness should be used, whilst the size of the detection head will become bigger and the system will be more sensitive to the wavelength fluctuation of the light source.

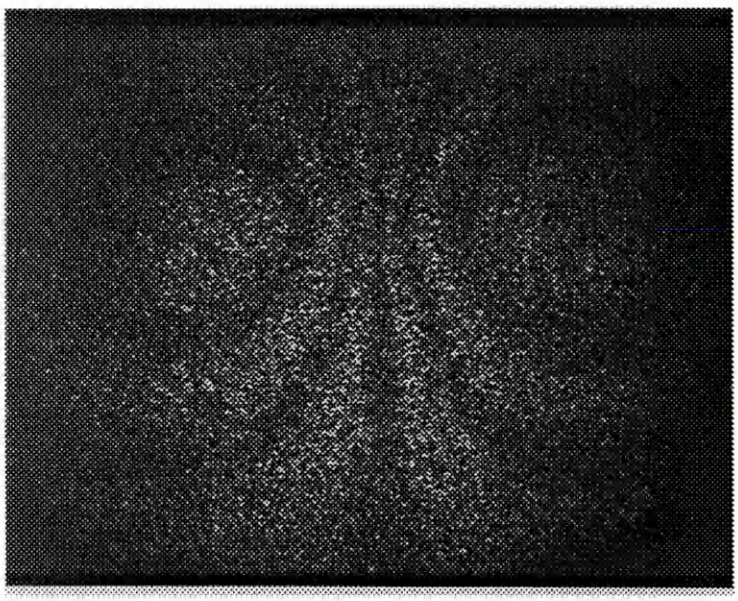

Fig. 5.3 Fringes of the flat plate under deformation, phase step = 0°

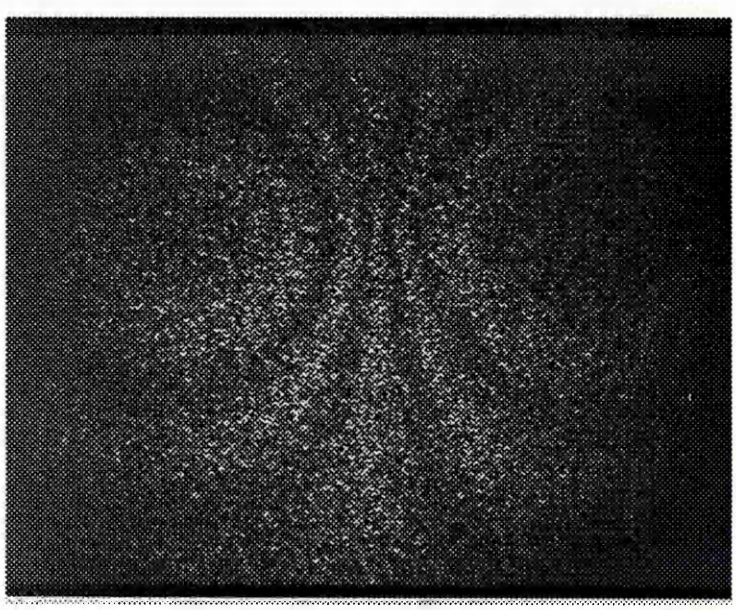

Fig. 5.4 Fringes of the flat plate under deformation, phase step = 120°

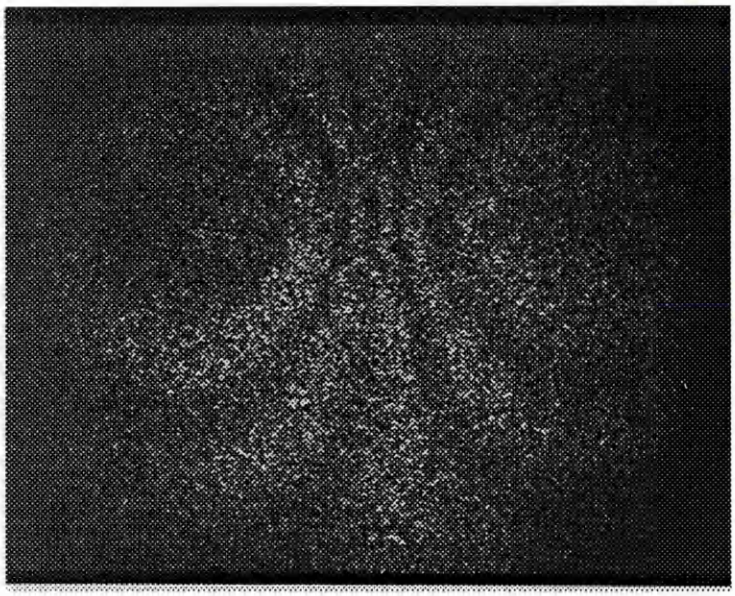

Fig. 5.5 Fringes of the flat plate under deformation, phase step = 240°

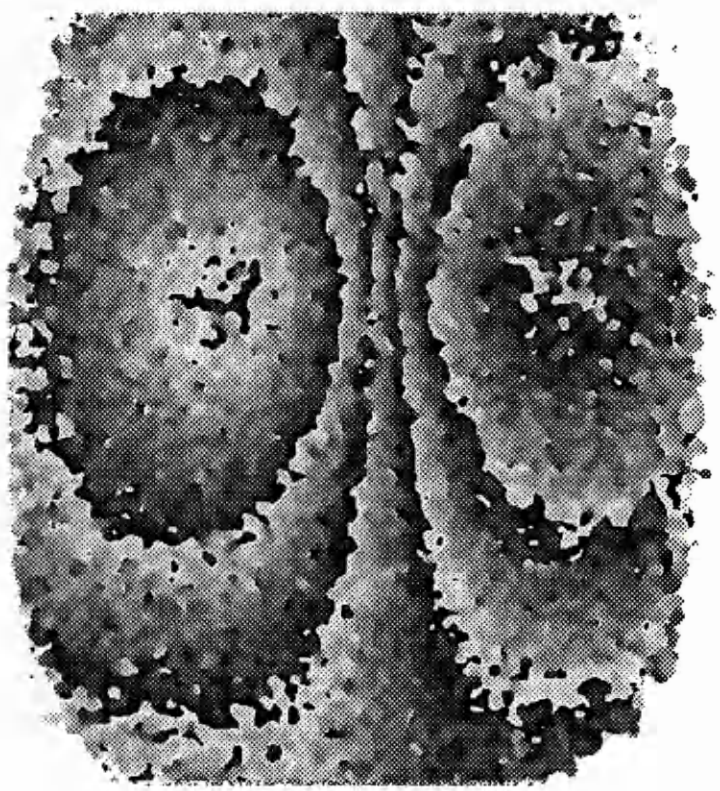

Fig. 5.6 Wrapped phase map calculated from the phase stepped fringes

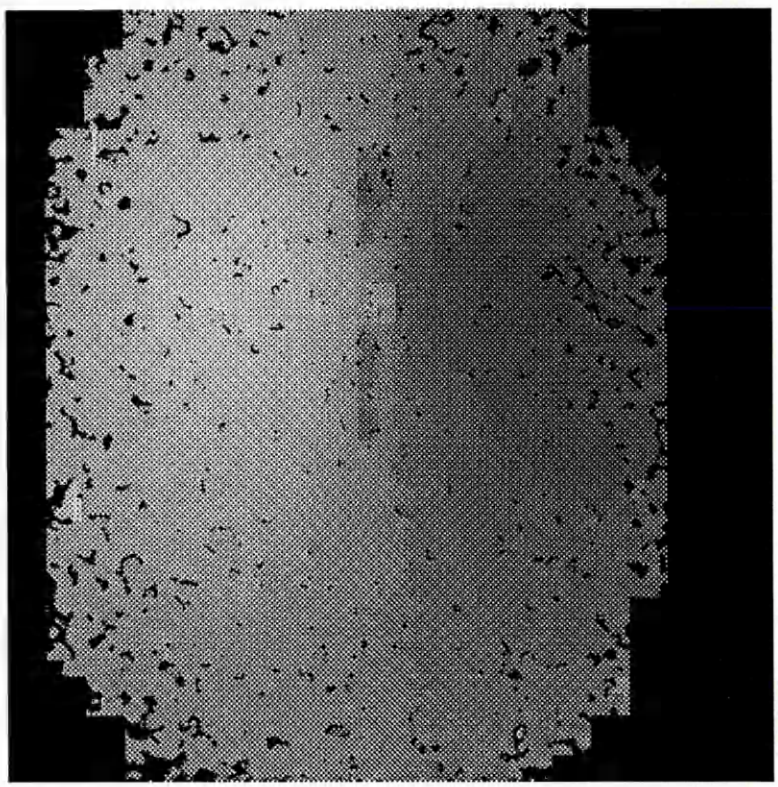

Fig. 5.7 Unwrapped phase map representing the gradient of deformation

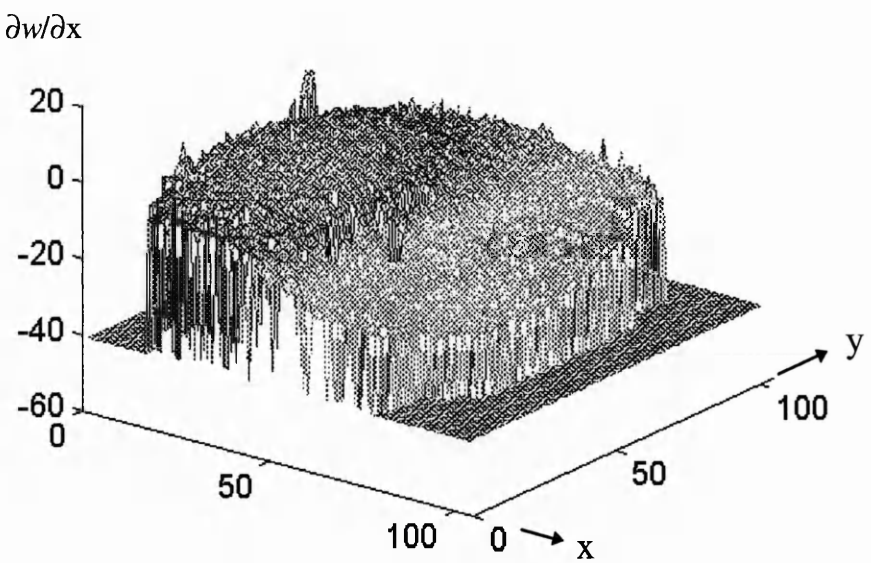

Fig. 5.8 Mesh plot of the deformation gradient in the x direction (the numbers in x and y axis represent the grid number and each grid is separated by 5 pixels)

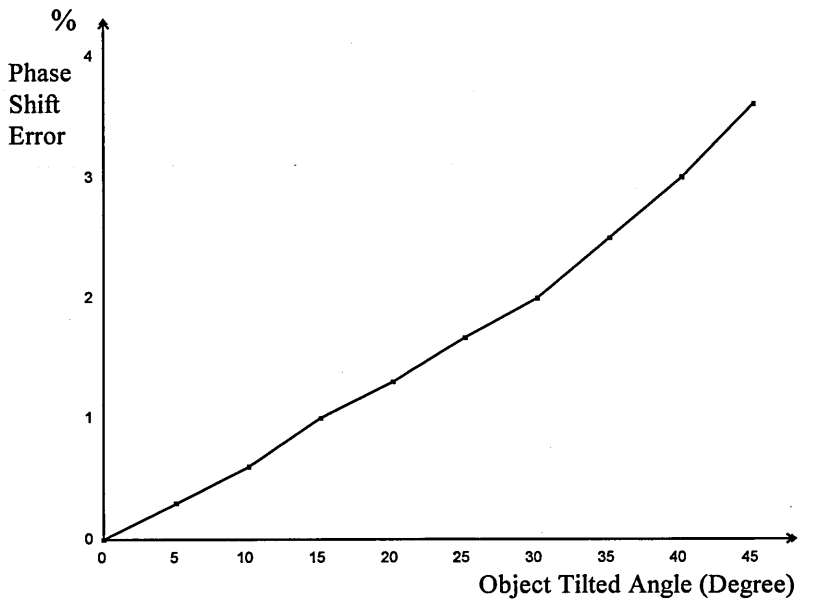

Fig. 5.9 The phase shift error with respect to the object tilted angle

References

5.1 Sommargren, G. E., Double-exposure holographic interferometry using common-path reference waves. *Appl. Opt.*, **16** (1977) 1736.

5.2 Hariharan, P., Oreb, B. F. and Brown, N., A digital phase-measurement system for real-time holographic interferometry. *Opt. Commun.*, 41 (1982) 393.

5.3 Nakadate, S. and Saito, H., Fringe scanning speckle-pattern interferometry. *Appl. Opt.*, **24** (14) (1985) 2172-2180.

5.4 Creath, K., Phase-shifting speckle interferometry. *Appl. Opt.*, **24** (18) (1985) 3053-58.

5.5 Robinson, D. W. and Williams, D. C., Digital phase stepping speckle interferometry. *Opt. Commun.*, **57** (1) (1986) 26-30.

5.6 Reid, G. T., Rixon, R. C., Messer, H. I., Absolute and comparative measurements of three dimensional shape by phase measuring moiré topography. *Opt. and Laser Technol.*, **16** (6) (1984) 315-319.

5.7 Srinivasan, V., Liu, H. C. and Halioua, M., Automated phase-measuring profilometry of 3-D diffuse object. *Appl. Opt.*, **23** (1984) 3105-08.

5.8 Asundi, A., Phase shifting in photoelasticity. *Exp. Techniques*, **17** (1) (1993) 19-23.

5.9 Wyant, J. C. and Shagam, R. N., Use of electronic phase measurement techniques in optical testing. *Proc. 11th Congr. of the Int. Commission for Optics*, Madrid, (1978) 659.

5.10 Creath, K., Phase-measurement interferometry techniques. *Progress in Optics XXVI*, ed. Wolf, E., (1988) 349-393.

5.11 Toyooka, S. and Kadono, H., Digital speckle shearography using a liquid-crystal phase shifter. *Proc. SEM, Hologram Interferometry and Speckle Metrology*, Bethel, Conn. USA, (1990) 158-163.

5.12 Kadono, H., Toyooka, S. and Iwasaki, Y., Speckle-shearing interferometry using a liquid-crystal cell as a phase modulator. *J. Opt. Soc. Am.*, **8** (12) (1991) 2001-08.

5.13 Kadono, H. and Toyooka, S., Liquid crystal phase modulator used in DSPI. *SPIE*, Vol. 1554A (1991) 628-638.

5.14 Stevenson, W. H., Optical frequency shifting by means of a rotating diffraction grating. *Appl. Opt.*, **9** (1970) 649-652.

5.15 Shagam, R. N. and Wyant, J. C., Optical frequency shifter for heterodyne interferometers using multiple rotating polarisation retarders. *Appl. Opt.*, **17** (1978) 3034-35.

5.16 Kothiyal, M. P. and Delisle, C., Shearing interferometer for phase shifting interferometry with polarisation phase shifter. *Appl. Opt.*, **24** (24) (1985) 4439-4442.

5.17 Davies, J. C., Jones, J. D. C. and Pannell, C. N., Development and application of a fibre optic electronic speckle pattern interferometry. *SPIE*, Vol. 863 (1987) 194-207.

5.18 Valera, J. D. and Jones, J. D. C., Phase stepping in fibre-based speckle shearing interferometry. *Opt. Lett.*, **19** (15) (1994) 1161-63.

5.19 Ishii, Y., Chen, J. and Murata, K., Digital phase-measuring interferometry with a tuneable laser diode. *Opt. Lett.*, 12 (1987) 233-235.

5.20 Hariharan, P., High-precision, digital, phase-stepping interferometry with laser diodes. *SPIE*, Vol. 1162 (1989) 86-91.

5.21 Atcha H, Optoelectronic Speckle Pattern Interferometry. PhD thesis, Cranfield University, 1995.

5.22 Mohan, N. K., Saldner, H. O. and Molin, N. E., Electronic shearography applied to static and vibrating objects. *Opt. Commun.*, **108** (1994) 197-202.

5.23 Dandridge, A. and Goldberg, L., Current induced frequency modulation in diode lasers. *Electron. Lett.*, **18** (1982) 302.

5.24 Ford, H. D., Atcha, H. and Tatam, R. P., Optical fibre technique for the measurement of small frequency separations: application to surface profile measurement using electronic speckle pattern interferometry. *Meas. Sci. Technol.*, **4** (1993) 601-607.

5.25 Seiler, F. and Srulijes, J., Doppler-pictures of velocity fields - an application to fluid mechanics. *Proc. 3rd Int. Symp. on Applications of Laser Anemometry to Fluid Mechanics (Lisbon, Portugal)*, 7-9 July 1986, Paper 191.

5.26 Creath, K., Temporal Phase Measurement Methods. *Interferogram Analysis - Digital Fringe Pattern Measurement Techniques*, ed. Robinson, D. W. and Reid, G. T., IOP Publishing Ltd, Bristol, (1993) 94-140.

5.27 Towers, D. P., Judge, T. R. and Bryanston-Cross, P. J., Automatic Interferogram Analysis Techniques Applied to Quasi Heterodyne Holography and ESPI. *Optics and Lasers in Eng*, **14** (1991) 239-282.

5.28 Hariharan, P., Phase-stepping interferometry with laser diodes: effect of changes in laser power with output wavelength. *Appl. Opt.*, 28 (1989) 27-29.

5.29 Tatsuno, K. and Tsunoda, Y., Diode laser direct modulation heterodyne interferometer. *Appl. Opt.*, **26** (1) (1987) 37-40.

5.30 Ishii, Y and Onodera, R., Laser-diode phase-shifting interferometer insensitive to the changes in laser power. *SPIE*, Vol. 2544 (1995) 173-176.

5.31 Onodera, R., Ishii, Y., Ohde, N., Takahashi, Y. and Yoshino, T., Effect of laser-diode power change on optical heterodyne interferometry. IEEE J. Lightwave Technol. 13 (1995) 675-681

6. VIBRATION MEASUREMENTS

6.1 Review of vibration techniques in ESPI and shearography

A very useful application of ESPI since its invention is in the visualisation and detection of vibrational mode shape of objects, e.g. turbine blades, engine blocks and car body panels etc. [6.1-6.6]. Normally in ESPI, movement of the object is restricted because it tends to decorrelate the speckle pattern. However in vibration measurements, if the movement of the object is small enough to keep the correlation of speckle patterns, correlation fringes related to the vibration mode shape are observed when the object vibrates resonantly.

Three vibration techniques are commonly used in ESPI. Time-averaged measurement is to realise vibration amplitudes across the object surface without knowing the phase information. If the phases of vibration motion are important, reference beam phase modulation (**heterodyning**) is applied and combined with the time-averaged method to map out the phase data. The above two methods are all based on continuous illumination, of which Bessel fringes are obtained due to the intensity-integration effect within the whole vibration cycle. Alternatively, Stroboscopic illumination can be applied and synchronised with the vibration frequency to obtain truly cosine fringes which represent the relative vibration motion, and phase stepping methods can be directly incorporated to automate the fringe analysis. These three techniques are detailed and reviewed as follows.

6.1.1 Time-averaged vibration measurement

Time-averaged vibration measurement was originally developed in holographic interferometry by Powell and Stetson [6.7]. The technique was then extended to ESPI

for vibration measurement by Butters et al [6.8] and Løkberg et al [6.9]. In an ordinary ESPI system, the image frame update rate is 25 Hz (the standard CCIR signal) which is much slower than the resonant frequencies of most test objects. When the system is used for vibration measurement, each interferogram represents the time-average of instantaneous intensities modulated by the cyclic vibration motion.

The theory of the time-averaged vibration method in ESPI is similar to that derived in holographic interferometry [6.7]. For the independent measurement of out-of-plane displacement, normal illumination and viewing directions are assumed. The motion of a sinusoidally vibrating object can be expressed as

$$A(\underline{r}_o,t) = a_o(\underline{r}_o)\sin\left[\omega t + \varphi_o(\underline{r}_o)\right] \tag{6.1}$$

where ω is the angular frequency of vibration, $\underline{r}_o$ is the position vector of a point on the object, and $a_o(\underline{r}_o)$ and $\varphi_o(\underline{r}_o)$ are the amplitude and phase of the vibration motion respectively. The electric fields of the reference beam and the object beam are given by

$$E_r = e_r \exp i\phi_r \tag{6.2}$$

$$E_o(\underline{r}_o,t) = e_o \exp i\left\{\phi_o + \phi_s + \frac{4\pi}{\lambda} a_o(\underline{r}_o)\sin\left[\omega t + \varphi_o(\underline{r}_o)\right]\right\} \tag{6.3}$$

where, e_r and e_o are the amplitudes of the reference and the object beams, and ϕ_r is the phase of the reference beam. The phase of the object beam expressed as ϕ_o is superimposed on a randomly varying speckle phase, ϕ_s. The instantaneous intensity at the camera is given by

$$I(\underline{r}_d,t) = (E_o + E_r)(E_o + E_r)^* \tag{6.3a}$$

where $\underline{r}_d$ represents a conjugate position vector of $\underline{r}_o$ in the image plane, and * implies a Hermitian conjugate. The instantaneous intensity in the image plane, $I(\underline{r}_d, t)$ becomes

$$I(\underline{r}_d,t) = I_r + I_o + 2\sqrt{I_r I_o}\cos\left\{\phi + \phi_s + \frac{4\pi}{\lambda}a_o(\underline{r}_o)\sin\left[\omega t + \varphi_o(\underline{r}_o)\right]\right\} \tag{6.4}$$

where $\underline{r}_d$ represents a conjugate position vector of $\underline{r}_o$ in the image plane, λ is the free space wavelength of the light, $I_r = e_r^2$ and $I_o = e_o^2$ are the intensities of the reference and object beams respectively, and $\phi = \phi_o - \phi_r$ is the phase difference between the object and the reference beams when the object is stationary.

Since the exposure time of one image frame is much greater than the period of vibration, $\tau = 2\pi/\omega$, each image frame records a continuous distribution of the instantaneous intensity corresponding to various positions of the object in its vibration cycles. Under this condition, the integrated intensity in one image frame can be expressed by the average of the instantaneous intensity over the vibration period τ as

$$I(\underline{r}_d) = \frac{1}{\tau}\int_0^{\tau} I(\underline{r}_d,t)dt$$

$$= I_r + I_o + 2\sqrt{I_r I_o}\cos(\phi + \phi_s)J_0\left[\frac{4\pi}{\lambda}a_o(\underline{r}_o)\right] \tag{6.5}$$

where J_0 is the zero-order Bessel function of the first kind.

To obtain correlation fringes related to the vibration amplitude, we can either high pass filter the single interferogram of equation (6.5), or use the sequential subtraction technique (one arm of the interferometer is modulated by a π phase shift in between image frames, and the incoming frame is subtracted with the previous frame sequentially) as described in section 2.4.3. The processed images are then rectified and

displayed on a TV monitor. Since most TV monitors have a gain of 2.2 (the gamma value), the displayed image can be approximately expressed as

$$I(\underline{r}_d) \propto I_r I_o \cos^2(\phi + \phi_s) J_o^2\left[\frac{4\pi}{\lambda} a_o(\underline{r}_o)\right] \tag{6.6}$$

Equation (6.6) represents a speckle pattern, $I_rI_o\cos^2(\phi+\phi_s)$, which is modulated by a J_o^2 function. Despite the intensity variation in each pixel due to the speckle effect, the intensity of the fringes observed follows a squared Bessel function distribution. The zero order fringe has an intensity approximately six times greater than the first order fringe intensity [6.10], as shown in Fig. 6.1.

To detect the mode shapes at different resonant frequencies, the object is excited from zero frequency to higher frequency with an appropriate amplitude, either by piezoelectric transducers, loud speakers, or electro dynamic shakers etc. An example of time-averaged fringes of a gas turbine blade vibrating resonantly at 2 kHz is shown in Fig. 6.2. It can be observed that the fringe visibility decreases rapidly as the vibration amplitude increases.

In the time-averaged vibration method, amplitudes of the excited resonant vibration motion can be observed. However the phase information is lost since the acquired intensity is the average over many vibration cycles. The vibration fringes obtained follow a Bessel function distribution making phase stepping methods difficult to apply directly. These two problems can be resolved by reference beam phase modulation (heterodyning) and stroboscopic illumination methods respectively.

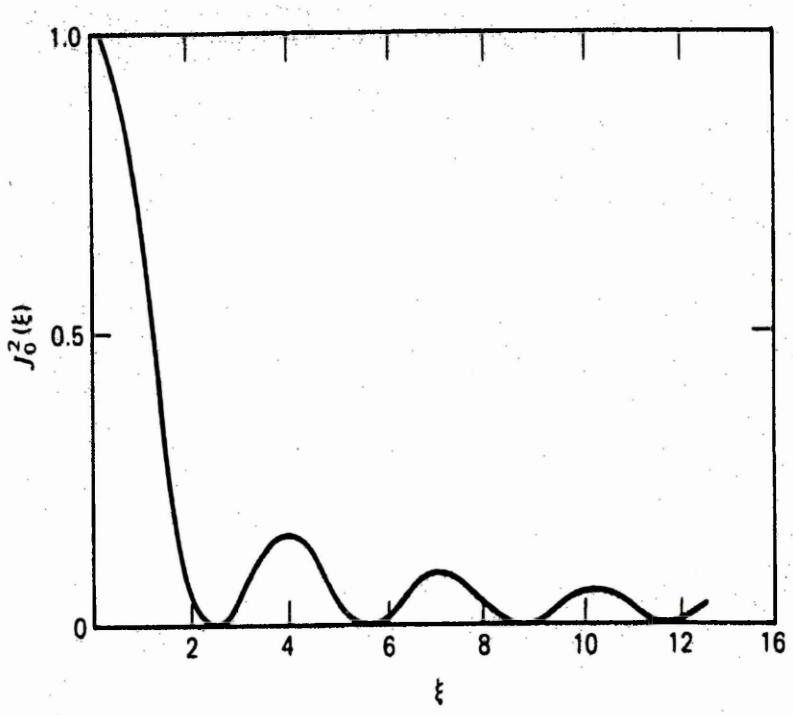

Fig. 6.1 Plot of $J_0^2(\xi)$ function

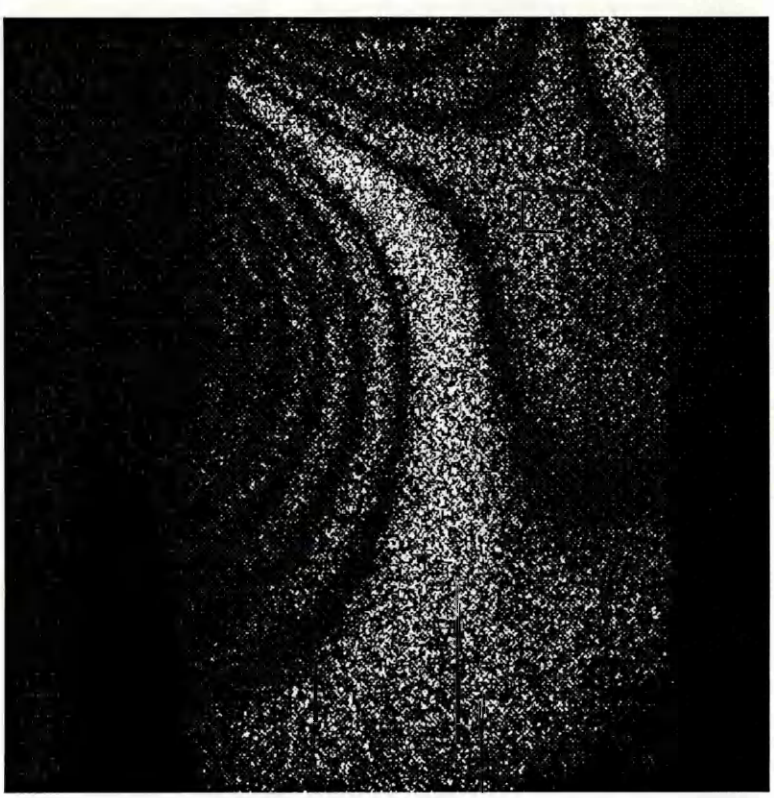

Fig. 6.2 ESPI time-averaged vibration fringes of a turbine blade vibrating at 2 kHz.

6.1.2 Heterodyning

As described in the time-averaged vibration method, the vibration fringes obtained are proportional to the rectification or the square of the zero-order Bessel function J_0. The intensity of the zero order fringe is much larger than those of the higher order fringes. This limits the number of resolvable fringes, in addition the phase of vibration motion is lost.

Phase modulation of the reference beam (heterodyning), to improve the visibility of higher order vibration fringes and also to determine the phase of vibration displacement, was first published by Aleksoff [6.11], and Neumann et al [6.12] in time-averaged holographic techniques. The reference beam of the interferometer is modulated at the same frequency as the vibrating object but with a variable amplitude and a relative phase with respect to the vibration motion. In the reconstructed images, the brightest fringes are no longer formed around the nodal positions of the object, but around a vibrating area determined by the modulation amplitude and the modulation phase of the reference beam.

A similar technique was then extended to ESPI by Løkberg and Høgmoen [6.13,6.14]. In their system, a mirror in the reference arm, modulated by a piezoelectric (PZT) actuator, was used to perform the heterodyning. The amplitude and relative phase of motion on the object surface were determined and a map of surface deformation was produced. The technique combines the time-averaged method with a phase modulation capability to become a phase sensitive technique and also extend the measurable range of vibration motion.

In fibre optic ESPI systems, heterodyning was also performed using a PZT stretcher to modulate the phase of light guided by an optical fibre [6.4,6.15-6.17]. However, certain limitations are expected by the use of a PZT for the phase modulation. These include the limited response of PZTs in high frequency modulation [6.18], the non-linear

response to applied voltage and the essential calibration of PZTs [6.19,6.20], and the complex vibration characteristics exhibited at different frequencies [6.21].

Heterodyning using an unbalanced all-fibre ESPI system, by modulating the wavelength of a laser diode through its injection current modulation, was reported by Atcha and Tatam [6.22,6.23]. For modulation frequencies below 1 GHz, the wavelength of light emitted by a laser diode is a relatively-linear function of its injection current [6.24]. Phase modulation in the unbalanced interferometer due to the wavelength change was then successfully implemented to perform the heterodyning [6.22,6.23]. The same technique is extended here for the heterodyning of vibration fringes in an electronic shearography system, and will be discussed in section 6.2.

The basic theory of heterodyning is described as follows.

When a test object is resonantly vibrating and measured using an out-of-plane ESPI system, the electric field of the object beam is expressed as in equation (6.3), and the electric field of the reference beam with sinusoidal phase modulation is given by

$$E_r(t) = e_r \exp i\left[\phi_r + \frac{4\pi}{\lambda} a_r \sin(\omega t + \varphi_r)\right] \tag{6.7}$$

where a_r and φ_r represent the amplitude and phase of the reference beam modulation. The instantaneous intensity in the image plane is now contributed by the interference of a vibrating object wave and a reference wave modulated with the same frequency as the vibrating object. The intensity of each image frame corresponds to the integration of the instantaneous intensity over the vibration period as described in equation (6.5). After the image processing either by sequential subtraction or by high pass filtering, the displayed vibration fringes can be expressed as [6.11] (or see Appendix A.1)

$$I(\underline{r}_d) \propto \cos^2(\phi + \phi_s) J_o^2\left(\frac{4\pi}{\lambda} a_m\right) \tag{6.8}$$

where, $\phi = \phi_o - \phi_r$ and

$$a_m = \left\{a_o^2(\underline{r}_o) + a_r^2 - 2a_o a_r \cos\left[\varphi_o(\underline{r}_o) - \varphi_r\right]\right\}^{1/2} \tag{6.9}$$

From equations (6.8) and (6.9), the intensity distribution is given by the same Bessel function J_0 as in time-averaged ESPI, equation (6.6). However, the fringe pattern is now dependent on the difference of amplitudes and phases between the object motion and the reference beam modulation. The brightest (zero order) fringes do not correspond to the nodal regions on the object but to those regions vibrating at the same amplitude and phase as the reference wave.

Reference beam phase modulation also can be used to map out the relative phase of vibration motion across the object, independent of vibration amplitudes [6.14]. In this application, the reference arm of the interferometer is modulated at the same frequency as the object vibration but with a variable amplitude and relative phase. If the phase of the reference beam is set to a certain value and the amplitude is varied between zero and a maximum value (determined by the object vibration amplitude), the fringe pattern will change. The bright zero order fringes, however, will always locate at the positions where the object phase equal to the reference beam phase. Hence, complete phase distribution of the object vibration can be obtained by varying the reference wave phase in appropriate steps and repeating the procedure with variations of the modulation amplitude in the reference beam.

Using the heterodyning method, the range of detectable vibration amplitude was reported to extend upwards to 8.4 μm [6.13], and downwards to 0.01 nm using photoelectric detection or 1 nm visually [6.25]. The amplitude and phase of vibration motion can be mapped out, which is very useful for the interpretation of vibration fringes, especially in dealing with a complex vibration mode shape.

To obtain higher resolution data from the heterodyning work, complementary techniques including the combination of a laser Doppler velocimeter to measure the motion of a point on the vibrating surface [6.15-6.17] or the monitoring of individual speckles [6.26-6.28] were applied. The measured signal representing the displacement of a vibrating point is then used to phase-lock and modulate the reference beam of an ESPI system. Automatic heterodyning can be performed by moving the reference point to different areas of the test surface. These techniques also can compensate the unwanted or environmentally induced out-of-plane motion of the test object.

6.1.3 Stroboscopic illumination

The use of stroboscopic illumination for vibration measurements was originally developed in holographic interferometry by several authors [6.29-6.34]. Stroboscopic holograms can be recorded by using two pulses from a pulse laser [6.29], or by chopping a continuous laser beam with a perforated disk driven by a synchronous motor [6.30-6.32] or with electro-optical devices such as Pockles cells [6.33,6.34].

In stroboscopic holography, a sequence of short pulses of laser light, of which the duration is much shorter than the period of vibration, are synchronised with the vibrating object and illuminate on the object surface. The hologram is recorded when the object is at two symmetrical positions of the vibration cycle, commonly at its maximum positive and negative positions. Due to the short illumination, the object is effectively frozen in these two positions of vibration, and the characteristic function of the interferogram is then of cosine form [6.30].

Stroboscopic illumination was also introduced to ESPI by Løkberg's group [6.9,6.35,6.36] and later by other authors [6.2,6.22,6.37-6.45]. By pulsing the laser beam at two symmetrical positions of the vibration cycle , commonly at the two extreme positions, only speckle fields of the two positions are recorded and cosinusoidal fringes are obtained.

The basic theory of stroboscopic illumination is described as follows.

When a test object vibrates sinusoidally, the instantaneous intensity can be expressed as in equation (6.4)

$$I(\underline{r}_d,t) = I_r + I_o + 2\sqrt{I_r I_o}\cos\left\{\phi + \phi_s + \frac{4\pi}{\lambda}a_o(\underline{r}_o)\sin\left[\omega t + \varphi_o(\underline{r}_o)\right]\right\} \tag{6.4}$$

If the light pulses are very short, only the instantaneous intensity when the object is at the illuminated positions of the vibration cycle is detected. For two pulses per vibration cycle, the averaged intensity in one vibration cycle can be expressed as

$$I(\underline{r}_d) = \frac{1}{2}\left[I(\underline{r}_d,t_s) + I(\underline{r}_d,t_s+\pi/\omega)\right]$$

$$= I_r + I_o + 2\sqrt{I_r I_o}\cos(\phi+\phi_s)\cos\left\{\frac{4\pi}{\lambda}a_o(\underline{r}_o)\sin\left[\omega t_s + \varphi_o(\underline{r}_o)\right]\right\} \tag{6.10}$$

where t_s is a specific time when the first pulse illuminates on the object in one vibration cycle. After image processing either by sequential subtraction or by high pass filtering, the vibration fringes obtained can be expressed as

$$\Delta I \propto \cos(\phi+\phi_s)\cos\left\{\frac{4\pi}{\lambda}a_o(\underline{r}_o)\sin\left[\omega t_s + \varphi_o(\underline{r}_o)\right]\right\} \tag{6.11}$$

When the timing of the pulses is adjusted to illuminate the object in its extreme positions of the vibration motion, then $\omega t_s+\varphi_o = (m+1/2)\pi$, where m is an integer, equation (6.11) simplifies to become

$$\Delta I \propto \cos(\phi + \phi_s)\cos\left[\frac{4\pi}{\lambda} a_o(\underline{r}_o)\right] \tag{6.12}$$

As seen from equations (6.11) and (6.12), the vibration fringes obtained in stroboscopic illumination are cosinusoidal functions. Compared with the Bessel fringes in the time-averaged method, the fringe contrast is uniform as the vibration amplitude increases and high order fringes can be clearly observed.

In practice, stroboscopic techniques performed by chopping a continuous laser beam using mechanical devices or using electro-optic and acousto-optic modulators [6.30-6.34] have two main problems. The chopping device is limited in frequency response and becomes more difficult to synchronise with the vibrating object when the vibration frequency is increased. The other is that most of the energy is wasted which gives very poor power efficiency.

Using a pulse laser in stroboscopic illumination [6.29,6.41-6.45] greatly reduces these two problems. Q-switching can produce pulses of very short duration which yield true sinusoidal fringe patterns even for very high frequency vibrations. Because the pulse timing and separation are variable, even transient vibration motions can be easily detected [6.45]. However, the main concern of using pulse lasers is that they are generally very expensive and large, and require high electric power to operate.

Stroboscopic illumination also can be performed by pulsing the injection current of a laser diode in ESPI systems [6.22,6.37-6.40]. Using this method, high frequency vibration motion can be well synchronised with a very good light efficiency, which is better than light chopping methods. In addition, laser diode is much cheaper and compact compared to pulse lasers. The technique is extended in this thesis to electronic shearography for vibration measurement and will be discussed in section 6.3.

6.1.4 Vibration techniques applied to shearography

In shearography, time-averaged [6.46-6.49] and heterodyning methods [6.50] have been reported in vibration measurements. The time-averaged method is to realise gradients of vibration amplitudes across the object surface without knowing the phase. To obtain phase information, heterodyning is applied and combined with the time-averaged method to map out the phase data. Similarly, stroboscopic illumination can be applied and synchronised with the vibration frequency to obtain cosine fringes which represent the gradients of vibration motion. Equations of the three methods are briefly described as follows.

Time-averaged vibration

In a shearography system, normal illumination and observation are necessary for the measurement of out-of-plane displacement [6.51]. If the image shearing is in the x direction by an amount δx, light reflected from a point (x, y) and light reflected from its neighbouring point (x+δx, y) on the object surface will be brought to interfere at the same point (x_d, y_d) in the image plane.

When the test object is vibrating at an angular frequency ω, amplitude $a_o(x, y)$ and a phase $\varphi_o(x, y)$, the light scattered from the point (x+δx, y) and point (x, y) can be expressed as

$$E_1(x+\delta x, y, t) = e_1(x+\delta x, y)\exp i(\phi_1 + \phi_{s1})\exp i\left[\frac{4\pi}{\lambda}a_o(x+\delta x, y)\sin(\omega t + \varphi_o)\right] \qquad (6.13)$$

$$E_2(x, y, t) = e_2(x, y)\exp i(\phi_2 + \phi_{s2})\exp i\left[\frac{4\pi}{\lambda}a_o(x, y)\sin(\omega t + \varphi_o)\right] \qquad (6.14)$$

where e_1 and e_2 represent the amplitudes of the two image-sheared wavefronts, ϕ_1 and ϕ_2 are the phase of the two beams, ϕ_{s1} and ϕ_{s2} are the randomly varying speckle phase terms. Correlation fringes generated and displayed on a TV monitor are described by

$$I(x_d, y_d) \propto \cos^2(\phi + \phi_s) J_o^2\left[\frac{4\pi}{\lambda}\left(\frac{\partial a_o}{\partial x}\right)\delta x\right] \tag{6.15}$$

where $\phi = \phi_1 - \phi_2$ and $\phi_s = \phi_{s1} - \phi_{s2}$. The fringe function is similar to that in time-averaged ESPI, as shown in equation (6.6), which follows a squared Bessel function distribution. However, these fringes represent gradients of vibration amplitude on the object surface. The brightest fringes locate on the areas (such as the peaks of vibration motion or a large stationary part on the object surface) where gradients of vibration displacement are equal to zero.

Heterodyning

When heterodyning is applied by modulating the phase of one arm of the interferometer, e.g. the light beam reflected from the point (x, y), the wavefront is then expressed as

$$E_2(x,y,t) = e_2(x,y)\exp i(\phi_2 + \phi_{s2})\exp i\left\{\frac{4\pi}{\lambda}\left[a_o(x,y)\sin(\omega t + \varphi_o) + a_r \sin(\omega t + \varphi_r)\right]\right\} \tag{6.16}$$

Where a_r and φ_r are the modulation amplitude and the modulation phase. Correlation fringes generated by subtraction are described by

$$I(x_d, y_d) \propto \cos^2(\phi + \phi_s) \cdot J_0^2\left(\frac{4\pi}{\lambda} a_m\right) \tag{6.17}$$

where,

$$a_m = \left[\left(\frac{\partial a_o}{\partial x} \delta x \right)^2 + a_r^2 - 2 \left(\frac{\partial a_o}{\partial x} \delta x \right) a_r \cos(\varphi_o - \varphi_r) \right]^{1/2} \tag{6.18}$$

When the heterodyning method is applied, the relative optical phase between the two arms of the interferometer is modulated at the same frequency as the vibrating object with a variable amplitude and a relative phase with respect to the vibration motions. As seen in equations (6.17) and (6.18), the brightest fringes are no longer formed on the areas where gradients of vibration displacement are equal to zero, but on the areas where gradients of vibration displacement multiplied by the shearing distance, i.e. $(\partial a_o/\partial x)\delta x$, is equal to the modulation amplitude a_r and the vibration phase φ_o is equal to the modulation phase φ_r.

Stroboscopic illumination

Applying stroboscopic illumination in shearography generates correlation fringes described by

$$\Delta I \propto \cos(\phi + \phi_s) \cos\left[\frac{4\pi}{\lambda} \left(\frac{\partial a_o}{\partial x} \delta x \right) \sin(\omega t_s + \varphi_o) \right] \tag{6.19}$$

The cosine fringe pattern represents the variation of gradients of vibration motion across the object surface.

6.2 Heterodyning in shearography using laser diode injection current modulation

In shearography, heterodyning is difficult to implement since the modulation frequency is relative high (in the order of kHz) and a general phase shifter, e.g. a mirror mounted on a piezoelectric transducer or a liquid crystal, does not respond adequately in this operating range.

Heterodyning using an optical fibre based shearography system was recently reported by Velera and Jones [6.50]. In their method, a highly birefringent (HiBi) fibre was used to illuminate a test object with equal intensities of light guided by the orthogonal polarisation eigenstates of the fibre and a Wollaston prism was used to generate two sheared images. Phase modulation was implemented by stretching the 19.2 meter long fibre wrapped around a cylindrical piezoelectric transducer. The technique was achieved successfully without obvious mechanical movement of components, however it relies on the preservation of polarisation states of the wavefronts scattered from the object surface. In addition the relative phase change between the polarisation states of the HiBi fibre is sensitive to temperature and strain [6.50] and therefore for practical applications an additional feedback circuit would be required to stabilise the interferometer phase with respect to thermal fluctuation.

To perform heterodyning in shearography using laser diode injection current modulation, the same optical configuration as that used in phase stepping work, an unbalanced Michelson interferometer arrangement, was used. The path length difference induces a relative phase difference between the two arms of the interferometer when the source optical frequency is modulated. Heterodyning was then demonstrated by modulating the injection current of the laser diode at the same frequency as the vibrating object with a variable amplitude and a relative phase with respect to the vibration motions. The theory of this method is described as follows.

6.2.1 Theory

In contrast to the reference beam phase modulation method implemented by piezoelectric phase shifters as described in section 6.1.2, heterodyning using the wavelength modulation of a laser light source affects the phase of both the two light beams simultaneously. The detailed derivation can be seen in Appendix A.2

When the test object is vibrating at an angular frequency ω, amplitude $a_o(x, y)$ and a phase $\varphi_o(x, y)$, and the optical frequency of the light source is modulated at the same frequency as the vibrating object but with a relative phase with respect to the vibration motion, the light scattered from the point $(x+\delta x, y)$ and point (x, y) are expressed as

$$E_1(x+\delta x, y, t) = e_1(x+\delta x, y)\exp i\phi_{s1}\exp i\left\{\frac{4\pi}{c}a_{m1}\right\} \tag{6.20}$$

$$E_2(x, y, t) = e_2(x, y)\exp i\phi_{s2}\exp i\left\{\frac{4\pi}{c}a_{m2}\right\} \tag{6.21}$$

where,

$$a_{m1} = a_o(x+\delta x, y)\nu\sin(\omega t+\varphi_o)+\left(\frac{L_1}{2}\right)\Delta\nu\sin(\omega t+\varphi_\nu) \tag{6.22}$$

$$a_{m2} = a_o(x, y)\nu\sin(\omega t+\varphi_o)+\left(\frac{L_2}{2}\right)\Delta\nu\sin(\omega t+\varphi_\nu) \tag{6.23}$$

e_1 and e_2 represent the amplitudes of the two wavefronts, ϕ_{s1} and ϕ_{s2} are the randomly varying speckle phase terms, ν is the optical frequency, $\Delta\nu$ and φ_ν are the amplitude and phase of the source frequency modulation, L_1 and L_2 are the optical paths of light reflected from the point $(x+\delta x, y)$ and (x, y) respectively, and c is the velocity of light.

The instantaneous intensity at the image detector is

$$I(x_d, y_d, t)$$
$$= e_1^2+e_2^2+2e_1e_2\cos\left\{\phi_s+\frac{4\pi}{c}\left[\left(\frac{\partial a_o}{\partial x}\delta x\right)\nu\sin(\omega t+\varphi_o)+\left(\frac{\Delta L}{2}+\delta z\right)\Delta\nu\sin(\omega t+\varphi_\nu)\right]\right\} \tag{6.24}$$

where $\phi_s = \phi_{s1} - \phi_{s2}$, ΔL is the path length difference generated in the Michelson interferometer, δz is the height variation between (x+δx, y) and (x, y). $\partial a_o/\partial x$ is the gradient of vibration motion.

The intensity of each image frame is the integration of the instantaneous intensity over the vibration period as described in equation (6.5). After the image processing either by sequential subtraction or by high pass filtering, the vibration fringes obtained can be expressed as

$$I(x_d,y_d) \propto J_0^2\left\{\left(\frac{4\pi\nu}{c}\right)\left[\left(\frac{\partial a_o}{\partial x}\delta x\right)^2+\left(\frac{\Delta L}{2}+\delta z\right)^2\left(\frac{\Delta\nu}{\nu}\right)^2+2\left(\frac{\partial a_o}{\partial x}\delta x\right)\left(\frac{\Delta L}{2}+\delta z\right)\left(\frac{\Delta\nu}{\nu}\right)\cos(\varphi_o-\varphi_\nu)\right]^{1/2}\right\} \quad (6.25)$$

As seen from equation (6.25), the heterodyning effect is related to the path length difference in the interferometer and the magnitude of the frequency modulation. The brightest fringes will be observed where the amplitude of the source frequency modulation is equal to the negative of gradients of vibration displacement multiplied by the shearing distance, i.e. $(\Delta L/2+\delta z)(\Delta\nu/\nu) = -[(\partial a_o/\partial x)\delta x]$ and the phase of the source frequency φ_ν is equal to the vibration phase φ_o .

The height variation δz is unknown in this technique, however it can be measured by the two-wavelength slope measurement method as described in chapter 4. If the path length difference generated in the Michelson interferometer, ΔL, is much greater than the object height variation, δz, equation (6.25) then simplifies to

$$I(x_d,y_d) \propto J_0^2\left\{\left(\frac{4\pi\nu}{c}\right)\left[\left(\frac{\partial a_o}{\partial x}\delta x\right)^2+\left(\frac{\Delta L}{2}\right)^2\left(\frac{\Delta\nu}{\nu}\right)^2+2\left(\frac{\partial a_o}{\partial x}\delta x\right)\left(\frac{\Delta L}{2}\right)\left(\frac{\Delta\nu}{\nu}\right)\cos(\varphi_o-\varphi_\nu)\right]^{1/2}\right\} \quad (6.26)$$

6.2.2 Experimental verification

The experimental arrangement of the shearography system used for heterodyning is as shown in Fig. 3.3. A 100 mW single longitudinal mode laser diode (Spectra Diode Labs, SDL-5411-G) emitting at 830 nm was coupled into a single mode optical fibre to illuminate the object. A Faraday isolator (isolation level of 30 dB) was used to prevent the light feedback into the laser cavity, because this feedback always cause an increase of the laser linewidth, mode hopping and other deleterious effects [6.52]. The use of optical fibres provides extra flexibility for the illumination and it also behaves as a very good spatial filter to provide a uniform illumination wavefront.

Light scattered from the object surface is then divided by a modified Michelson interferometer into two beams, as shown in Fig. 5.1. The image shearing is generated by tilting one of the mirrors, and these two beams are collected by a zoom lens onto a CCD camera.

The test object is a gas turbine compressor blade (with 10 cm wide and 15 cm high) which was coated with retroreflective tape. The amount of shear used in the measurement was 4 mm in the x direction (the horizontal axis). Sinusoidal signals from one output of a dual channel function generator were input into a high voltage amplifier to drive a piezoelectric transducer bonded on to the back of the blade. The blade was excited by this transducer to produce a range of resonate vibration frequencies.

The second output of the function generator, with the same frequency as the first output but with its own amplitude and phase adjustment, was synchronised by a synthesised function generator (Stanford Research System, DS 345) which was used to modulate the injection current of the laser diode.

To detect the mode shapes of different resonant frequencies, the blade is excited from zero frequency to higher frequency with an appropriate amplitude by the piezoelectric

transducer. The image signals detected by the CCD camera were processed by the frame grabber housed in the PC. Correlation fringes obtained were then displayed on the TV monitor.

To ensure high visibility of the vibration fringes, the π phase shift needed for sequential subtraction was performed by sending a DC voltage from a D/A board and synchronised with the image frame update rate, to dither one of the interferometer mirrors.

The optical frequency modulation of the laser diode was measured by a confocal Fabry-Pérot interferometer with 2 GHz free spectral range and a finesse of ~200. The injection current of the laser diode was modulated by different amounts (from 1 mA to 8 mA and each step is 0.5 mA). The ratio of the optical frequency change to the injection current change was measured to be 1.433 GHz/mA with an error of ±1% (the diode temperature is 18.01°C and the initial current is 100.01 mA).

6.2.3 Results and discussion

Fig 6.3 shows time-averaged vibration fringes of the turbine blade vibrating at 2 kHz, 3.4 kHz and 5.6 kHz recorded by the ESPI and shearography systems. For ESPI fringes, the brightest areas represent the nodal positions on the blade where the vibration displacement is equal to zero. In contrast, for shearography fringes, the brightest areas represent the positions where gradients of vibration displacement are equal to zero, i.e. the peaks of vibration motion and the large stationary areas on the object surface. It can be seen from these pictures that, as expected, the zero-order fringes of shearography pass through the peak positions and link with the large stationary areas at the bottom of the object.

Fig 6.4 shows the results of heterodyning in ESPI by modulating the optical frequency of the laser diode with an amplitude of 0.2 GHz. The brightest fringes have shifted from the nodal positions to the areas that vibrate with the same amplitude and phase. Fig.

6.4(b) and 6.4(c) show the same amplitude of heterodyning with a 180° phase difference, which reveal the positions of the anti-phase areas. The amplitude and phase information is then used to characterise the vibration motion across the object surface.

Fig. 6.5 shows the results of heterodyning in shearography by modulating the wavelength of the laser diode by 10.9 GHz. As seen from these images, the brightest fringe has shifted from the original peak positions, where the gradient of vibration displacement is equal to zero, to nearby areas. Fig 6.5(c) shows the same amplitude of heterodyning with a phase shift of 180° with respect to Fig. 6.5(b), and we find that the brightest fringes have shifted to the opposite nearby areas. This effect is an inherent characteristics of shearography, since gradients of vibration displacement are in anti-phase (one positive and one negative) next to the peak positions of the vibration motion.

By applying heterodyning in vibration measurements, the measurable range can be extended to higher amplitude of vibration motion [6.13]. However, for heterodyning using diode modulation, the fringe visibility will be reduced if the intensity changes greatly due to the current modulation. This effect can be released by increasing the path length imbalance in the interferometer. The diode used in this work has been modulated up to 15 GHz and the intensity variation is nearly 6% which does not show much effect in the fringe visibility. The measurable range is actually limited by the continuous tuning range of this laser diode.

Vibration fringe patterns obtained in shearography depend on the image-sheared direction and also the shearing amount. When the shearing amount is big, the fringes obtained no longer represent the variation of gradients of vibration but only the variation of the relative vibration displacement. The interpretation of shearographic vibration fringes is rather difficult and needs very good experience. Theoretically, the integration of gradients of vibration displacement can generate the vibration mode shape. This work is also tedious and requires a special-purpose program to accomplish it.

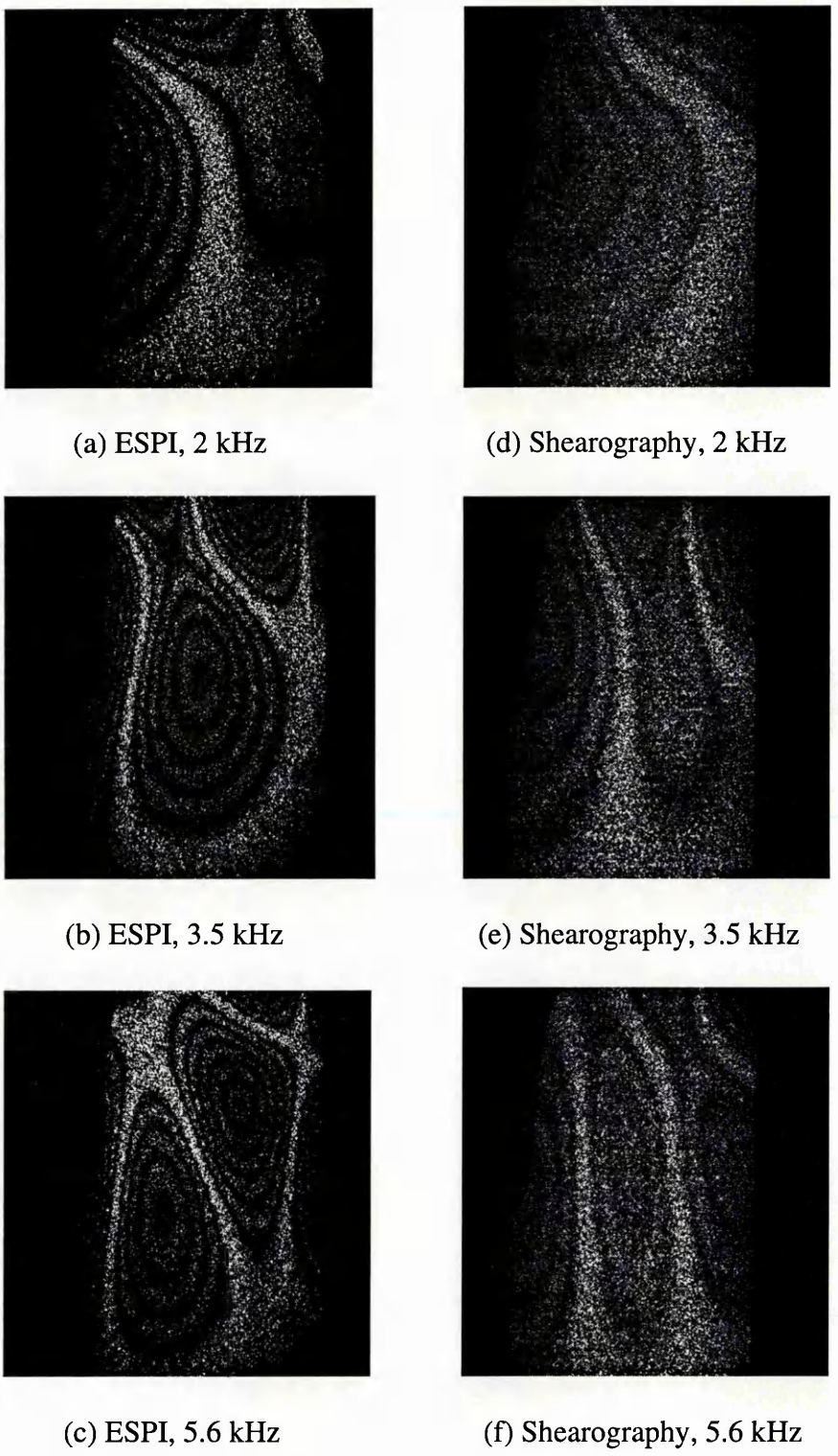

(a) ESPI, 2 kHz (d) Shearography, 2 kHz

(b) ESPI, 3.5 kHz (e) Shearography, 3.5 kHz

(c) ESPI, 5.6 kHz (f) Shearography, 5.6 kHz

Fig. 6.3 Comparisons of time-averaged vibration fringes of turbine blade measured by ESPI and shearography systems.

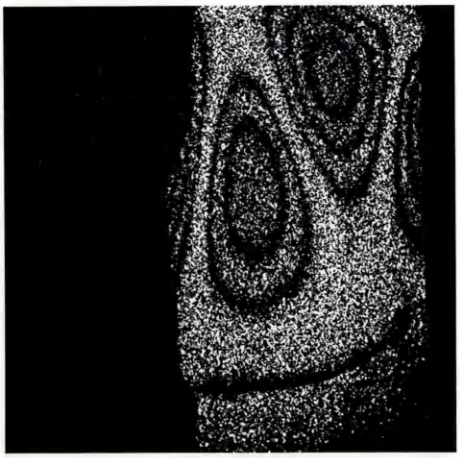

(a) Time-averaged fringes without heterodyning.

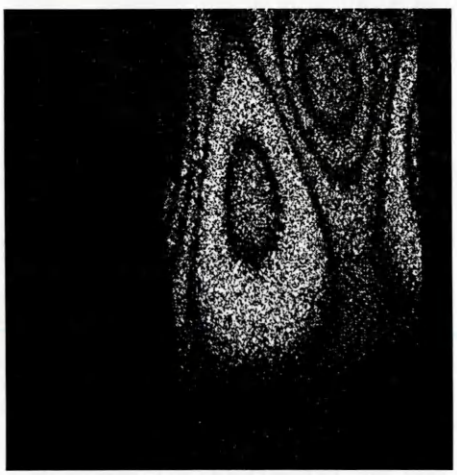

(b) Heterodyne fringes with 0° relative phase modulation.

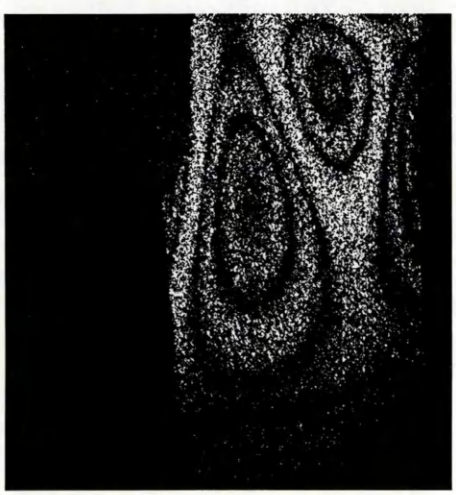

(c) Heterodyne fringes with 180° relative phase modulation.

Fig. 6.4 ESPI vibration fringes (a) time-averaged (b) heterodyned by 0.2 GHz and 0° relative phase (c) heterodyned by 0.2 GHz and 180° relative phase

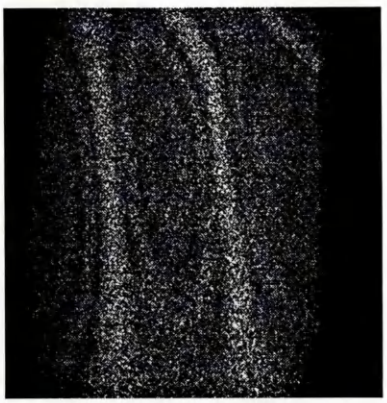

(a) Time-averaged fringes without heterodyning

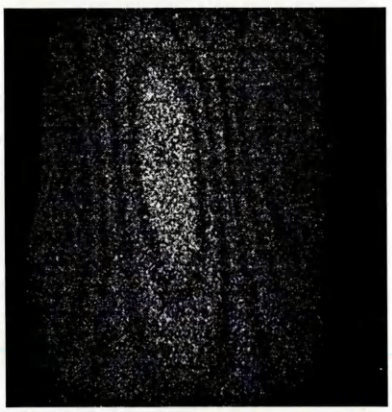

(b) Heterodyne fringes with 0° relative phase modulation.

(c) Heterodyne fringes with 180° relative phase modulation.

Fig. 6.5 Shearographic vibration fringes (a) time-averaged (b) heterodyned by 10.9 GHz and 0° relative phase (c) heterodyned by 10.9 GHz and 180° relative phase.

6.3 Stroboscopic illumination in shearography using laser diode injection current modulation

Stroboscopic illumination in shearography was achieved by pulsing the injection current of the laser diode between its nominal operating point and a point below threshold. When the modulation frequency of the injection current is below 10 MHz, the thermal sensitivity of the laser diode induces chirps in the optical frequency which creates an unstable wavelength during the pulse duration [6.53,6.54] and also deteriorates the fringe visibility quickly. This effect can be suppressed by the use of equalisation electronics (pulse shaping) in the diode drive current [6.55,6.56] or by balancing the optical path lengths between the two arms of the interferometer.

As mentioned in section 6.1.3, the stroboscopic method is normally performed by illuminating the vibrating object in its two extreme positions (the peak and the trough), as shown in Fig. 6.6. Speckle patterns modulated by the peak position are superimposed (correlated) with the speckle patterns modulated by the trough in the same image frame. Correlation fringes are then generated by either sequential subtraction or high-pass filtering. To phase step the stroboscopic fringes obtained by this method, the phase difference must be introduced to the interferometer between the two pulses and synchronised with the vibration motion (similar to the simultaneous two-wavelength contouring, as described in section 4.3.2). In practice, most phase shifter can not synchronise with the vibration frequency properly, hence the fringe visibility is reduced.

An alternative method is performed by illuminating the vibrating object in one of the two extreme positions (the peak or the trough), as shown in Fig. 6.7. When the object is stationary and illuminated by the stroboscopic light, a speckle image is first stored as a reference frame. The object is then excited to vibrate and the incoming frames are continuously subtracted from the reference frame to generate the stroboscopic vibration fringes. In this method, phase stepping can be easily implemented either by generating a phase step to one arm of the interferometer either in the reference frame or the

incoming frames. An modified method to one pulse illumination was published by Jones et al [6.37-6.40]. In their method, the reference frame is selected by adjusting the phase of the stroboscopic illumination when the object is vibrating. If the undeformed situation of the vibration is illuminated and synchronised, the stored reference frame is the same as that obtained when the object is stationary. In this method, relative vibration motion can be obtained by adjusting the phases of the illumination for the reference and the incoming frames.

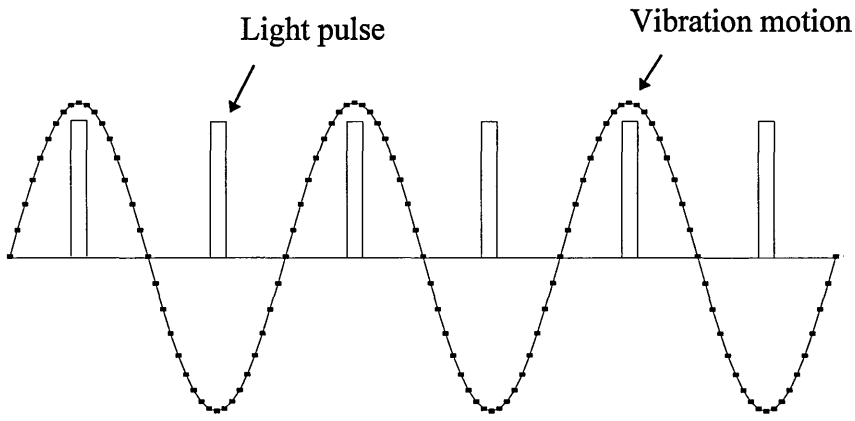

Fig. 6.6 Stroboscopic illumination using two pulses per vibration cycle.

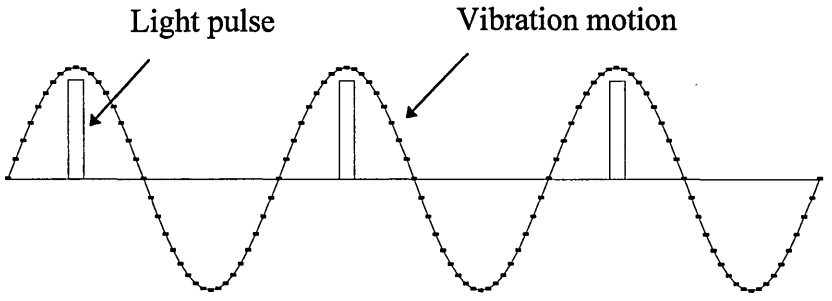

Fig. 6.7 Stroboscopic illumination using one pulse per vibration cycle.

6.3.1 Experimental

To reduce the chirping effect in stroboscopic illumination, the two optical paths in the interferometer were balanced to ± 0.2 mm (except the height variation on the object surface). The injection current of the laser diode was modulated by a synthesised function generator (Stanford Research System, DS 345) which generates an offset sinusoidal voltage, $V(t) = V_s[1+\sin(\omega t+\varphi_s)]$, to modulate the laser diode injection current from below threshold current (25 mA) to nominal operating current (100~123 mA). For the laser diode (Spectra Diode Labs, SDL-5411-G) used in this work, the threshold current is approximately 30 mA. The amplitude of voltage used is 4 volt, which generates a modulation range of 80 mA (20 mA/volt).

For quantitative analysis of vibration fringes obtained by stroboscopic illumination, phase stepping techniques [6.57] were implemented by moving one of the mirrors which was mounted on a PZT actuator. The phase stepped fringe patterns were stored in the frame grabber and low pass filtered by a 5x5 convolution filter. The pre-processed images were then processed by the fringe analysis program [6.58], provided by Dr. P. J. Bryanston-Cross at Warwick University, to get the wrapped and unwrapped phase maps which represent the gradients of vibration on the object surface.

6.3.2 Results and discussion

Fig. 6.8 and Fig. 6.9 show time-averaged and stroboscopic fringes of the turbine blade resonantly vibrating at 2.1 kHz, 3.4 kHz and 5.6 kHz, measured using the ESPI and shearography systems respectively. The visibility of stroboscopic fringes is uniform across the object even in the area of the higher vibration amplitude, or the higher gradient of vibration in shearography.

Figs 6.10-6.21 show stroboscopic shearographic fringes of the turbine blade vibrating at different resonant mode and the wrapped, unwrapped and 3D plot representing the gradient of vibration in each mode obtained from phase calculation algorithm.

The application of diode lasers in stroboscopic illumination offers the advantage of straightforward modulation via control of their injection current. However, the peak optical powers available are low, thus requiring that the illuminating pulses have a certain duty cycle to provide sufficient light [6.39]. If other than the extreme positions are measured, the light pulses need to be much shorter because the velocity of the blade surface at these positions is much larger. The fringe visibility will decrease as the velocity of the detecting positions increases for a given laser pulse width. The worst situation is within the linear region of a sinusoidal vibration motion, where the velocity of most vibrating points is approaching a maximum.

6.4 Summary

Heterodyning and stroboscopic techniques based on the wavelength modulation of a laser diode in an electronic shearography system have been presented. Heterodyning has been successfully demonstrated in a mechanical passive manner, which is in contrast to modulating the mirror mounted on a piezoelectric transducer. In order to enhance the understanding of vibration fringes measured by shearography, results of a vibrating turbine blade measured by shearography and ESPI systems respectively have been compared.

For heterodyning using ESPI, the brightest fringes locate at the areas where the vibration amplitude and phase correspond to the amplitude and phase of modulation. In contrast, for heterodyning using shearography, the brightest fringes locate at the positions where gradients of vibration displacement multiplied by the shearing distance is equal to the modulation amplitude and the vibration phase is equal to the modulation

phase. The brightest fringes by anti-phase modulations always locate at the opposite side surrounding the peak positions and the large stationary areas on the object surface.

In time-averaged vibration measurement, heterodyning can be easily applied to map out the phase and the amplitude of vibration motion. However, the process is performed manually, which need a high level of user intervention and sometimes need a photo detector to observe the intensity variation on a TV monitor. Automatic heterodyning that helps to release the disadvantage has been reported using Pockels cells [6.26] and the combination of a velocimeter [6.15].

Stroboscopic illumination produces uniform fringe visibility across the object surface and the fringe can be easily phase stepped to obtain vibration amplitude and phase maps. However, the available optical power of this method is normally low which will restrict its application within a certain frequency or velocity range unless pulse lasers are used.

The detection of resonant frequencies and mode shapes of test objects, using ESPI and shearography systems, is very useful for the assessment of the performance of mechanical components, e.g. the range of the operating speed and the noise level etc. Especially, they can be used to compare with the results obtained by numerical methods, e.g. finite element (FEM) [6.59,6.60], to verify the accuracy of simulation data and are helpful for the modification of assumed parameters and conditions if necessary. At this moment, vibration measurements using shearography are not as popular as using ESPI systems. The main reason is perhaps that vibration fringes in shearography are more difficult to interpret than those in ESPI. Since shearography systems have better robustness against environmental perturbations, the combination of shearography and ESPI systems or the development of interpretation software might resolve this problem.

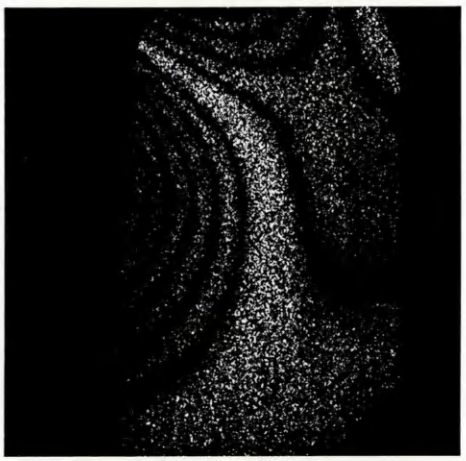

(a) Time-averaged, 2 kHz

(d) Stroboscopic, 2 kHz

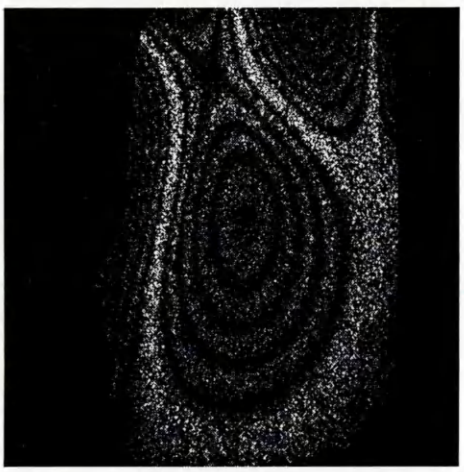

(b) Time-averaged, 3.5 kHz

(e) Stroboscopic, 3.5 kHz

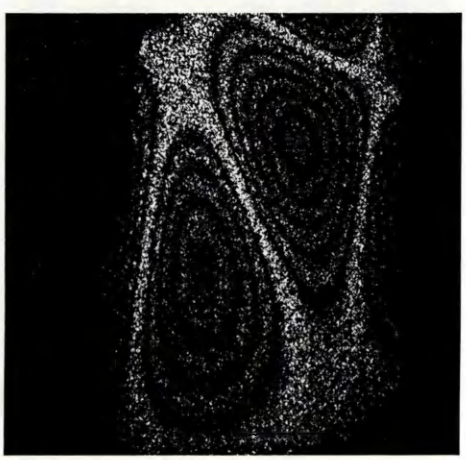

(c) Time-averaged, 5.6 kHz

(f) Stroboscopic, 5.6 kHz

Fig. 6.8 Time-averaged and stroboscopic vibration fringes of turbine blade measured using ESPI.

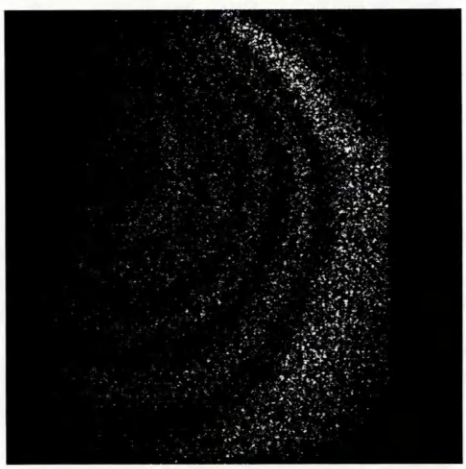

(a) Time-averaged, 2 kHz

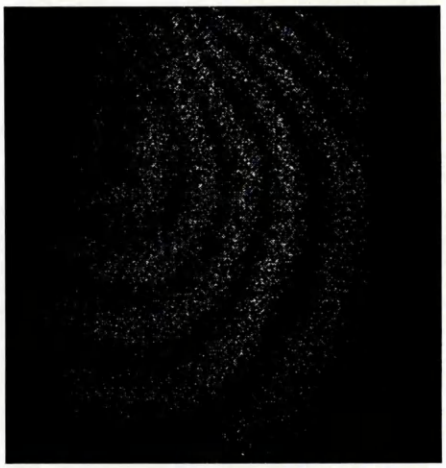

(d) Stroboscopic, 2 kHz

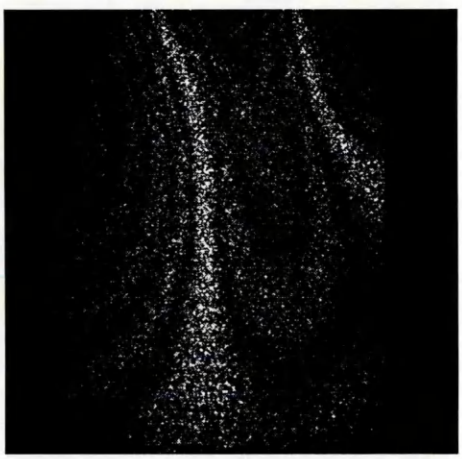

(b) Time-averaged, 3.5 kHz

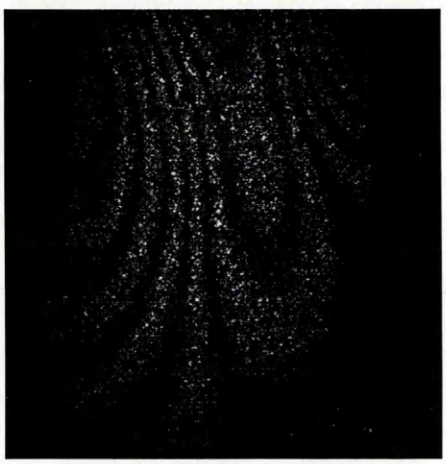

(e) Stroboscopic, 3.5 kHz

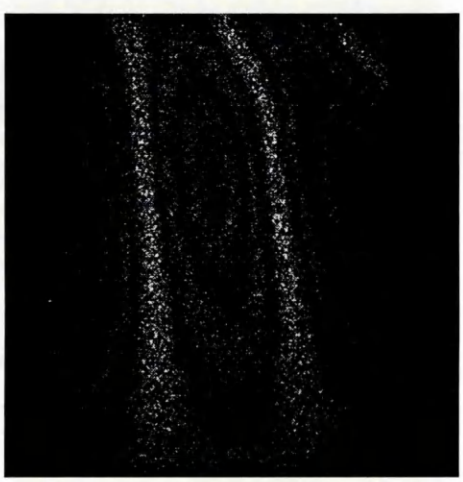

(c) Time-averaged, 5.6 kHz

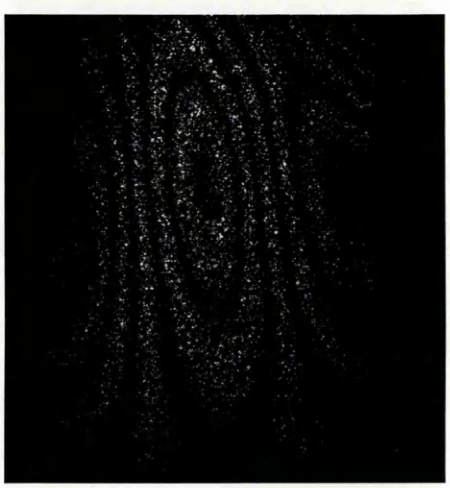

(f) Stroboscopic, 5.6 kHz

Fig. 6.9 Time-averaged and stroboscopic vibration fringes of turbine blade measured using shearography

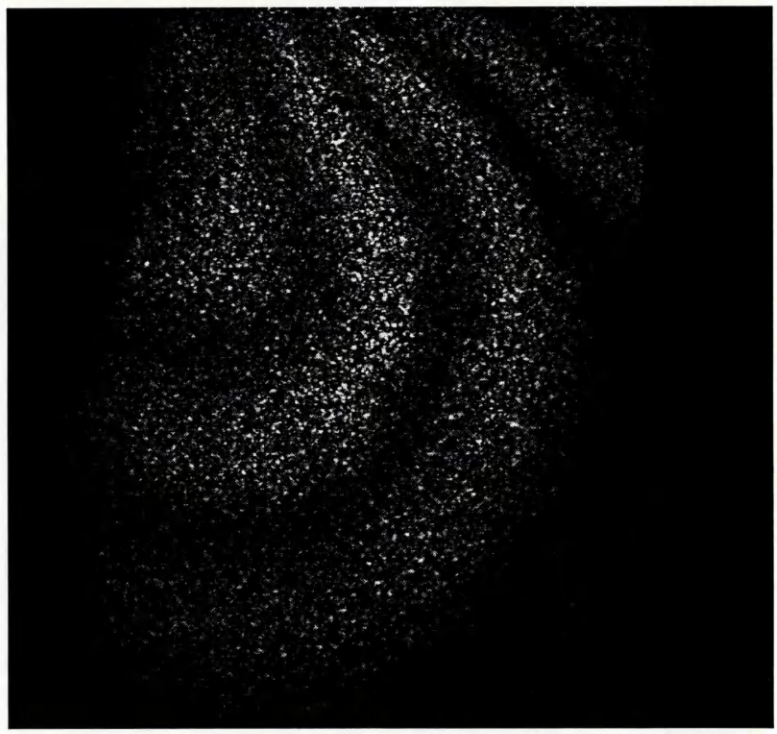

Fig. 6.10 Stroboscopic fringes of turbine blade vibrating at 2 kHz, measured using shearography with 0° phase shift

Fig. 6.11 Wrapped phase map calculated from the phase stepped fringes (2 kHz mode)

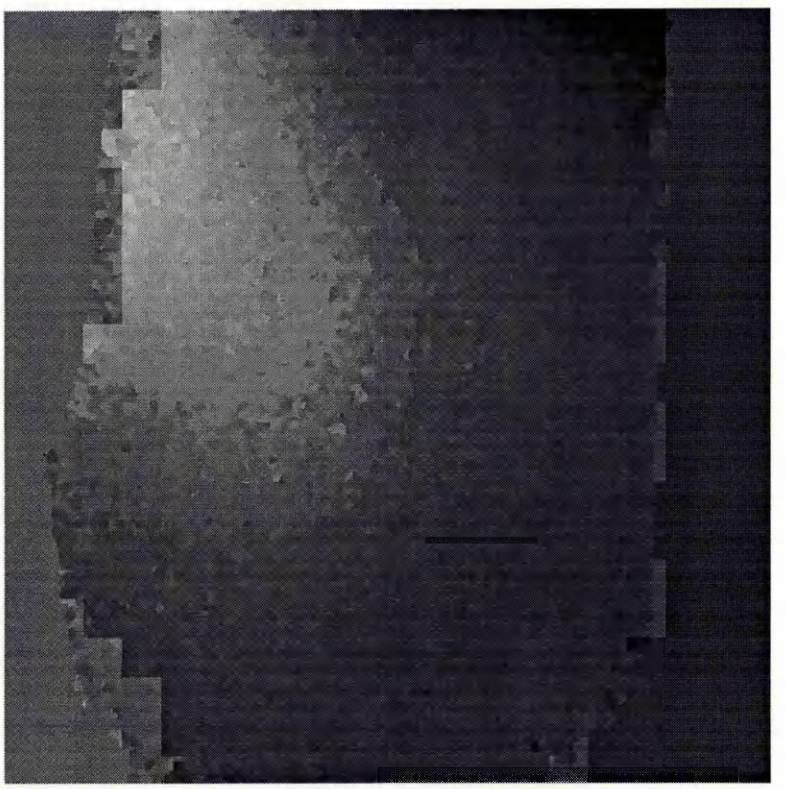

Fig. 6.12 Unwrapped phase map of the turbine blade (2 kHz mode)

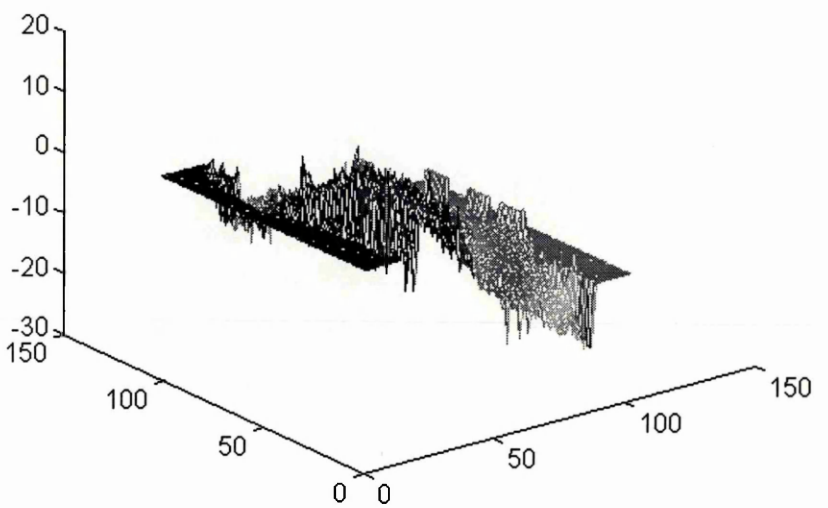

Fig. 6.13 Mesh plot representing the gradient of vibration motion (2 kHz mode)

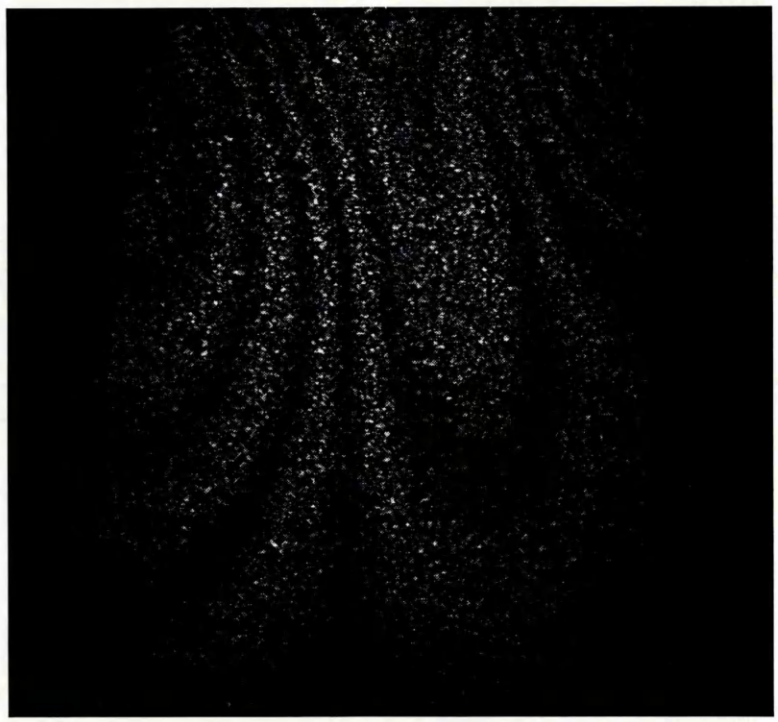

Fig. 6.14 Stroboscopic fringes of turbine blade vibrating at 3.5 kHz, measured by shearography with 0° phase shift

Fig. 6.15 Wrapped phase map calculated from the phase stepped fringes (3.5 kHz mode)

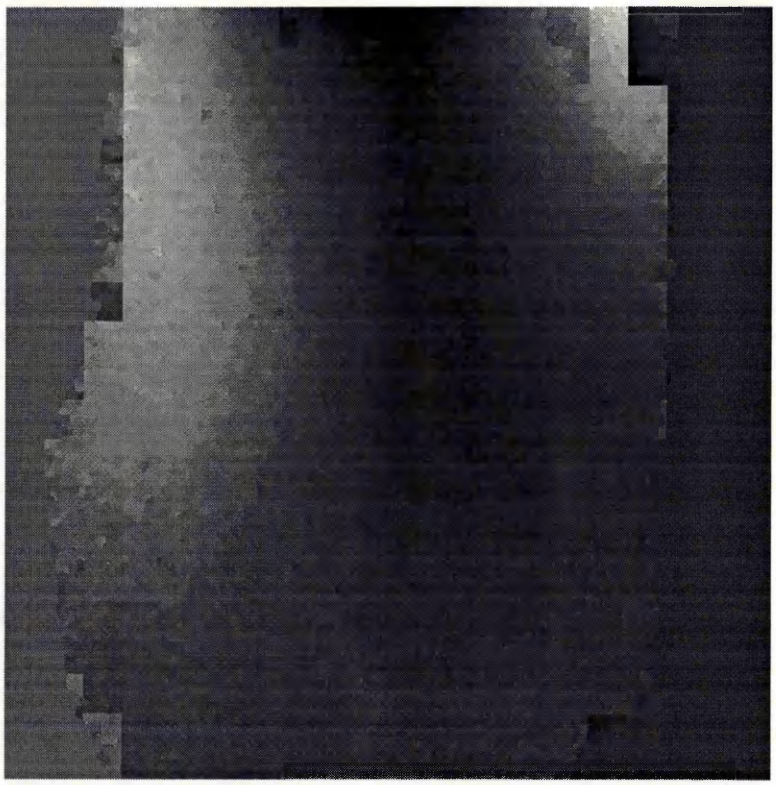

Fig. 6.16 Unwrapped phase map of the turbine blade (3.5 kHz mode)

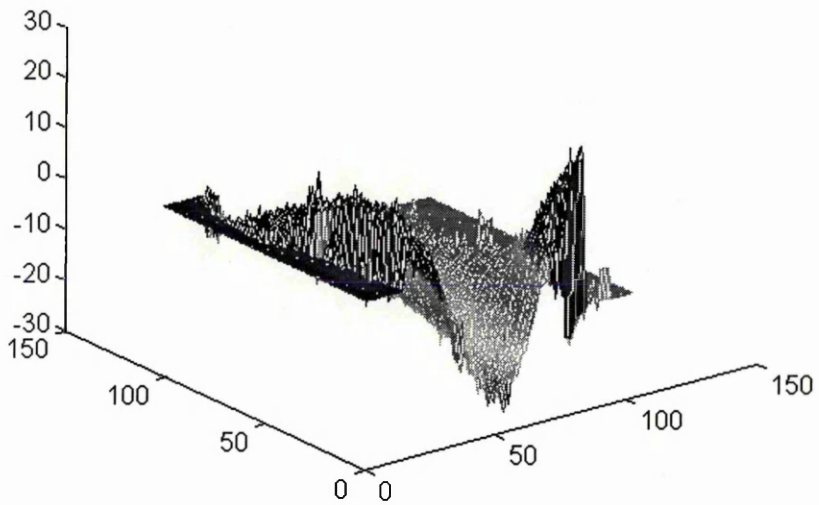

Fig. 6.17 Mesh plot representing the gradient of vibration motion (3.5 kHz mode)

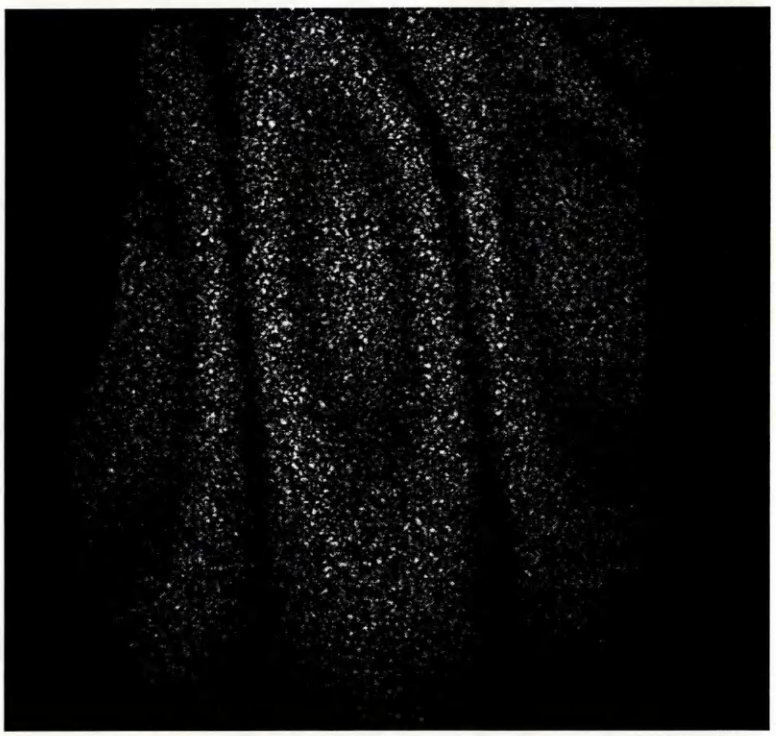

Fig. 6.18 Stroboscopic fringes of turbine blade vibrating at 5.6 kHz, measured using shearography with 0° phase shift

Fig. 6.19 Wrapped phase map calculated from the phase stepped fringes (5.6 kHz mode)

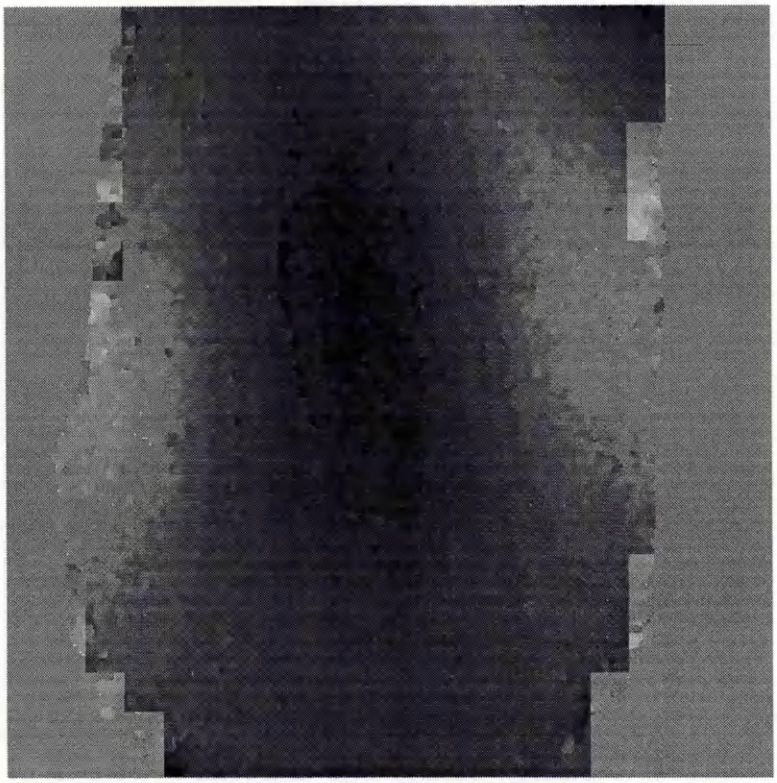

Fig. 6.20 Unwrapped phase map of the turbine blade (5.6 kHz mode)

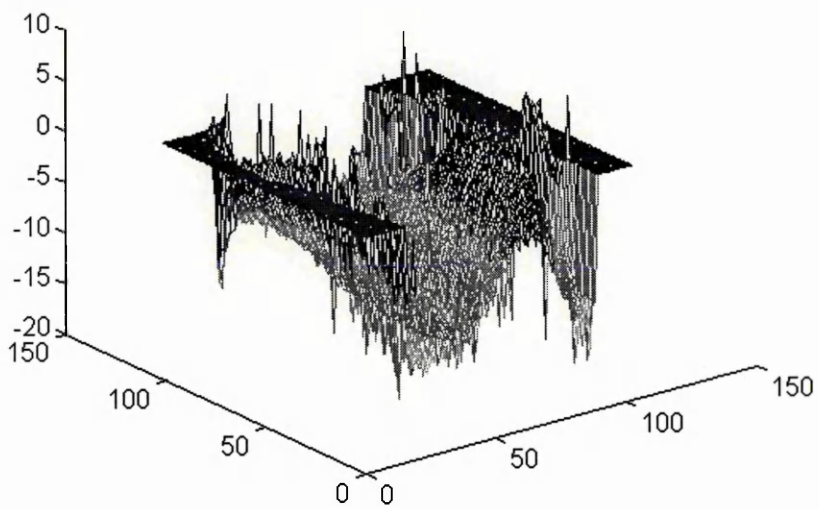

Fig. 6.21 Mesh plot representing the gradient of vibration motion (5.6 kHz mode)

References

6.1 Løkberg, O. J. and Svenke, P., Design and use of an electronic speckle pattern interferometer for testing of turbine parts. *Opt. and Lasers in Eng*, **2** (1981) 1-12.

6.2 Davies, J. C., The application of electronic speckle pattern interferometry to modal analysis. Proc. Int. Symp. on Automotive Technol. and Automation, Graz Austra, (1985) 73-92.

6.3 Davies, J. C. and Buckberry, C. H., Application of electronic speckle pattern interferometry in automotive product development. VDI Berichte, (617) (1986) 279-293.

6.4 Davies, J. C., Jones, J. D. C. and Pannell, C. N., Development and application of a fibre optic electronic speckle pattern interferometry. *SPIE*, Vol. 863 (1987) 194-207.

6.5 Løkberg, O. J., Industrial applications of ESPI. *SPIE*, Vol. 952 (1988) 208-217.

6.6 Buckberry, C. H. and Davies, J. C., The application of TV holography to engineering problems in the automotive industry. *Proc. Soc. for Exp. Mechanics on hologram interferometry and speckle metrology*, Bethel, Conn. USA, (1990) 268-278.

6.7 Powell, R. L. and Stetson, K. A., Interferometric vibration analysis by wavefront reconstruction. *J. Opt. Soc. Am.*, **55** (12) (1965) 1593-98.

6.8 Butters, J. N. and Leendertz, J. A., Holographic and video techniques applied to engineering measurement. *Transactions of the Institute of Measurement and Control*, **4** (12) (1971) 349-354.

6.9 Pedersen, H. M., Løkberg, O. J. and Forre, B. M., Holographic vibration measurement using a TV speckle interferometer with silicon target Vidicon. *Opt. Commun.*, 12 (4) (1974) 421-426.

6.10 Jones, R. and Wykes, C., *Holographic and Speckle Interferometry*. Cambridge University Press, Cambridge, 2nd ed., (1989) 109.

6.11 Aleksoff, C. C., Time average holography extended. *Appl. Phys. Lett.*, **14** (1) (1969) 23-24.

6.12 Neumann, D. B., Jacobson, C. F. and Brown, G. M., Holographic technique for determining the phase of vibrating objects. *Appl. Opt.*, **9** (6) (1970) 1357-62.

6.13 Løkberg, O. J. and Høgmoen, K., Use of modulated reference wave in electronic speckle pattern interferometry. *J. Phys. E: Sci. Instrum.*, **9** (1976) 847-851.

6.14 Løkberg, O. J. and Høgmoen, K., Vibration phase mapping using electronic speckle pattern interferometry. *Appl. Opt.*, **15** (11) (1976) 2701-04.

6.15 Valera, J. D., Harvey, D. and Jones, J. D. C., Automatic heterodyning of fibre optic speckle pattern interferometry. *SPIE*, Vol. 1508 (1991) 170-179.

6.16 Valera, J. D., Harvey, D. and Jones, J. D. C., Automatic heterodyning in fibre optic speckle pattern interferometry using laser velocimetry. *Opt. Eng.*, 31 (1992) 1646.

6.17 Valera, J. D., Doval, A. F. and Jones, J. D. C., Combined fibre optic laser velocimeter and electronic speckle pattern interferometer with a common reference beam. *Meas. Sci. Technol.*, **4** (1993) 578-582.

6.18 Martini, G., Analysis of a single-mode optical fibre piezo-ceramic phase modulator. Opt. Quantum Electron., **19**, 179.

6.19 Cheng, Y. Y. and Wyant, J. C., Phase shifter calibration in phase-shifting interferometry. *Appl. Opt.*, **24** (18) (1985) 3049-52.

6.20 Hariharan, P., Oreb, B. F. and Eiju, T., Digital phase-shifting interferometry: a simple error-compensating phase calibration. *Appl. Opt.*, **26** (13) (1987) 2504-05.

6.21 Dakin, J. P., Wade, C. A. and Haji, M., A fibre optic sensodyne frequency translator based on piezoelectrically-strained fibre phase shifter. *IEE*, Vol. 132 (1) (1985) 287.

6.22 Atcha, H. and Tatam, R. P., Optoelectronic ESPI: applications to surface contouring and vibration measurements. Proc. 9th Optical Fibre Sensors Conference (IEEE/OSA) Firenze, Italy, (1993) 337-340.

6.23 Atcha, H. and Tatam, R. P., Heterodyning of fibre optic electronic speckle pattern interferometers using laser diode wavelength modulation. *Meas. Sci. Technol.*, **5** (1994) 704-709.

6.24 Kobayashi, S., Yamamoto, Y. and Kimura, T., Modulation frequency characteristics of directly modulated optical frequency modulated AlGaAs semiconductor lasers. *Electron. Lett.*, **17** (7) 350-351.

6.25 Høgmoen, K. and Løkberg, O. J., Detection and measurement of small vibrations using electronic speckle pattern interferometry. *Appl. Opt.*, 16 (7) (1977) 1869-75.

6.26 Moran, S. E., Law, R. L., Craig, P. N. and Goldberg, W. M., Optically phase locked electronic speckle pattern interferometer. *Appl. Opt.*, **26** (1987) 475-491.

6.27 Moran, S. E., Lugannani, R., Craig, P. N. and goldberg, W. M., Optically phase locked electronic speckle pattern interferometer: system performance for vibration measurements in random displacement field. *J. Opt. Soc. Am.*, **A6** (1989) 252.

6.28 Dupont, C., Optoelectronic stabilisation for electronic speckle pattern interferometry. MSc thesis, Cranfield University, (1992).

6.29 Macchia, J. T. L., Stroboscopic holography with a mode-locked laser. *J. Appl. Phys.*, **39** (1968) 5340-41.

6.30 Archbold, E. and Ennos, A. E., Observation of surface vibration modes by stroboscopic hologram interferometry. *Nature*, **217** (1968) 942-943.

6.31 Watrasiewicz, B. M. and Spicer, P., Vibration analysis by stroboscopic holography. *Nature*, **217** (1968) 1142-43.

6.32 Zaidel, A. N., Malkhasyan, L. G., Markova, G. V. and Ostrovskii, Y. I., Holographic strobe method for studying vibrations. *Sov. Phys. Tech. Phys.*, **13** (1969) 1470-73.

6.33 Sajenko, P. and Johnson, C. D., Stroboscopic holographic interferometry. *Appl. Phys. Lett.*, 13 (1968) 22-24.

6.34 Mayer, G. M., Vibration phase measurement by rotation-strobe holography. *J. Appl. Phys.*, **40** (1969) 2863-66.

6.35 Løkberg, O. J., Use of chopped laser light in electronic speckle pattern interferometry. *Appl. Opt.*, **18** (14) (1979) 2377-84.

6.36 Løkberg, O. J., ESPI-the ultimate holographic tool for vibration analysis. *J. Opt. Soc. Am.*, **75** (6) (1984) 1784.

6.37 Valera, J. D., Doval, A. F. and Jones, J. D. C., Determination of vibration phase with electronic speckle pattern interferometry (ESPI). *Electron. Lett.*, **28** (25) (1992) 2292-94.

6.38 Valera, J. D., Doval, A. F. and Jones, J. D. C., Vibration phase measurement by fibre optic electronic speckle pattern interferometry (ESPI) with stroboscopic illumination. Proc. 9th Optical Fibre Sensors Conference (IEEE/OSA) Firenze, Italy, (1993) 381-384.

6.39 Anderson, D. J., Valera, J. D. and Jones, J. D. C., Electronic speckle pattern interferometry using diode laser stroboscopic illumination. *Meas. Sci. Technol.*, **4** (1993) 982-987.

6.40 Valera, J. D. and Jones, J. D. C., Whole field vibration phase measurement with ESPI. *SPIE*, Vol. 2342 (1994) 201-208.

6.41 Tyrer, J. R., Application of pulsed holography and double pulsed electronic speckle pattern interferometry to large vibrating engineering structures. *SPIE*, Vol. 599 (1985) 181.

6.42 Soares, O. D. D., Synchronous stroboscopic electronic speckle pattern interferometry. *SPIE*, Vol. 655 (1986) 390.

6.43 Tyrer, J. R., Critical review of recent developments in electronic speckle pattern interferometry. *SPIE*, Vol. 604 (1986) 95.

6.44 Shellabear, M. C., Santoyo, F. M. and Tyrer, J. R., Processing of addition and subtraction fringes from pulse ESPI for study of vibrations. *Proc. Soc. for Exp.*

Mechanics on hologram interferometry and speckle metrology, Bethel, Conn. USA, (1990) 238-244.

6.45 Santoyo, F. M., Shellabear, M. C. and Tyrer, J. R., Four cases of engineering studies using pulsed ESPI. *SPIE*, Vol. 1508 (1991) 143-152.

6.46 Nakadate, S., Yatagai, T. and Saito, H., Digital speckle-pattern shearing interferometry. *Appl. Opt.*, **19** (24) (1980) 4241-46.

6.47 Toh, S. L., Sang, H. M., Chau, F. S. and Tay, C. J., Flaw detection in composites using time-average shearography. *Opt. Laser Technol.*, **23** (1991) 25-30.

6.48 Pryputniewicz, R. J., Electronic shearography and electronic holography working side by side. *SPIE*, Vol. 1821 (1992) 27-37.

6.49 Mohan, N. K., Saldner, H. O. and Molin, N. E., Electronic shearography applied to static and vibrating objects. *Opt. Commun.*, **108** (1994) 197-202.

6.50 Valera, J. D. R. and Jones, J. D. C., Vibration analysis by modulated time-averaged speckle shearing interferometry. *Meas. Sci. Technol.*, **6** (1995) 965-970.

6.51 Hung, Y. Y. and Liang, C. Y., Image-shearing camera for direct measurement of surface strains. *Appl. Opt.*, **18** (7) (1979) 1046-51.

5.52 Buus, J., Single frequency semiconductor lasers. Tutorial Texts in Optical Eng., Vol. TT5, SPIE Optical Eng. Press (1991).

6.53 Ito, M. and Kimura, T., Stationary and transient thermal properties of semiconductor laser diodes. IEEE J. Quant. Electron., 17 (1981) 787-795.

6.54 Linke, R. A., Modulation induced transient chirping in single frequency lasers. IEEE J. Quant. Electron., QE-21 (1985) 593.

6.55 Bickers, L. and Westbrook, L. P., Reduction in laser chirp in 1.5 μm DFB lasers by modulation pulse shaping. *Electron. Lett.*, **21** (1985) 103.

6.56 Anderson, D. J., Jones, J. D. C., Sinha, P. G., Kidd, S. P. and Barton, J. S., Scheme for extending the bandwidth of injection-current-induced laser diode optical frequency modulation. *J. Modern Optics*, **38** (1991) 2459.

6.57 Creath, K., Temporal Phase Measurement Methods. *Interferogram Analysis - Digital Fringe Pattern Measurement Techniques*, ed. Robinson, D. W. and Reid, G. T., IOP Publishing Ltd, Bristol, (1993) 94-140.

6.58 Towers, D. P., Judge, T. R. and Bryanston-Cross, P. J., Automatic Interferogram Analysis Techniques Applied to Quasi Heterodyne Holography and ESPI. *Optics and Lasers in Eng*, **14** (1991) 239-282.

6.59 Pryputniewicz, R. J., A hybrid approach to deformation analysis. SPIE, Vol. 2342 (1994) 282-296.

6.60 Crema, L. B., Caponero, M. A., Castellani, A., Angelis, A. D. and Ermio, A., Analysis of coupled vibration modes by use of holographic interferometry and finite elements method. SPIE, Vol. 2545 (1995) 24-32.

7. CONCLUSIONS AND FUTURE WORK

7.1 Conclusions

This thesis has presented the implementation of enhanced signal processing techniques in electronic speckle shearing interferometry using laser diode wavelength modulation, including two-wavelength slope measurement, phase stepping, and heterodyning and stroboscopic illumination in vibration analysis.

Two-wavelength slope measurement is a mechanically passive method which does not require shifting or tilting of the illuminating beam, producing better fringe-visibility due to reduced speckle decorrelation. An accurate measurement can be obtained by increasing the illumination and viewing distances, or by calculating the related parameters C_x , C_y and C_z in the fringe function, since they are very simple equations. This technique offers the advantage, compared to illumination-shifting and object-tilting techniques, of no mechanical movement of any of the components required to produce the fringes combined with variable sensitivity and robustness to environmental perturbations compared to ESPI configurations.

A novel phase stepping technique using laser diode injection current modulation has been demonstrated. An unbalanced Michelson-interferometer arrangement, with a thick perspex block inserted into the longer arm of the interferometer, was used to accomplish the task. Advantages of this technique include the removal of an active phase-shifting component for phase stepping which reduces electrical signals in the detection head and a greater linearity in the phase shifts through the wavelength modulation of laser diodes. The technique has provided an additional phase shifting method in electronic shearography.

In vibration measurement, heterodyning and stroboscopic illumination have also been successfully achieved in a mechanical passive manner. For shearing systems using Michelson interferometer or wedge arrangements, heterodyning was originally difficult to perform. With the unbalanced optical configuration as used in the phase stepping work, this problem has been overcome. In shearography, the optical path length difference is not effected by the viewing distance which is in contrast to an out-of-plane ESPI system. This is an advantage for performing heterodyning using diode wavelength modulation, because the path length difference is nearly constant and is not necessary to re-calibrate when the viewing distance is changed.

By pulsing the laser diode, stroboscopic illumination has been performed to obtain cosine fringes along with greatly improved visibility. The chirping effect was suppressed by calibrating the two optical paths in the interferometer well balanced to ± 0.2 mm. Phase stepping methods were then incorporated to automate the fringe analysis.

Together with the theoretical and experimental work, a software program has been written to integrate the electronic shearography and ESPI systems in a PC. The program, which has facilitated most of the functions required, has been a useful tool and is specific to the frame grabber that we used. Combined with the phase unwrapping software provided by Dr P. J. Bryanston-Cross, automatic analysis of correlation fringes can be achieved.

The main contribution of this thesis is the development of signal processing techniques which can be used to extend the applicability of electronic speckle shearing interferometry.

7.2 Future work

Some ideas about future work in shearography are discussed below.

Measurement of in-plane strain

In experimental mechanics, a complete strain analysis is a very useful information for design verification and product testing. Although shearography can measure gradients of out-of-plane deformation directly, the gradients of in-plane deformation can not be independently measured without the effect of out-of-plane deformation. To resolve this problem, one possibility is to investigate optical configurations that can measure gradients of in-plane deformation separately [7.1,7.2]. Up to this moment, there is no really successful solution to this approach and it is regarded as a very difficult task [7.5].

Another approach is to obtain two fringe patterns resulting from different illuminating positions to separate the in-plane components point by point, originally proposed by Hung et al [7.3-7.5]. In the papers reported by Fang et al [7.4,7.5], the phase of the fringe pattern was determined by the fringe order number and a fringe carrier technique was applied [7.6]. If using phase stepping and phase unwrapping methods in this approach, the phase of the fringe pattern in each illuminating position can be determined unambiguously without generating carrier fringes. Phase stepping can be more readily automated than fringe counting methods, and is suggested here as an improvement to the technique of Fang et al.

The development of a multi-wavelengths shearography system is also a future trend for strain measurements. In this system, the test object is simultaneously illuminated using three different wavelengths and the speckle images are recorded by a colour CCD camera. Phase stepping can be performed simultaneously in each wavelength, instead of recording phase stepped images sequentially. This is specially suitable for the measurements in harsh environmental conditions or using pulse lasers. For simultaneous measurements of three-dimensional strain [7.3], the illuminating

configuration of one wavelength, λ_1 , is located to be collinear with the viewing axis (z axis), the second wavelength, λ_2 , must lie on the xz plane at an angle (e.g. 45°) with respect to the viewing axis, and the third wavelength, λ_3 , must lie on the yz plane at an angle with respect to the viewing axis. The configuration of λ_1 is used to obtain gradients of out-of-plane deformation directly. However, the configurations of λ_2 and λ_1 are used to obtain the x gradients of in-plane deformation, and the configurations of λ_3 and λ_1 are used to obtain the y gradients of in-plane deformation.

Separation of two vibration modes

In vibration measurement, we have demonstrated stroboscopic illumination by pulsing the laser diode. The method can also be used to separate two sinusoidal vibration modes which was originally proposed in holographic interferometry [7.7] and also reported by Valera et al [7.8] in ESPI. When the stroboscopic illumination is synchronised at the same frequency of one vibration mode, but with a phase such that only the undeformed situation of that mode is illuminated, the fringes obtained will then contain the information of the second mode.

This method can measure the composite vibration motion with irrationally related modes, i.e. ω_1/ω_2 is not an integer, and also the motion with rationally related modes, i.e. ω_1/ω_2 is an integer. A typical structure with two-mode vibration characteristics is a circular plate supported at its centre by a beam with a small cross section. Composite vibration occurs when this object is excited at a certain frequency, of which two different modes vibrate at the same frequency but with a phase difference. The two modes are rationally related ($\omega_1/\omega_2 = 1$) and can be separated using stroboscopic illumination by pulsing the laser diode. The method is simpler compared to the vibration comparative method proposed by Ganesan et al [7.9], since no master object

(an object similar to the test object) is required. In their method, the test object is excited simultaneously in two different modes, and the reference beam is modulated by the master object vibrating in one of the two modes. This vibration comparative method is only suitable for objects that vibrate in irrationally related modes, and is not practical because the discrimination of vibration modes between the test and master objects is difficult to implement.

Fringe Interpretation

For shearography, the most promising application is in NDT. Image interpretation is now an area of active research, since the fringes obtained in flaw detection can be very complex. Some of the more sophisticated data analysis techniques could alleviate this problem and are still under development. The use of an ESPI system can also help to interpret the shearographic fringes. The construction of a compact and portable combined system is still ongoing in this laboratory.

References

7.1 Dai, F. L., Wang, S. Y. and Zhong, G. C., Speckle-shearing moire for strain fields. *Proc. 4th Conf. on Exp. Mec.*, Wuhan, China, (1984).

7.2 Petzing, J. N. and Tyrer, J. R., In-plane electronic speckle pattern interferometry: A theoretical analysis supported with experimental results. *SPIE*, Vol. 2342 (1994) 27-36.

7.3 Hung, Y. Y. and Liang, C. Y., Image-shearing camera for direct measurement of surface strains. *Appl. Opt.*, **18** (7) (1979) 1046-51.

7.4 Fang, J. and Shi, H. M., Fringe modulation for the separation of displacement derivative components in speckle-shearing interferometry. *SPIE*, Vol. 1163 (1989) 172-175.

7.5 Fang, J. and Laermann, K. H., A carrier method of speckle-shearing interferometry for individual-component patterns of in-plane strain. *Opt. and Laser Technol.*, **27** (3) (1995) 139-143.

7.6 Hung, Y. Y., Hovanesian, J. D. and Takezaki, J., A fringe carrier technique for unambiquous determination of fringe orders in shearography. *Optics. and Lasers in Eng*, **8** (1988) 73-81.

7.7 Vikram, C. S., Stroboscopic holographic interferometry of vibration simultaneously in two sinusoidal modes. *Opt. Commun.*, **11** (4) (1974) 360-364.

7.8 Valera, J. D., Doval, A. F. and Jones, J. D. C., Determination of vibration phase with electronic speckle pattern interferometry (ESPI). *Electron. Lett.*, **28** (25) (1992) 2292-94.

7.9 Ganesan, A. R., Meinlschmidt, P. and Hinsch, K. D., Vibration mode separation using comparative electronic speckle pattern interferometry (ESPI). *Opt. Commun.*, **107** (1994)28-34.

APPENDIX A

A.1 Heterodyning in ESPI using reference beam modulation

When a test object is resonantly vibrating and measured using an out-of-plane ESPI system, the electric field of the object beam is expressed as

$$E_o(\underline{r}_o,t) = e_o \exp i\left\{\phi_o + \phi_s + \frac{4\pi}{\lambda} a_o(\underline{r}_o)\sin\left[\omega t + \varphi_o(\underline{r}_o)\right]\right\} \tag{A.1}$$

where $a_o(\underline{r}_o)$ and $\varphi_o(\underline{r}_o)$ are the amplitude and phase of the vibration motion. If the reference beam is sinusoidally modulated, its electric field is expressed as

$$E_r(t) = e_r \exp i\left[\phi_r + \frac{4\pi}{\lambda} a_r \sin(\omega t + \varphi_r)\right] \tag{A.2}$$

where a_r and φ_r represent the amplitude and phase of the reference beam modulation. The instantaneous intensity at the camera is

$$\begin{aligned} I(\underline{r}_d,t) &= (E_o + E_r)(E_o + E_r)^* \\ &= e_r^2 + e_o^2 + e_r e_o \exp i(\phi + \phi_s)\exp i\left\{\frac{4\pi}{\lambda}\left[a_o \sin(\omega t + \varphi_o) - a_r \sin(\omega t + \varphi_r)\right]\right\} \\ &\quad + e_r e_o \exp i\left[-(\phi + \phi_s)\right]\exp i\left\{-\frac{4\pi}{\lambda}\left[a_o \sin(\omega t + \varphi_o) - a_r \sin(\omega t + \varphi_r)\right]\right\} \end{aligned} \tag{A.3}$$

where $\phi = \phi_o - \phi_r$, $\underline{r}_d$ represents a conjugate position vector of $\underline{r}_o$ in the image plane, and * implies a Hermitian conjugate. It can be seen from equation (A.3) that

$$\begin{aligned} &a_o \sin(\omega t + \varphi_o) - a_r \sin(\omega t + \varphi_r) \\ &= a_o \sin\omega t \cos\varphi_o + a_o \cos\omega t \sin\varphi_o - a_r \sin\omega t \cos\varphi_r - a_r \cos\omega t \sin\varphi_r \end{aligned}$$

$$= \cos\omega t\left(a_o \sin\varphi_o - a_r \sin\varphi_r\right) + \sin\omega t\left(a_o \cos\varphi_o - a_r \cos\varphi_r\right) \tag{A.4}$$

Using the cosine law, equation (A.4) can be simplified to become

$$a_m \cos(\omega t - \alpha) \tag{A.5}$$

where,

$$a_m = \left[a_o^2 + a_r^2 - 2a_o a_r \cos(\varphi_o - \varphi_r)\right]^{1/2}, \tag{A.6}$$

$$\cos\alpha = \left(a_o \sin\varphi_o - a_r \sin\varphi_r\right)/a_m, \tag{A.7}$$

$$\sin\alpha = \left(a_o \cos\varphi_o - a_r \cos\varphi_r\right)/a_m \tag{A.8}$$

The instantaneous intensity in the image plane, equation (A.3), becomes

$$I(\underline{r}_d, t) = I_r + I_o + \sqrt{I_r I_o}\exp i(\phi + \phi_s)\exp i\left[\frac{4\pi}{\lambda} a_m \cos(\omega t - \alpha)\right]$$
$$+\sqrt{I_r I_o}\exp i\left[-(\phi + \phi_s)\right]\exp i\left[-\frac{4\pi}{\lambda} a_m \cos(\omega t - \alpha)\right] \tag{A.9}$$

where $I_r = e_r^2$ and $I_o = e_o^2$ are the intensities of the reference and object beams respectively. The integrated intensity in one image frame can be expressed by the average of the instantaneous intensity over the vibration period τ as

$$I(\underline{r}_d) = \frac{1}{\tau}\int_0^\tau I(\underline{r}_d, t)dt$$
$$= I_r + I_o + \sqrt{I_r I_o}\exp i(\phi + \phi_s)\frac{1}{\tau}\int_0^\tau \exp i\left[\frac{4\pi}{\lambda} a_m \cos(\omega t - \alpha)\right]dt$$

$$+\sqrt{I_r I_o}\exp i\left[-(\phi+\phi_s)\right]\frac{1}{\tau}\int_0^{\tau}\exp i\left[-\frac{4\pi}{\lambda}a_m\cos(\omega t-\alpha)\right]dt \tag{A.10}$$

As seen from equation (A.10),

$$\frac{1}{\tau}\int_0^{\tau}\exp i\left[\frac{4\pi}{\lambda}a_m\cos(\omega t-\alpha)\right]dt = J_o\left(\frac{4\pi}{\lambda}a_m\right) \tag{A.11}$$

and

$$\frac{1}{\tau}\int_0^{\tau}\exp i\left[-\frac{4\pi}{\lambda}a_m\cos(\omega t-\alpha)\right]dt = J_o\left(-\frac{4\pi}{\lambda}a_m\right) = J_o\left(\frac{4\pi}{\lambda}a_m\right) \tag{A.12}$$

Substituting equations (A.11) and (A.12) into equation (A.10) and rearranging yields

$$I(\underline{r}_d) = I_r + I_o + 2\sqrt{I_r I_o}\cos(\phi+\phi_s)J_0\left(\frac{4\pi}{\lambda}a_m\right) \tag{A.13}$$

After the image processing either by sequential subtraction or by high pass filtering, the displayed vibration fringes can be expressed as

$$I(\underline{r}_d) \propto \cos^2(\phi+\phi_s)J_o^2\left(\frac{4\pi}{\lambda}a_m\right) \tag{A.14}$$

A.2 Heterodyning in shearography using laser diode wavelength modulation

In an interferometer, the phase of a light beam travels a distance L in the free space can be expressed as

$$\phi = \frac{2\pi}{\lambda} L = \frac{2\pi\nu}{c} L \tag{A.15}$$

When the optical frequency of the light source has been changed by $\Delta\nu$, the phase change $\Delta\phi$ is given by

$$\Delta\phi = \frac{2\pi L}{c} \Delta\nu \tag{A.16}$$

In a shearography system with an x shear of δx, light reflected from two neighbouring points (x, y) and (x+δx, y) will be brought to interfere at the same point (x_d, y_d) in the image plane. To perform heterodyning using laser diode wavelength modulation, the optical frequency of the light source is modulated at the same frequency, ω, as the vibrating object but with a relative phase with respect to the vibration motion. The optical frequency change can be expressed as

$$A_\nu = \Delta\nu \sin(\omega t + \varphi_\nu) \tag{A.17}$$

where, $\Delta\nu$ and φ_ν are the amplitude and phase of the optical frequency change respectively. The phase of light reflected from (x+δx, y) and (x, y) can be expressed as

$$\phi_1 = \frac{2\pi\nu}{c} \cdot 2a_o(x + \delta x, y)\sin(\omega t + \varphi_o) + \frac{2\pi}{c}(L_1)\Delta\nu \sin(\omega t + \varphi_\nu) \tag{A.18}$$

$$\phi_2 = \frac{2\pi\nu}{c} \cdot 2a_o(x, y)\sin(\omega t + \varphi_o) + \frac{2\pi}{c}(L_2)\Delta\nu \sin(\omega t + \varphi_\nu) \tag{A.19}$$

where, a_o(x+δx, y) and a_o(x, y) are the vibration amplitudes of the positions (x+δx, y) and (x, y) respectively, φ_o is the vibration phase, and L_1 and L_2 are the path lengths of the light reflected from (x+δx, y) and (x, y). The path length difference between these two beams is then given by

$$L_2 - L_1 = \Delta L + 2\delta z \tag{A.20}$$

where, ΔL is the path length difference generated in the Michelson interferometer, and δz is the height variation between (x+δx, y) and (x, y). The electric fields of the light reflected from these two points are expressed as

$$E_1(x+\delta x, y, t) = e_1(x+\delta x, y)\exp i\phi_{s1}\exp i\left\{\frac{4\pi}{c}a_{m1}\right\}$$

$$E_2(x, y, t) = e_2(x, y)\exp i\phi_{s2}\exp i\left\{\frac{4\pi}{c}a_{m2}\right\} \tag{A.21}$$

where,

$$a_{m1} = a_o(x+\delta x, y)\nu\sin(\omega t+\varphi_o) + \left(\frac{L_1}{2}\right)\Delta\nu\sin(\omega t+\varphi_\nu) \tag{A.22}$$

$$a_{m2} = a_o(x, y)\nu\sin(\omega t+\varphi_o) + \left(\frac{L_2}{2}\right)\Delta\nu\sin(\omega t+\varphi_\nu) \tag{A.23}$$

e_1 and e_2 represent the amplitudes of the two wavefronts, and ϕ_{s1} and ϕ_{s2} are the randomly varying speckle phase terms. The instantaneous intensity at the image detector is

$$\begin{aligned} I(x_d, y_d, t) &= (E_1 + E_2)(E_1 + E_2)^* \\ &= e_1^2 + e_2^2 + 2e_1e_2\cos\left\{\phi_s + \frac{4\pi}{c}(a_{m1} - a_{m2})\right\} \\ &= e_1^2 + e_2^2 + 2e_1e_2\cos\left\{\phi_s + \frac{4\pi}{c}\left[\left(\frac{\partial a_o}{\partial x}\delta x\right)\nu\sin(\omega t+\varphi_o) + \left(\frac{\Delta L}{2} + \delta z\right)\Delta\nu\sin(\omega t+\varphi_\nu)\right]\right\} \end{aligned} \tag{A.24}$$

where, $\phi_s = \phi_{s1} - \phi_{s2}$. Using the cosine law, equation (A.24) can be simplified to become

$$I(x_d, y_d, t) = e_1^2 + e_2^2 + 2e_1 e_2 \cos\left[\phi_s + \frac{4\pi\nu}{c} a_{m3} \cos(\omega t - \beta)\right] \tag{A.25}$$

where,

$$a_{m3} = \left[\left(\frac{\partial a_o}{\partial x}\delta x\right)^2 + \left(\frac{\Delta L}{2} + \delta z\right)^2 \left(\frac{\Delta\nu}{\nu}\right)^2 + 2\left(\frac{\partial a_o}{\partial x}\delta x\right)\left(\frac{\Delta L}{2} + \delta z\right)\left(\frac{\Delta\nu}{\nu}\right)\cos(\varphi_o - \varphi_\nu)\right]^{1/2} \tag{A.26}$$

$$\cos\beta = \left[\left(\frac{\partial a_o}{\partial x}\delta x\right)\sin\varphi_o + \left(\frac{\Delta L}{2} + \delta z\right)\left(\frac{\Delta\nu}{\nu}\right)\sin\varphi_\nu\right] \Big/ a_{m3} \tag{A.27}$$

$$\sin\beta = \left[\left(\frac{\partial a_o}{\partial x}\delta x\right)\cos\varphi_o + \left(\frac{\Delta L}{2} + \delta z\right)\left(\frac{\Delta\nu}{\nu}\right)\cos\varphi_\nu\right] \Big/ a_{m3} \tag{A.28}$$

The integrated intensity in one image frame can be expressed by the average of the instantaneous intensity over the vibration period τ as

$$I(x_d, y_d) = \frac{1}{\tau}\int_0^\tau I(x_d, y_d, t) = e_1^2 + e_2^2 + 2e_1 e_2 \cos\phi_s J_o\left(\frac{4\pi}{c} a_{m3}\right) \tag{A.29}$$

After the image processing either by sequential subtraction or by high pass filtering, the displayed vibration fringes can be expressed as

$$I(x_d, y_d) \propto J_0^2\left\{\left(\frac{4\pi\nu}{c}\right)\left[\left(\frac{\partial a_o}{\partial x}\delta x\right)^2 + \left(\frac{\Delta L}{2} + \delta z\right)^2 \left(\frac{\Delta\nu}{\nu}\right)^2 + 2\left(\frac{\partial a_o}{\partial x}\delta x\right)\left(\frac{\Delta L}{2} + \delta z\right)\left(\frac{\Delta\nu}{\nu}\right)\cos(\varphi_o - \varphi_\nu)\right]^{1/2}\right\} \tag{A.30}$$

APPENDIX B: DSPI program listing

```
/* Main Program: dspi.c */

#include <graph.h>
#include <process.h>
#include <stdio.h>

#define AT
#include "itex.h"
#include "itex100.h"
#include "menu1.h"
#include "stdtyp.h"

int DTA_VOLT=1336;

/* Array and enum for main menu1 */

ITEM mnuMain1[] =
{
   { 0, "Quit"              },
   {11, "select a caMera"    },
   {10, "reset 100 Board"    },
   {11, "continuous Grab"    },
   { 3, "snaP an image"      },
   { 1, "sTatic SUB"         },
   { 1, "sEquential SUB"     },
   { 1, "sWap up 2 bits"     },
   { 0, "Save a page"        },
   { 0, "Read an image"      },
   { 2, "enHence an image"   },
   { 5, "view All pages"     },
   { 0, "Clear active page"  },
   { 1, "cLear all pages"    },
   { 1, "bIt map of regs"    },
   { 0, "static MOD: p0"     },
   { 1, "Contr-frame-p1"     },
   { 1, "Contr-fast-p1"      },
   { 0, "Log Image"          },
   { 1, "Log look-up table"  },
   { 0, "Next"               },
   { 0,""                    }
};

/* Define constants (0, 1, 2,...) for menu1 choices */

enum CHOICE1
{
   QUIT, SCAM, REST, GRB, SNP, STAS, SEQS, SWA2, SPGE, RIMG, EHIM,
   VALL, CPGE, CLAL, DTA0, CTR1, CTR2, LOIM, LOLU, NEXP
};

/* Array and enum for main menu2 */

ITEM mnuMain2[] =
{
   { 0, "Previous"           },
   { 0, "Change PZT volt"    },
```

```
    { 1, "sEquential SUB2"        },
    { 4, "specKle average1"       },
    { 0, "Read pixel value"       },
    { 0, "Electronic Noise"       },
    { 0, "Nonlinear Enhence"      },
    { 3, "conVol filter"          },
    { 0, "Low pass filter"        },
    { 7, "Change Brightness"      },
    { 0, "Static MOD: p4"         },
    { 0, "FP calibration"         },
    { 1, "Pixel averaged"         },
    { 1, "PZT calibration"        },
    { 0, "Histogram"              },
    { 0, "Diode calibration"      },
    { 0, "Dual grab"              },
    { 0,""                        }

};

/* Define constants (0, 1, 2,...) for menu2 choices */

enum CHOICE3
{
    PRES, CHVT, SEQ2, SPCA, RPL, SNR, NON, CVF, LPF, BRI, DTA4,
    FPC, PAV, PZC, HIS, DIOC, DUGR
};

/* Global video configuration */

 struct videoconfig vc;


int main()
{
    int rowMid, colMid;
    int iMainCur1 = 1;
    int iMainCur2 = 1;
    int CAMSEL;
    int mnuidx2;

    _getvideoconfig( &vc );
    rowMid = vc.numtextrows / 2;
    colMid = vc.numtextcols / 2;

    board_reset();

    system("\\utils\\keyemu");

    while( TRUE )
    {
            _clearscreen( _GCLEARSCREEN );

            /* Select from menu1. */

            iMainCur1 = Menu1( rowMid, colMid, mnuMain1, iMainCur1 );

            /* Branch to menu1 choice. */

            switch( iMainCur1 )
            {
              case QUIT:
                    quit_subroutine();
```

```
            return FALSE;

    case SCAM:
            CAMSEL= camera_selection(rowMid, colMid);
            setcamera(CAMSEL);
            break;

    case REST:
            stopgrab(1);
            board_reset();
            setcamera(CAMSEL);
            break;

    case GRB:
            waitvb();
            grab(0);
            break;

    case SNP:
            img_snap();
            break;

    case STAS:
            static_subtraction();
            break;

    case SEQS:
            sequential_subtraction();
            break;

    case SWA2:
            swap2_subroutine();
            break;

    case SPGE:
            imgsave_sub();
            break;

    case RIMG:
            imgread_sub();
            break;

    case EHIM:
            enhence_img_sub();
            break;

    case VALL:
            pages();
            break;

    case CPGE:
            sclear(0);
            break;

    case CLAL:
            aclear( 0,  0, 1024, 1024, 0);
            break;

case BTMP:
      test_register();
      break;
```

```
case DTA0:
        dta_ch0();
        break;

case CTR1:
        contour1_func();
        break;

case CTR2:
        contour2_func();
        break;

case LOIM:
        log_img_sub();
        break;

case LOLU:
        loglut(0x0000, 0);
        loglut(0x2000, 0);
        loglut(0x4000, 0);
        break;

case NEXP:
        mnuidx2=1;
        while( mnuidx2==TRUE )
        {
         _clearscreen( _GCLEARSCREEN );

         /* Select from menu2. */

         iMainCur2 = Menu1( rowMid, colMid, mnuMain2, iMainCur2 );

         /* Branch to menu2 choice. */

         switch( iMainCur2 )
         {
          case PRES:
                mnuidx2=0;
                break;

          case CHVT:
                volt_change();
                break;

          case SEQ2:
                sequential_subtraction2();
                break;

          case SPCA:
                speckle_average_sub1();
                break;

          case RPL:
                read_pixel();
                break;

          case SNR:
                signal_noise_func();
                break;

          case NON:
                enhence_img_sub2();
```

```
                    break;

                case CVF:
                    convol_5x5();
                    break;

                case LPF:
                    lopass( 0, 0, 512, 512, ABS );
                    break;

                case BRI:
                    brightness_sub();
                    break;

                case DTA4:
                    dta_ch4();
                    break;

                case FPC:
                    fp_cali_func();
                    break;

                case PAV:
                    fp_cali_func2();
                    break;

                case PZC:
                    pzt_cal1_func();
                    break;

                case HIS:
                    hist_func();
                    break;

                case DIOC:
                    diode_cal1_func();
                    break;

                case DUGR:
                    dualgrab();
                    break;
                }
               }

        }
    }
}

/************************************* End of main program *********************************/


/* DSPI Program: gt11.c */

/*  Header files included  */

#include <graph.h>
#include <math.h>   /* for pow( x, y) func */
#include <stdio.h>

#define AT
#include "itex.h"
#include "itex100.h"
```

```
#include "menu1.h"
#include "stdtyp.h"

/* Array and enum for camera selection */

ITEM mnuCam[] =
{
   { 9, "Port: CAM1"  },
   { 9, "Port: CAM2"  },
   { 9, "Port: CAM3"  },
   { 0, ""      }
};

enum CHOICE2
{
    CAM1, CAM2, CAM3
};

void quit_subroutine()
{
   static quit_pattern[8]= { 0, 0, 0, 0, 128, 128, 128, 128 };

   stopgrab(1);
   board_reset();
   pclear(quit_pattern);
   _clearscreen( _GCLEARSCREEN );
   system("\\utils\\menu off");
}

int camera_selection(rowMid, colMid)
 int rowMid, colMid;
{
   int iCamCur = 0;
   _clearscreen(_GCLEARSCREEN );
   iCamCur = Menu1( rowMid, colMid, mnuCam, iCamCur );
   return(iCamCur);
}

int board_reset()  /* Reset vs100 board  */
{
   sethdw(0x300, 0xd0000, 2, 1);
   setdim(1024, 1024, 12);
   orreg( LUT_CONTROL, 0x4000 ); /* Software reset- to remove vibration */
                                 /* image at grab function */
   initialize();
   crystal();
/*  extsync();    output screen will blink when there is no ext signal */

   setgain(255);
   setoffset(0);
}

void img_snap()
{
   waitvb();
   andreg(STATUS_CONTROL, 0xafff);
   if(testreg(STATUS_CONTROL, 0x2000) == 0 )
   orreg(STATUS_CONTROL, 0x2000);
   while(testreg(STATUS_CONTROL, 0x2000));
}

void static_subtraction()
```

```
{
  andreg(STATUS_CONTROL, 0x8fff);
  aclear(0, 0, 512, 512, 0);
  setinmux(MODE_A6_R0_F6);
  _clearscreen(_GCLEARSCREEN );
  printf("\n\t\tHit any key to acquire a reference frame\n");
  getch();
  snap(WAIT);
  swap6();
  rtsubtract(0);
  waitvb();
  grab(-1);
}

void sequential_subtraction()
{
  rtdiffs(4);
  static_luts();
  setlut(RED, 4);
  waitvb();
  grab(-1);
}

void swap2_subroutine()
{
  int x, y;
  int xarray[512], *xarray_ptr;

/*  andreg(STATUS_CONTROL, 0xafff);
  while (testreg(STATUS_CONTROL, 0x2000));  */
  setpmask(0x03f);
  aclear(0, 0, 512, 512, 0);
  while(testreg(STATUS_CONTROL, 0x1000));
  setpmask(0x000);
  initluts();
  xarray_ptr = xarray;
  for (y=0; y<512; y++)
  {
        rhline( 0, y, 512, xarray);
        for ( x=0; x<512; x++)
        {
          *(xarray_ptr+x) = (int) (*(xarray_ptr+x) * 4);
        }
        whline(0, y, 512, xarray);
  }
}

void imgsave_sub()
{
  char name[30], comment[80];
  int err;

  _clearscreen(_GCLEARSCREEN );
  printf("\n\n Save this page into file name:\n");
  scanf("%s",name);
  printf("comment is: \n");
  scanf("%s",comment);
  if((err=saveim(0, 0, 512, 512, EIGHT_BIT, name, comment)) < 0)
  {
        switch(err)
        {
          case FILE_ERROR:
```

```
                printf("Error opening file!\n");
                break;
            case FORMAT_ERROR:
                printf("Unknown format selected!\n");
                break;
            default:
                printf("? Unknown error ?\n");
                break;
            }
            getch();
    }
}

void imgread_sub()
{
    char name[80], comment[100];
    int x, y, dx, dy, format;

//  _clearscreen(_GCLEARSCREEN );
    if(filehunt( strcpy(name,"\\*.*") ) == NULL) return (0);
//  printf(" Enter the file name to read in: ");
//  scanf("%s",name);
    readim(0, 0, 512, 512, name);
    image_header(&x, &y, &dx, &dy, &format, name, comment);
    printf("\n\n comment: ");
    printf("%s", comment);
    printf("\n\n Press any key to continue!");
    getch();
}

void pages()
{
    int saoi[4], daoi[4];

    saoi[0]=0;
    saoi[1]=0;
    saoi[2]=1024;
    saoi[3]=1024;

    daoi[0]=0;
    daoi[1]=0;
    daoi[2]=512;
    daoi[3]=512;
    scale( saoi, daoi, 0.5, 0.5);
}

void test_register()
{
    unsigned int offset, newval;
    _clearscreen( _GCLEARSCREEN );
    printf(" Bit map of registers\n\n" );
    for (offset=0; offset <=0x1E; offset+=2)
    {
            newval=getreg(offset);
            pbin(offset, newval);
    }
    printf("\n\n Hit any key to continue" );
    getch();
}

int pbin(offset, num)
  unsigned int offset, num;
```

```
{
   unsigned int mask;
   int j, bit;
   mask=0x8000;
   printf("%04x   ",offset);
   for(j=0; j<16; j++)
   {
    bit=(mask & num) ? 1 : 0;
    printf("%d ", bit);
    if(j==7)
          printf("-- ");
    mask>>= 1;
   }
   printf("\n");
}

void enhence_img_sub()
{
   int x, y;
   int th;
   float n;
   int xarray[512], *xarray_ptr;
   xarray_ptr = xarray;

   _clearscreen(_GCLEARSCREEN );
   printf("\n\t\tEnter the enhence number( 2 - 10 )\n");
   scanf("%f", &n );
   printf("\n\t\tEnter the threshold number( 0 - 30 )\n");
   scanf("%d", &th );

   for (y=0; y<512; y++)
   {
          rhline( 0, y, 512, xarray);
          for ( x=0; x<512; x++)
          {
            if(*(xarray_ptr+x) > th )
              {
               *(xarray_ptr+x) =(int) *(xarray_ptr+x) * n ;
               if(*(xarray_ptr+x) > 255 )  *(xarray_ptr+x) = 255;
              }
          }
          whline(0, y, 512, xarray);
   }
}

void enhence_img_sub2()
{
   int x, y, th;
   double n, temp;
   int xarray[512], *xarray_ptr;

   xarray_ptr = xarray;

   _clearscreen(_GCLEARSCREEN );
   printf("\n\t\tEnter the enhence number( 1.38 - 2 )\n");
   scanf("%lf", &n );
   printf("\n\t\tEnter the threshold number( 0 - 30 )\n");
   scanf("%d", &th );
   for (y=0; y<512; y++)
   {
          rhline( 0, y, 512, xarray);
          for ( x=0; x<512; x++)
```

```
            {
              if( *(xarray_ptr+x) > th )
                {
                 temp = pow( (double) *(xarray_ptr+x) , n );
                 if( temp > 255.0 )      temp = 255.0;
                 *(xarray_ptr+x) = (int) temp;
                }
            }
            whline(0, y, 512, xarray);
    }
}

void log_img_sub()
{
    int x, y;
    double temp;
    int xarray[512], *xarray_ptr;

    xarray_ptr = xarray;

    _clearscreen(_GCLEARSCREEN );
    for (y=0; y<512; y++)
    {
            rhline( 0, y, 512, xarray);
            for ( x=0; x<512; x++)
            {
//        temp = log( (double) ( *(xarray_ptr+x)/13.0+1.0) )*84.268;
              temp = log( (double) ( *(xarray_ptr+x)/20.0+1.0) )*97.28;
              *(xarray_ptr+x) = (int) temp;
            }
            whline(0, y, 512, xarray);
    }
}

void brightness_sub()
{
    int x, y;
    int n;
    int xarray[512], *xarray_ptr;
    xarray_ptr = xarray;

    _clearscreen(_GCLEARSCREEN );
    printf("\n\t\tEnter the offset number( 0 - 50 )\n");
    scanf("%d", &n );

    for (y=0; y<512; y++)
    {
            rhline( 0, y, 512, xarray);
            for ( x=0; x<512; x++)
            {
                *(xarray_ptr+x) = *(xarray_ptr+x) + n ;
                if(*(xarray_ptr+x) > 255 )  *(xarray_ptr+x) = 255;
            }
            whline(0, y, 512, xarray);
    }
}

convol_5x5()
{
 int kernel[25];

  kernel[0]=1;  kernel[1]=2;  kernel[2]=2;  kernel[3]=2;  kernel[4]=1;
```

```
  kernel[5]=2; kernel[6]=3; kernel[7]=4; kernel[8]=3; kernel[9]=2;
  kernel[10]=2; kernel[11]=4; kernel[12]=8; kernel[13]=4; kernel[14]=2;
  kernel[15]=2; kernel[16]=3; kernel[17]=4; kernel[18]=3; kernel[19]=2;
  kernel[20]=1; kernel[21]=2; kernel[22]=2; kernel[23]=2; kernel[24]=1;

  conv5x5( 0, 0, 512, 512, 6, 0, ABS, kernel );
}

/************************************** End of gt11.c ************************************/

  /* DSPI Program: gt21.c */

/*  Header files included  */

#include <graph.h>
#include <malloc.h>

#define AT
#include "itex.h"
#include "itex100.h"
#include "menu1.h"
#include "stdtyp.h"

#define DTA_ADRS 0x350
#define F_OFF  1

void volt_change()
{
   extern DTA_VOLT;

   _clearscreen(_GCLEARSCREEN );
   printf(" Key in a volt number(0~4095) in DTA port 3:");
   printf("\n\n (default Vnum is 1800 for pig tailed system)");
   printf("\n\n Vnum = ");
   scanf("%d", &DTA_VOLT);
}


void sequential_subtraction2()
{
   extern DTA_VOLT;
   int volt1, volt2;
   float step;

   _clearscreen(_GCLEARSCREEN );
LP1:printf(" Input phase step (0-270): ");
   scanf("%f", &step);
   if( (step < 0) || (step > 270) ) goto LP1;
   volt1=(int) DTA_VOLT*(step/180);
   volt2=(int) DTA_VOLT*(1+step/180);
   if( volt2 > 4095 ) volt2=(volt2-2*DTA_VOLT);
   printf("\n\n %d %d", volt1, volt2);
   printf("\n\n Self dithering from DTA port 3 ( 0 - 10 V )");
   printf("\n\n Hit space bar to snap a frame");
   rtdiffs(4);
   static_luts();
   setlut(RED, 4);
   waitvb();
   grab(-1);
   while(!kbhit())
   {
     waitvb();
```

```
    waitvb();
    outp(DTA_ADRS+6 , volt1 & 0x00ff);
    outp(DTA_ADRS+7 , (volt1 >>8) & 0x000f);
    waitvb();
    waitvb();
    outp(DTA_ADRS+6 , volt2 & 0x00ff);
    outp(DTA_ADRS+7 , (volt2 >>8) & 0x000f);
  }
  andreg(STATUS_CONTROL, 0xafff);
  while(testreg(STATUS_CONTROL, 0x2000));
}

void speckle_average_sub1()
{
  char ch;
  int count=0, stop=0;
  extern DTA_VOLT;


  rtdiffs(4);
  static_luts();
  setlut(RED, 4);

 while(stop== 0)
 {
  _clearscreen(_GCLEARSCREEN );
  printf("\n\t\tSequential subtraction is processing!\n");
  printf("\n\t\tHit space bar to snap a frame\n\n");
  waitvb();
  grab(-1);
  while(!kbhit())
  {
    waitvb();
    waitvb();
    outp(DTA_ADRS , DTA_VOLT & 0x00ff);
    outp(DTA_ADRS+1, (DTA_VOLT >>8) & 0x000f);
    waitvb();
    waitvb();
    outp(DTA_ADRS , 0);
    outp(DTA_ADRS+1 , 0);
  }
/*  waitvb();   */
  andreg(STATUS_CONTROL, 0xafff);
  while(testreg(STATUS_CONTROL, 0x2000));

  while(kbhit()==1)
  {
   ch= getch();
  }
  setpmask(0x03f);
  aclear( 0, 0, 512, 512, 0);
  setpmask(0x000);

  sum_sub(count);
  count++;
  printf(" count = %d\n\n\n",count);
  printf("Stop averaging(type 1) If you want to continue, change illumitation! \n");
  scanf("%d", &stop );
  while(kbhit()==1)
  {
    ch= getch();
  }
```

```
 }
avg_sub(count);
}

sum_sub(count)
 int count;
{
 int x,y;
 int x0array[512], x1array[512];
 int *x0_ptr, *x1_ptr;
 x0_ptr = x0array;
 x1_ptr = x1array;
 if( count == 0)
 {
  for (y=0; y<512; y++)
  {
   rhline( 0, y, 512, x0array );
   whline(512, y, 512, x0array );
  }
 }
/*  else
 {
    for (y=0; y<512; y++)
    {
      rhline( 0, y, 512, x0array );
      rhline( 512, y, 512, x1array );
      whline( 0, y+512, 512, x1array);
      for (x=0; x<512; x++)
      {
        *(x1_ptr+x) = ( *(x0_ptr+x) ) + ( *(x1_ptr+x) );
      }
      whline(512, y, 512, x1array);
    }
 }   */
}

avg_sub(count)
 int count;
{
  int x, y, x3array[512];
  int *x3_ptr;
  x3_ptr = x3array;
  for (y=0; y<512; y++)
  {
    rhline( 512, y, 512, x3array );
    for( x=0; x< 512; x++)
    {
     *(x3_ptr+x) = (int) (*(x3_ptr+x) / count);
    }
    whline(512, y, 512, x3array );
  }
}

/*  read_pixel()
{
   int i, pix_array[512];
   int x=255, y=255;
   char ch;
   _clearscreen(_GCLEARSCREEN );
   setpmask(0x7ff);
   dynamic_luts();
   printf("\n\n Move the cross on the image to where you want to read!");
```

```
    while(TRUE)
    {
     if( x > 509 ) x=509;
     if( y > 509 ) y=509;
     if( x < 2 ) x=2;
     if( y < 2 ) y=2;
     line( x, 0, x, 511, 0x800);
     line( 0, y, 511, y, 0x800);
     if((ch=getch()) == 43) break;
     if(ch==0) hair_cross(&y, &x,F_OFF);
     sclear(0);
    }
    setpmask(0x000);
    static_luts();
LOOP: printf("\n\n Read Horizontal or vertical line(H/V)?");
    scanf("%c", &ch);
    if( ch == 'H' || ch == 'h' ) rhline(0, y, 512, pix_array);
    else if( ch == 'V' || ch == 'v' ) rvline(x, 0, 512, pix_array);
    else
    {
      printf(" Typing error");
      goto LOOP;
    }
    _clearscreen(_GCLEARSCREEN );

    for( i=0; i<512; i++)
    {
     printf( "%4d", pix_array[i] );
    }
printf(" Press any key to continue! ");
getch();
}
*/

read_pixel()
{
    int i, pix_array[512];
    int xy, ch;
    int *pix_ptr;

    pix_ptr= pix_array;
    _clearscreen(_GCLEARSCREEN );
LP: printf("\n\n Read Horizontal(1) or vertical(2) line: ");
    scanf("%d",&ch);
    printf("\n\n Line position (5~500):");
    scanf("%d", &xy);

    if( ch == 1 )
    {
     rhline(0, xy, 512, pix_array);
     setpmask(0x7ff);
     dynamic_luts();
     line( 0, xy, 511, xy, 0x800);
    }
    else if( ch == 2 )
    {
     rvline(xy, 0, 512, pix_array);
     setpmask(0x7ff);
     dynamic_luts();
     line( xy, 0, xy, 511, 0x800);
    }
    else
```

```
    {
      printf("\n\n Typing error");
      goto LP;
    }
    contrast_drawing( pix_ptr, 512, 1, 127);
    aclear( 0, 0, 512, 512, 0 );
    setpmask(0x000);
    static_luts();
}

contrast_drawing( array_ptr, size, scale, h_level )
int *array_ptr, size, scale, h_level;
{
   int i, j=0, k=0, flag1, flag2, centre;
   char _far *image;
   unsigned numbytes;
   long int value;

   centre= size/2-1;
   if(_setvideomode(_ERESCOLOR) == 0 )
   {
    printf("\nMode not supported, press any key to continue!\n");
    getch();
    exit(0);
   }
   _clearscreen(_GCLEARSCREEN );
   _setcolor(4);
   _rectangle(_GBORDER, 63, 73, 576, 329 );
   h_ruler(k, 15, h_level);
   numbytes= (unsigned int) _imagesize(64, 328-h_level+k, 575, 328-h_level+k);
   image= (char _far *) malloc(numbytes);
   _getimage(64, 328-h_level+k, 575, 328-h_level+k, image );
   h_ruler(k, 0, h_level);
   _setcolor(14);
   for ( i=0; i < size; i++ )
   {
    _moveto( 64+i, 328 );
    _lineto( 64+i, 328- *(array_ptr + i) );
   }
   ruler(j, 15, centre);
   _putimage( 64, 328-h_level+k, image, _GXOR );
   _settextwindow ( 0, 0, 1, 42);
   _settextposition(0,0);
   _settextcolor(5);
   value= ( (long int) *(array_ptr+centre) ) * ( (long int) scale );
   printf(" X= %3d  Y= %3d  Scale= %d  Value= %ld", centre, *(array_ptr+centre), scale, value );
   while( (flag1=getch())!=27 )
   {
    if( flag1==0)
    {
     if( (flag2=getch()) == 77)
     {
      _putimage( 64, 328-h_level+k, image, _GXOR );
      ruler(j, 0, centre);
      redraw_line( array_ptr, j, 14, centre);
      if( centre+j < size-1) j++;
      ruler(j, 15, centre);
      _putimage( 64, 328-h_level+k, image, _GXOR );
      _clearscreen(_GWINDOW);
      _settextposition(0,0);
      value= ( (long int) *(array_ptr+centre+j) ) * ( (long int) scale );
      printf(" X= %3d  Y= %3d  Scale= %d  Value= %ld", centre+j, *(array_ptr+centre+j), scale, value );
```

```
      }
      if(flag2 == 75)
      {
       _putimage( 64, 328-h_level+k, image, _GXOR );
       ruler(j, 0, centre);
       redraw_line( array_ptr, j, 14, centre);
       if( centre+j > 0) j--;
       ruler(j, 15, centre);
       _putimage( 64, 328-h_level+k, image, _GXOR );
       _clearscreen(_GWINDOW);
       _settextposition(0,0);
       value= ( (long int) *(array_ptr+centre+j) ) * ( (long int) scale );
       printf(" X= %3d  Y= %3d  Scale= %d  Value= %ld", centre+j, *(array_ptr+centre+j), scale, value );
      }
      if(flag2 == 72)
      {
       _putimage( 64, 328-h_level+k, image, _GXOR );
       if( 328-h_level+k > 73) k--;
       _putimage( 64, 328-h_level+k, image, _GXOR );
      }
      if(flag2 == 80)
      {
       _putimage( 64, 328-h_level+k, image, _GXOR );
       if( 328-h_level+k < 328) k++;
       _putimage( 64, 328-h_level+k, image, _GXOR );
      }
     }
    }

    _ffree(image);
    _setvideomode(_DEFAULTMODE );
}

redraw_line( array_ptr, j, color, centre )
int *array_ptr, j, color, centre;
{
    _setcolor(color);
    _moveto( 64+centre+j, 328);
    _lineto( 64+centre+j, 328- *(array_ptr +centre+j) );
}

ruler( j, color, centre )
int j, color, centre;
{
    _setcolor(color);
    _moveto( 64+centre+j, 328);
    _lineto( 64+centre+j, 328-254 );
}

h_ruler( k, color, h_level )
int k, color, h_level;
{
    _setcolor(color);
    _moveto( 64,328-h_level+k ) ;
    _lineto( 64+510, 328-h_level+k );
}

signal_noise_func()
{
    int xval, yval;
    int prev=0, pread;
```

```
  _clearscreen(_GCLEARSCREEN );
  printf("\n\tInput pixel position: x= ");
  scanf("%d", &xval );
  printf("   y= ");
  scanf("%d", &yval );
  printf("\n\n\t\tHit any key to start, and hit space bar to stop!\n");
  getch();
  while(!kbhit())
  {
    waitvb();
    waitvb();
    pread= rpixel(xval, yval) & 0x003f;
    printf( "%4d", pread-prev );
    prev= pread;
  }
}

fp_cali_func()
{
  int yval, i, count;
  int *pix_ptr, ptr_array[40];

  pix_ptr=ptr_array;
  _clearscreen(_GCLEARSCREEN );
  printf("\n\t\tInput height position: y= ");
  scanf("%d", &yval );
  snap(1);
  setpmask(0x7ff);
  dynamic_luts();
  line( 236, yval, 275, yval, 0x800);
  printf("\n\n\t\tHit any key to start, and hit space bar to stop!\n");
  getch();
  aclear( 0, 0, 512, 512, 0 );
  setpmask(0x000);
  static_luts();
  waitvb();
  grab(-1);
  while(!kbhit())
  {
    for( count=0; count < 50; count++ )
    {
     waitvb();
     waitvb();
    }
    rhline(236, yval, 40, ptr_array);
    printf("\n\n");
    for( i=0; i< 40; i++)
    {
     printf("P(%2d)=%3d ", i+1, *(pix_ptr+i) );
    }
  }
}

fp_cali_func2()
{
  int yval, i, count;
  int *pix_ptr, ptr_array[80], sum[80];
  int *sum_ptr, max, imax;

  pix_ptr=ptr_array;
  _clearscreen(_GCLEARSCREEN );
  yval = 420;
```

```
  snap(1);
  setpmask(0x7ff);
  dynamic_luts();
  line( 216, yval, 295, yval, 0x800);
  printf("\n\n\t\tHit any key to start, and hit space bar to stop!\n");
  getch();
  aclear( 0, 0, 512, 512, 0 );
  setpmask(0x000);
  static_luts();
  waitvb();
  grab(-1);
  while(!kbhit())
  {
    max=0;
    printf("\n\n");
    for( i=0; i< 80; i++)
    {
     sum[i] =0;
    }
    for( count=0; count < 150; count++ )
    {
     waitvb();
     waitvb();
     rhline(216, yval, 80, ptr_array);
     for( i=0; i< 80; i++)
     {
        sum[i]= sum[i]+ *(pix_ptr+i);
     }
    }
    for( i=0; i< 80; i++)
    {
      sum[i]= sum[i] / (count+1);
      if( max < sum[i] )
      {
       max= sum[i];
       imax= i;
      }
    }
    printf("Pmax(%2d)=%3d ", imax+1, max );
  }
  getch();
  getch();
}

hist_func()
{
 LONG histval[256], max=0;
 int i, *hist_ptr, hist_array[256], scale;
 int flag=1, count=0;

 hist_ptr= hist_array;
 histogram( 0, 0, 512, 512, 1, 1, 0, histval );
 for (i=1; i < 256; i++)
 {
  if( histval[i] > max ) max= histval[i];
 }
 scale= (int) (max/255+1);
 for (i=0; i < 256; i++)
 {
  hist_array[i]= (int) ( histval[i]/scale );
  if( hist_array[i] > 255 ) hist_array[i] = 255;
 }
```

```
 contrast_drawing( hist_ptr, 256, scale, 127 );

 _clearscreen(_GCLEARSCREEN );
 i=0;
 while( (flag!=27) && (i<256) )
 {
  printf(" N(%d)=%ld ", i, histval[i] );
  count++;
  i++;
  if(count > 200)
  {
   flag=getch();
   count=0;
  }
 }
 if(i>=256) getch();
}

/************************************ End of gt21.c ***************************************/

 /* DSPI Program: gt31.c */

/*  Header files included  */

#include <graph.h>
#include <stdio.h>

#define AT
#include "itex.h"
#include "itex100.h"
#include "menu1.h"
#include "stdtyp.h"

#define DTA_ADRS 0x350


void dta_ch0()
{
   int volt=0, vlim=900;

   outp(DTA_ADRS, 0);
   outp(DTA_ADRS+1 , 0);
   _clearscreen(_GCLEARSCREEN );

   Printf(" This function is mainly for diode temp. modulation");
   Printf("\n\n The limit of Vnum on CH.0 is set to 900");
   printf("\n\n The max volt change is %5.4f", (float) 5*vlim/4095 );
   printf("\n\n Key in Vnum ( Quit, when Vnum < 0 )\n\n");
   for( ; ; )
   {
     printf(" Vnum = ");
     scanf("%d", &volt);
     printf("\n Volt = %5.4f", (float) 5*volt/4095 );
     if( (volt > vlim) )
     {
      printf("\n\n Vnum is too big and has been reset to 0!");
      volt =0;
     }
     if( volt < 0 ) break;
     outp(DTA_ADRS , volt & 0x00ff);
     outp(DTA_ADRS+1 , (volt >>8) & 0x000f);
```

```
    printf("\n\n");
  }
}

void dta_ch4()  /* DTA volt change for static modulation */
{
  int volt=0, vlim=4095;
  int port=4;

  outp(DTA_ADRS+port*2, 0);
  outp(DTA_ADRS+port*2+1 , 0);
  _clearscreen(_GCLEARSCREEN );
  printf(" This function is for PZT phase shifting ( manually )");
  Printf("\n\n The limit of Vnum on CH.4 is set to 4095");
  printf("\n\n The max volt change is %5.4f", (float) 10*vlim/4095 );
  printf("\n\n Key in volt number ( Quit, when Vnumb < 0 )\n\n");
  for( ; ; )
  {
    printf(" Vnumb = ");
    scanf("%d", &volt);
    printf("\n Volt = %5.4f", (float) 5*volt/4095 );
    if( (volt > vlim) )
    {
     printf("\n\n Vnum is too big and has been reset to 0!");
     volt =0;
    }
    if( volt < 0 ) break;
    outp(DTA_ADRS+port*2 , volt & 0x00ff);
    outp(DTA_ADRS+port*2+1 , (volt >>8) & 0x000f);
    printf("\n\n");
  }
}


void contour1_func()
{
  extern DTA_VOLT;
  int volt, vlim = 900;
  int p3=3;
  float step;
  int volt1;

  _clearscreen(_GCLEARSCREEN );
LP1:printf(" Input phase step (0-270): ");
  scanf("%f", &step);
  if( (step < 0) || (step > 270) ) goto LP1;
  volt1=(int) DTA_VOLT*(step/180);
  printf("\n\n step= %d ", volt1);
  printf("\n\n laser diode current modulation on CH.1 (0 - 5 V )");
  Printf("\n\n The limit of Vnum on CH.1 is set to 900");
  printf("\n\n Self dithering on CH.3 ( 0 - 10 V )");
  printf("\n\n Hit space bar to snap a frame");
  printf("\n\n Key in Vnum on CH.1 ( 0 - 900 )");
  printf("\n\n Vnum = ");
  scanf("%d", &volt );
  if( (volt > vlim) || (volt < 0) ) volt=0;
  rtdiffs(4);
  static_luts();
  setlut(RED, 4);
  waitvb();
  waitvb();
  grab(-1);
```

```
  while(!kbhit())
  {
    waitvb();
    waitvb();
    outp(DTA_ADRS+p3*2, 0);
    outp(DTA_ADRS+p3*2+1, 0);
    outp(DTA_ADRS+2 , volt & 0x00ff);
    outp(DTA_ADRS+3 , (volt >>8) & 0x000f);
    waitvb();
    waitvb();
    outp(DTA_ADRS+p3*2, volt1 & 0x00ff);
    outp(DTA_ADRS+p3*2+1, (volt1 >>8) & 0x000f);
    outp(DTA_ADRS+2 , 0 );
    outp(DTA_ADRS+3 , 0 );
  }
  andreg(STATUS_CONTROL, 0xafff);
  while(testreg(STATUS_CONTROL, 0x2000));
}


void contour2_func()
{
  extern DTA_VOLT;
  int volt, vlim = 1200;
  int p3=3, delay;
  int count=0, initial =1;
  float step;
  int volt1;


  _clearscreen(_GCLEARSCREEN );
LP1:printf(" Input phase step (0-270): ");
  scanf("%f", &step);
  if( (step < 0) || (step > 270) ) goto LP1;
LP2:printf("\n\n Input delay (3000-30000): ");
  scanf("%d", &delay);
  if( (delay < 0) || (delay >30000) ) goto LP2;
  volt1= (int) ( DTA_VOLT*(step/180) );
  printf("Stepping Volt= %d", volt1);
  printf("\n\n laser diode current modulation on CH.1 (0 - 5 V )");
  Printf("\n\n The limit of Vnum on CH.1 is set to 1200");
  printf("\n\n Self dithering on CH.3 ( 0 - 10 V )");
  printf("\n\n Hit space bar to snap a frame");
  printf("\n\n Key in Vnum on CH.1 ( 0 - 1200 )");
  printf("\n\n Vnum = ");
  scanf("%d", &volt );
  if( (volt > vlim) || (volt < 0) ) volt=0;
  rtdiffs(4);
  static_luts();
  setlut(RED, 4);
  waitvb();
  waitvb();
  grab(-1);
  waitvb();
  waitvb();
  while(!kbhit())
  {
    outp(DTA_ADRS+p3*2 , 0);
    outp(DTA_ADRS+p3*2+1 , 0);
    while( !testreg(STATUS_CONTROL, 0x0400) );
    while( testreg(STATUS_CONTROL, 0x0400) )
    {
```

```
      dta1_mod(volt, delay, volt1);
      count+=1;
     }
     while( !testreg(STATUS_CONTROL, 0x0400) );
     while( testreg(STATUS_CONTROL, 0x0400) )
     {
      dta1_mod(volt, delay, volt1);
      count+=1;
     }
     outp(DTA_ADRS+p3*2 , DTA_VOLT & 0x00ff);
     outp(DTA_ADRS+p3*2+1 , (DTA_VOLT >>8) & 0x000f);
     while( !testreg(STATUS_CONTROL, 0x0400) );
     while( testreg(STATUS_CONTROL, 0x0400) )
     {
      dta1_mod(volt, delay, volt1);
      count+=1;
     }
     while( !testreg(STATUS_CONTROL, 0x0400) );
     while( testreg(STATUS_CONTROL, 0x0400) )
     {
      dta1_mod(volt, delay, volt1);
      count+=1;
     }
     if( initial==1)
     {
      printf("\n\n modulation freq. = %6.3f k", (float) 12.5*count/1000 );
     }
     initial=0;
   }
   andreg(STATUS_CONTROL, 0xafff);
   while(testreg(STATUS_CONTROL, 0x2000));
}

int dta1_mod(volt,delay, volt1)
int volt, delay, volt1;
{
   int i, p4=4;
     outp(DTA_ADRS+p4*2 , volt1 & 0x00ff);
     outp(DTA_ADRS+p4*2+1 , (volt1 >>8) & 0x000f);
     outp(DTA_ADRS+2 , volt & 0x00ff);
     outp(DTA_ADRS+3 , (volt >>8) & 0x000f);
     for(i=0; i < delay; i++);
     outp(DTA_ADRS+p4*2 , 0);
     outp(DTA_ADRS+p4*2+1 , 0);
     outp(DTA_ADRS+2 , 0 );
     outp(DTA_ADRS+3 , 0 );
     for(i=0; i < delay; i++);
}

/************************************** End of gt31.c ************************************/

/* DSPI program: pzt_cal1.c */

#include <graph.h>

#include "itex.h"
#include "itex100.h"

#define DTA_ADRS 0x350

void pzt_cal1_func()
{
```

```
   int vnum, port, vnum_limit=4096, psum[4096], max=0;
   int i, j, scale;
//   int array[10][200];
   int array[50][50];
   int pwin, sum;
//   int *ptr_psum, cx =255, cy=255;
   int *ptr_psum, cx, cy;

   ptr_psum=psum;
   _clearscreen(_GCLEARSCREEN );
LP1:printf("\n Select a DTA port ( 3-5): ");
   scanf("%d", &port );
   if( port<3 || port>5) goto LP1;
LP2:printf("\n Enter window size (2-50): ");
   scanf("%d", &pwin );
   if( pwin<2 || pwin>50) goto LP2;
   printf("\n Enter x coord. of window: ");
   scanf("%d", &cx );
   printf("\n Enter y coord. of window: ");
   scanf("%d", &cy );
   printf("\n");
/*
LP2:printf("\n Enter window size (20-200): ");
   scanf("%d", &pwin );
   if( pwin<20 || pwin>200) goto LP2;
*/
   rtdiffs(4);
   static_luts();
   setlut(RED, 4);
   waitvb();
   grab(-1);
   for ( i=0; i < 50; i++)
   {
    waitvb();
    waitvb();
   }
   for ( vnum=0; vnum< vnum_limit; vnum++)
   {
     sum=0;
     outp(DTA_ADRS+port*2, 0);
     outp(DTA_ADRS+port*2+1, 0);
     waitvb();
     waitvb();
     outp(DTA_ADRS+port*2, vnum & 0x00ff);
     outp(DTA_ADRS+port*2+1, (vnum >>8) & 0x000f);
     waitvb();
     waitvb();
     for (i=0; i < pwin; i++)
     {
      rhline( cx-pwin/2, cy-pwin/2+i, pwin, array[i] );
     }
     for(i=0; i< pwin; i++)
     {
      for (j=0; j < pwin; j++)
      {
       sum+=( *(*(array+i)+j) & 0x003f );
      }
     }
/*
     for (i=0; i <10; i++)
     {
      rhline( cx-pwin/2, cy+(i-5)*i, pwin, array[i] );
```

```
    }
    for(i=0; i< 10; i++)
    {
     for (j=0; j < pwin; j++)
     {
      sum+= ( *(*(array+i)+j) & 0x003f );
     }
    }
*/
    *( ptr_psum + vnum ) = sum;
    if( *(ptr_psum+ vnum) > max ) max= *(ptr_psum+ vnum);
    printf("V=%4d  Sum=%6d  ", vnum, sum );
  }
  scale = (int) (max/255 +1);
  for (vnum=0; vnum < vnum_limit; vnum++)
  {
   psum[vnum]= (int) ( psum[vnum]/scale );
   if( psum[vnum] > 255 ) psum[vnum] = 255;
  }
  for( i=0; i < 8; i++)
  {
   contrast_drawing(ptr_psum+512*i, 512, scale, 20);
  }
  outp(DTA_ADRS+port*2, 0);
  outp(DTA_ADRS+port*2+1, 0);
}

void diode_call_func()
{
  int vnum, port, vnum_limit=512, psum[512], max=0;
  int i,j, scale;
  int array[50][50];
  int sum, pwin;
  int *ptr_psum, cx, cy;

  ptr_psum=psum;
  _clearscreen( _GCLEARSCREEN );
LP1:printf("\n Select a DTA port ( 0-2): ");
  scanf("%d", &port );
  if( port<0 || port>2) goto LP1;
LP2:printf("\n Enter window size (2-50): ");
  scanf("%d", &pwin );
  if( pwin<2 || pwin>50) goto LP2;
  printf("\n Enter x coord. of window: ");
  scanf("%d", &cx );
  printf("\n Enter y coord. of window: ");
  scanf("%d", &cy );
  printf("\n");
  rtdiffs(4);
  static_luts();
  setlut(RED, 4);
  waitvb();
  grab(-1);
  for ( i=0; i < 10; i++)
  {
   waitvb();
   waitvb();
  }
  for ( vnum=0; vnum< vnum_limit; vnum++)
  {
    sum=0;
    outp(DTA_ADRS+port*2, 0);
```

```
    outp(DTA_ADRS+port*2+1, 0);
    waitvb();
    waitvb();
    outp(DTA_ADRS+port*2, vnum & 0x00ff);
    outp(DTA_ADRS+port*2+1, (vnum >>8) & 0x000f);
    waitvb();
    waitvb();
    for (i=0; i < pwin; i++)
    {
     rhline( cx-pwin/2, cy-pwin/2+i, pwin, array[i] );
    }
    for(i=0; i< pwin; i++)
    {
     for (j=0; j < pwin; j++)
     {
      sum+=( *(*(array+i)+j) & 0x003f );
     }
    }
    *(ptr_psum+ vnum) = sum;
    if( *(ptr_psum+ vnum) > max ) max= *(ptr_psum+ vnum);
  }
  scale= max/255 +1;
  for (vnum=0; vnum < vnum_limit; vnum++)
  {
   psum[vnum]= (int) ( psum[vnum]/scale );
   if( psum[vnum] > 255 ) psum[vnum] = 255;
  }
  contrast_drawing(ptr_psum, vnum_limit, scale, 80);
  outp(DTA_ADRS+port*2, 0);
  outp(DTA_ADRS+port*2+1, 0);
}

/************************* End of pzt_cal1.c ************************************************/


/* A typical compiling batch file */

cl /G2 /c dspi.c > comp.err
type comp.err


/* The linking batch file */

link dspi gt11 gt21 gt31 pzt_cal1 mouse menu1 dualgrab ,,, \lib\tvh \lib\mouse \lib\slibce \lib\itx100ms /stack:30000
/NOD /E


/****************************** End of program listing ***************************************/
```

PUBLICATIONS

1. Huang, J-R and Tatam, R. P., Optoelectronic speckle interferometry. *IOP Short Contributions Meeting*, (1995).

2. Huang, J-R, Ford, H. D. and Tatam, R. P., Speckle techniques for material testing. *IEE Colloquium on "Optical Techniques for Structural Monitoring"*, (1995).

3. Huang, J-R and Tatam, R. P., Optoelectronic shearography: Two wavelength slope measurement. *SPIE*, Vol. 2544 (1995) 300-308.

4. Huang, J-R, Ford, H. D. and Tatam, R. P., Slope measurement by two-wavelength electronic shearography. Accepted for publication in *Optics. and Lasers in Eng.*

5. Huang, J-R, Ford, H. D. and Tatam, R. P., Source modulation techniques for static deformation and vibration measurement in optoelectronic shearography. *OFS* (1996) 348-351.

6. Huang, J-R, Ford, H. D. and Tatam, R. P., Phase-stepped speckle shearing interferometer using source wavelength modulation. Accepted for publication in *Opt. Lett.*

7. Huang, J-R, Ford, H. D. and Tatam, R. P., Source modulation for phase shifting in static and dynamic speckle shearing interferometry. *SPIE*, Vol. 2860, (1996).